An investigation into the location of the heparan sulphate/heparin-binding site of human bone morphogenetic protein-7

David John McClarence

School of Biological Sciences
Royal Holloway, University of London

A thesis submitted for the degree of
Doctor of Philosophy

2011

Declaration of authorship

I, David John McClarence, hereby declare that this thesis and the work presented in it is entirely my own. Where I have consulted the work of others, this is always clearly stated.

Signed:

Date:

Abstract

The bone morphogenetic proteins (BMPs) are small cystine-knot-containing cytokines that serve pivotal functions during the development of a wide range of tissues. Consisting of approximately twenty structurally and functionally related proteins, the BMP family makes up the largest branch of the transforming growth factor beta (TGF-β) superfamily. At least three of the BMPs have the ability to bind to heparan sulphate (HS) and heparin, which are highly sulphated, complex polysaccharides that are found in abundance on cell surfaces and in the extracellular matrix. The functional significance of these interactions remains unclear, but it has been demonstrated that BMPs -2 and -4 bind to HS/heparin via a small cluster of basic amino acids in their N-terminal regions. BMP-7 has also been shown to interact with HS and heparin. However, it belongs to a different BMP sub-group to BMPs -2 and -4, and it differs from them considerably in this key N-terminal region. This raises the question as to where the HS/heparin-binding site of BMP-7 is situated. The aim of this study was to answer this question using a combination of predictive computational molecular docking calculations, site-directed mutagenesis techniques and heparin-affinity chromatography.

The findings from a series of predictive docking calculations suggested that BMP-7 binds to HS/heparin through three basic residues close to the C-terminal ends of each of its constituent monomers. However, experimental studies have shown that this is unlikely, as removing two of these three basic residues from each monomer had no affect on the heparin-binding affinity of BMP-7. The same was true when two of seven basic residues were removed from the N-terminal regions of each BMP-7 monomer, both alone and in combination with the C-terminal mutations. Further investigation is therefore required in order to resolve this matter.

Table of contents

List of figures

List of tables

Abbreviations

ACTR	Activin receptor
ALK	Activin receptor-like kinase
ALP	Alkaline phosphatase
AMBER	Assisted model building with energy refinement
APS	Ammonium persulphate
ATIII	Antithrombin III
BBSRC	Biotechnology and Biological Sciences Research Council
BMP	Bone morphogenetic protein
BMPR	Bone morphogenetic protein receptor
bp	Base pair
BSA	Bovine serum albumin
CDMP	Cartilage-derived morphogenetic protein
cDNA	Complementary deoxyribonucleic acid
CHO	Chinese hamster ovary
CMV	Cytomegalovirus
Dam	DNA adenine methylase
dATP	Deoxyadenosine triphosphate
Dly	Dally-like
DNA	Deoxyribonucleic acid
dNTP	Deoxynucleotide triphosphate
Dpp	Decapentaplegic
DTT	1,4-Dithiothreitol
ECACC	European Collection of Cell Cultures

ECD	Extracellular domain
ECM	Extracellular matrix
ECMV	Encephalomyocarditis virus
E. coli	*Escherichia coli*
EDTA	Ethylenediaminetetraacetic acid
ELISA	Enzyme-linked immunosorbent assay
EMT	Epithelial-to-mesenchymal transition
EXT	Exostosin
FBS	Foetal bovine serum
FGF	Fibroblast growth factor
FGFR	Fibroblast growth factor receptor
GAG	Glycosaminoglycan
Gbb	Glass bottom boat
GDF	Growth and differentiation factor
GDNF	Glial cell line-derived neurotrophic factor
GlcA	β-D-glucuronic acid
GlcA2S	β-D-glucuronic acid *O*-sulphated at C-2
GlcNAc	*N*-acetyl-α-D-glucosamine
$GlcNH_3$	*N*-unsubstituted α-D-glucosamine
GlcNS	*N*-sulphated-α-D-glucosamine
GlcNS3S	*N*-sulphated-α-D-glucosamine *O*-sulphated at C-3
GlcNS6S	*N*-sulphated-α-D-glucosamine *O*-sulphated at C-6
GPI	Glycosylphosphatidylinositol
IFN-γ	Interferon gamma

IL-8	Interleukin 8
IPTG	Isopropyl-β-D-1-thiogalactopyranoside
HEK	Human embryonic kidney
HEPES	4-(2-hydroxyethyl)-1-piperazineethanesulphonic acid
HRP	Horseradish peroxidase
HS	Heparan sulphate
HSPG	Heparan sulphate proteoglycan
HS2ST	Heparan sulphate 2-*O*-sulphotransferase
HS3ST	Heparan sulphate 3-*O*-sulphotransferase
HS6ST	Heparan sulphate 6-*O*-sulphotransferase
IdoA	α-L-iduronic acid
IdoA2S	α-L-iduronic acid *O*-sulphated at C-2
IRES	Internal ribosome entry site
kb	Kilobase
kcal	Kilocalorie
K_d	Dissociation constant
kDa	KiloDalton
LB	Luria-Bertani
Lys-C	Endoproteinase Lys-C
MCK	Muscle creatine kinase
MCS	Multiple cloning site
MET	Mesenchymal-to-epithelial transition
MOI	Multiplicity of infection
mRNA	Messenger ribonucleic acid
NDST	*N*-acetylglucosamine *N*-deacetylase/*N*-sulfotransferase

NIBSC	National Institute for Biological Standards and Control
OE-PCR	Overlap extension polymerase chain reaction
OP	Osteogenic protein
PBS	Phosphate buffered saline
PCR	Polymerase chain reaction
PDB	Protein Data Bank
PF4	Platelet factor 4
pfu	Plaque forming units
PG	Proteoglycan
RCSB	Research Collaboratory for Structural Bioinformatics
RE	Restriction endonuclease
RHUL	Royal Holloway, University of London
RNA	Ribonucleic acid
ROS	Rat osteosarcoma
RT-PCR	Reverse transcription polymerase chain reaction
SAP	Shrimp alkaline phosphatase
SDM	Site-directed mutagenesis
SDS	Sodium dodecyl sulphate
SDS-PAGE	Sodium dodecyl sulphate polyacrylamide gel electrophoresis
SEC	Size-exclusion chromatography
Sf9	*Spodoptera frugiperda* cell line
SOC	Super optimal broth with catabolite repression
SV40	Simian vacuolating virus 40
TAE	Tris-acetate-ethylenediaminetetraacetic acid

TBS	Tris buffered saline
TEMED	Tetramethylethylenediamine
TGF-β	Transforming growth factor beta
UTR	Untranslated region
UV	Ultraviolet
USFDA	United States Food and Drug Administration
X-gal	5-bromo-4-chloro-3-indolyl-beta-D-galactopyranoside

Chapter 1: Introduction

1.1 Bone morphogenetic proteins

1.1.1 Discovery and early work

The study of the bone morphogenetic proteins (BMPs) began in the 1960s when Marshall R. Urist first discovered their activity whilst searching for the principles that give bone its regenerative capacity. The pioneering work of Urist (1965) demonstrated that demineralised bone matrix had the ability to induce *de novo* bone formation when ectopically implanted in subcutaneous and intramuscular pockets in a number of host animals, including rats and rabbits. Reddi and Huggins (1972) later revealed that the observed matrix-induced bone formation occurred via a tightly coordinated sequential cascade of events. The first step in this process was chemotaxis, in which the demineralised bone matrix implant was colonised by migrating mesenchymal cells. These mesenchymal cells proliferated before differentiating into cartilage-forming cells (chondroblasts and chondrocytes). Following this, vascular invasion of the site occurred, and differentiated osteoblast and osteoclast bone cells began to appear in the area. These bone cells gradually removed the cartilage and deposited new bone in its place. This process recapitulated all of the events that occur during embryonic skeletogenesis in the limb bud and fracture healing in developed bones (Reddi and Huggins, 1972; Reddi, 1981). Together, these studies therefore suggested that the demineralised bone matrix extracts contained the key signals that are required for bone morphogenesis.

These early findings demonstrated the importance and considerable regenerative potential of the matrix factors, and provoked the interest of both skeletal and developmental biologists. However, the identities of the proteins within the matrix extracts that were responsible for the bone inductive properties remained unknown until the first human BMPs were purified (Sampath *et al.*, 1987; Luyten *et al.*, 1989) and cloned (Wozney *et al.*, 1988) many years later.

1.1.2 The BMP family

Upon peptide sequencing and gene cloning, the BMPs were found to be members of the transforming growth factor beta (TGF-β) protein superfamily (Wozney *et al.*, 1988). Whilst the members of this family fulfill an incredibly diverse range of functions (reviewed in Kingsley, 1994; Hogan, 1996b; Massague, 2000; Attissano and Wrana, 2002; Chang *et al.*, 2002), they are structurally very closely related (Lin *et al.*, 2006). TGF-β superfamily proteins display homology in their highly conserved pattern of seven characteristically-spaced cysteine residues (Herpin *et al.*, 2004), which produces a common cystine-knot fold (Avsian-Kretchmer and Hsueh, 2004). They also share sequence similarity within these cystine-knot regions. The one exception in the BMP family is BMP-1, a metalloproteinase that is structurally unrelated to TGF-β (Mac Sweeney *et al.*, 2008). BMP-1 exercises its pro-BMP activity during morphogenesis by cleaving the extracellular BMP antagonist chordin (Pappano *et al.*, 2003). It also serves to activate GDF-8 and BMP-11 by releasing them from their latent pro-protein complexes (Wolfman *et al.*, 2003; Ge *et al.*, 2005).

Work carried out since the initial discovery of the first BMPs has shown that the BMP family contains around twenty cytokines, which are highly related both structurally and functionally (reviewed by Reddi, 1997; Ducy and Karsenty, 2000). Many of the BMP family cytokines were independently characterised prior to them being recognised as members of the larger BMP family. As a result, some of the BMPs were originally classified as osteogenic proteins (OPs), cartilage-derived morphogenetic proteins (CDMPs), or growth and differentiation factors (GDFs) (Ducy and Karsenty, 2000). However, it is now apparent that there is a high degree of overlap between these nomenclatures, and that these designations do not represent separate cytokine lineages. In many cases the terms BMP and GDF are redundant. An example of such a case is BMP-13, which is also known as GDF-6.

Following phylogenetic analyses, a number of the BMPs have been grouped into sub-sets based on similarities in the amino acid sequences of their mature protein regions. These groupings are: BMPs -2 and -4; BMPs -3 and -3b; BMPs -5 to -8; BMPs -9 and -10; BMP-11 and GDF-8; and finally BMPs -12 to -14 (Kingsley, 1994; Hogan, 1996; Yamashita *et al.*, 1996; Mehler *et al.*, 1997; Ebendal *et al.*, 1998). The

same phylogenetic analyses have also revealed that the BMPs that make up two of these sub-sets exhibit close homology to the *Drosophila* morphogens decapentaplegic, Dpp (BMPs -2 and -4) and glass bottom boat, Gbb (BMPs -5 to -8). Comparison of their mature protein sequences shows that the most obvious difference between these two sub-sets is that the Gbb-type BMPs possess considerably longer amino-terminal extensions upstream of their TGF-β-like cystine-knot domains than the Dpp-type BMPs.

1.1.3 Synthesis and processing

The BMPs, like other TGF-β family proteins, are initially translated as large monomeric pre-pro-proteins that are generally in the region of 400-500 amino acids in length (Jones *et al.*, 1994). Following translation, these pre-pro-proteins undergo a number of processing events. First, cleavage takes place between the short signal peptide sequence and the pro-domain (Jones *et al.*, 1994). Some of the BMPs, including BMP-2 and BMP-7 (Israel *et al.*, 1992; Sampath *et al.*, 1992; Jones *et al.*, 1994), are then glycosylated at a conserved N-glycosylation sequence (NXS/T) before dimerisation takes place. BMP dimerisation generally occurs via a covalent inter-chain disulphide bridge (Griffith *et al.*, 1996), although there are some exceptions to this. In the cases of GDFs -3 and -9, and also BMP-15, dimerisation occurs non-covalently as they lack the fourth conserved cysteine residue that is required to form inter-chain disulphide bonds (Liao *et al.*, 2003). Once dimerised, the pro-proteins are proteolytically cleaved at a dibasic arginine-X-X-arginine site to release the 30-38 kiloDalton (kDa) mature BMP dimers from their latent complexes prior to secretion (Ozkaynak *et al.*, 1992; Cui *et al.*, 1998). It has been shown that the efficiency of this cleavage step is determined by the downstream sequences that lie adjacent to the precursor cleavage site (Constam and Robertson, 1999).

In most instances, the mature BMP dimers are secreted without their pro-regions, which dissociate after cleavage (Brown *et al.*, 2005). However, there is evidence to suggest that the mature GDF-8 and BMP-9 dimers remain non-covalently associated with their pro-regions after secretion; for GDF-8, this association inhibits the binding of the mature ligand to its receptor (Thies *et al.*, 2001), whereas the activities of BMP-9 and the BMP-9 dimer-pro-region complex are equal (Brown *et*

al., 2005). When expressed and characterised in Chinese hamster ovary (CHO) cells (Jones *et al.*, 1994) or human embryonic kidney 293 (HEK 293) cells (Gregory *et al.*, 2005), the majority of the secreted mature BMP-7 dimers were also found to remain associated with their pro-regions. In this case, the non-covalent complexes of mature BMP-7 dimers and pro-BMP-7 domains had greater solubility in physiological buffers than the purified mature dimers alone (Jones *et al.*, 1994).

The monomeric constituents of the mature BMP dimers each contain around 100-140 amino acid residues (Jones *et al.*, 1994). Although the BMPs are normally homodimeric in nature, natural heterodimers are known to exist. The bioactivity of some of these heterodimers has been reported to be equal to, if not greater than, that of their homodimeric counterparts (Hazama *et al.*, 1995).

1.1.4 Structure

The three-dimensional structures of a number of BMPs have been resolved to high resolution, and their coordinates have been deposited in the Research Collaboratory for Structural Bioinformatics (RCSB) Protein Data Bank (PDB) archive (http://www.rcsb.org/pdb). These structures include BMPs -1, -2, -3, -6, -7, -9 and GDF-5, with their respective PDB identifications being 3EDG, 3BMP, 2QCQ, 2R52, 1LXI, 1ZKZ and 2BHK. In each of these reported structures, most of the N-terminal sequence that lies upstream of the cystine-knot domain remains unresolved and is therefore absent. It is likely that this component of the structures was not resolved as a result of it being disordered (Griffith *et al.*, 1996; Greenwald *et al.*, 2003). In contrast, the N-terminal extensions of TGF-βs -1, -2 and -3 were resolved due to them being held in place (close to the cystine-knot domains of the structures) by an additional disulphide bond (Daopin *et al.*, 1992; Schlunegger and Grutter, 1992; Hinck *et al.*, 1996; Mittl *et al.*, 1996).

The available structures confirm that the BMPs, with the exception of BMP-1, possess the cystine-knot structural motif that is characteristic of all the TGF-β superfamily members (McDonald and Hendrickson, 1993). Examination of the X-ray crystal structure of BMP-7, which was first resolved by Griffith *et al.* (1996), reveals that these knots form the core of each BMP monomer and consist of three intra-chain disulphide bonds (Figure 1.1). Two of these bonds, which connect cysteine 2 to

cysteine 6, and cysteine 3 to cysteine 7, create a ring through which the third disulphide bond passes, linking cysteine 1 and cysteine 5. Emanating from this cystine-knot are two elongated, thin and slightly curved finger-like projections. Both of these projections are antiparallel beta-sheet structures, and are termed fingers 1 and 2 (Figure 1.1). On the opposite side of the knot is an alpha-helix. In its monomeric form, this fold is often likened to an open left hand, with the beta-sheets making up the two fingers, the cystine-knot acting as the palm, and the helix as the wrist/thumb (Griffith *et al.*, 1996).

Upon dimerisation, the wrist/thumb region of one BMP monomer tucks into the concave face that is formed by the fingers of the other (Figure 1.2). In most cases (see section 1.1.3 for exceptions), a disulphide bond forms between the fourth conserved cysteine residues of each monomer to link the two together covalently (Figure 1.2).

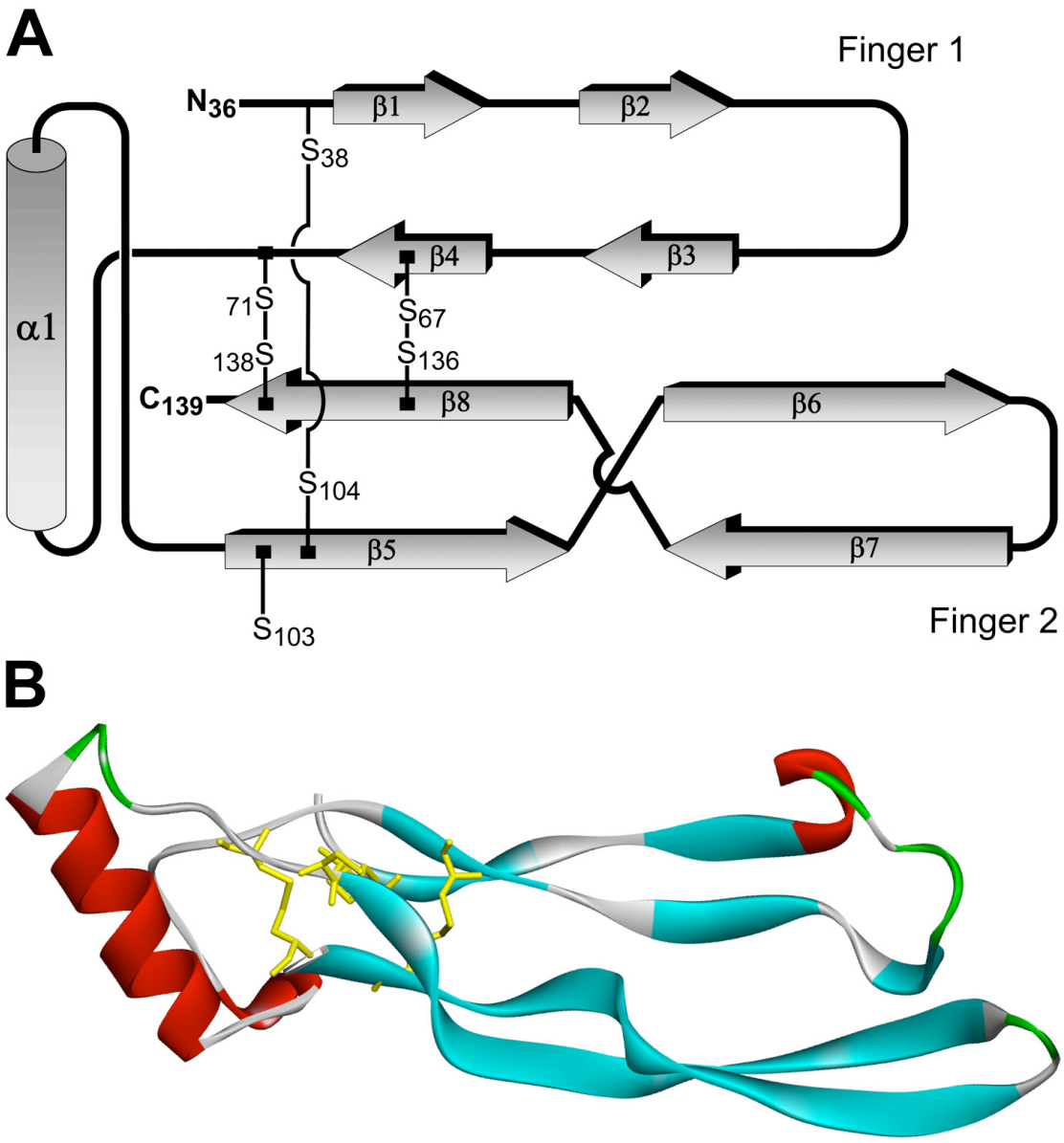

Figure 1.1 The BMP-7 monomer fold
A schematic (A) and ribbon (B) representation of a BMP-7 monomer. The cystine-knot forms the core of each BMP monomer and consists of three intra-chain disulphide bonds. The first bond connects cysteine 2 to cysteine 6 and the second bond connects cysteine 3 to cysteine 7. A ring is created by these two bonds through which the third disulphide bond passes, linking cysteine 1 to cysteine 5. Two elongated, thin and slightly curved finger-like projections emanate from the cystine-knot. Both of these projections are antiparallel beta-sheet structures, and are termed fingers 1 and 2 (shown in turquoise in B). On the opposite side of the knot is an alpha-helix (shown in red in B). The side chains of the cysteine residues that partake in forming the cystine-knot can be seen in yellow in B. [Figure 1.1A adapted from that presented in Griffith *et al.*, (1996). The image shown in Figure 1.1B was generated from the PDB file 1LXI using the Accelrys Discovery Studio software package].

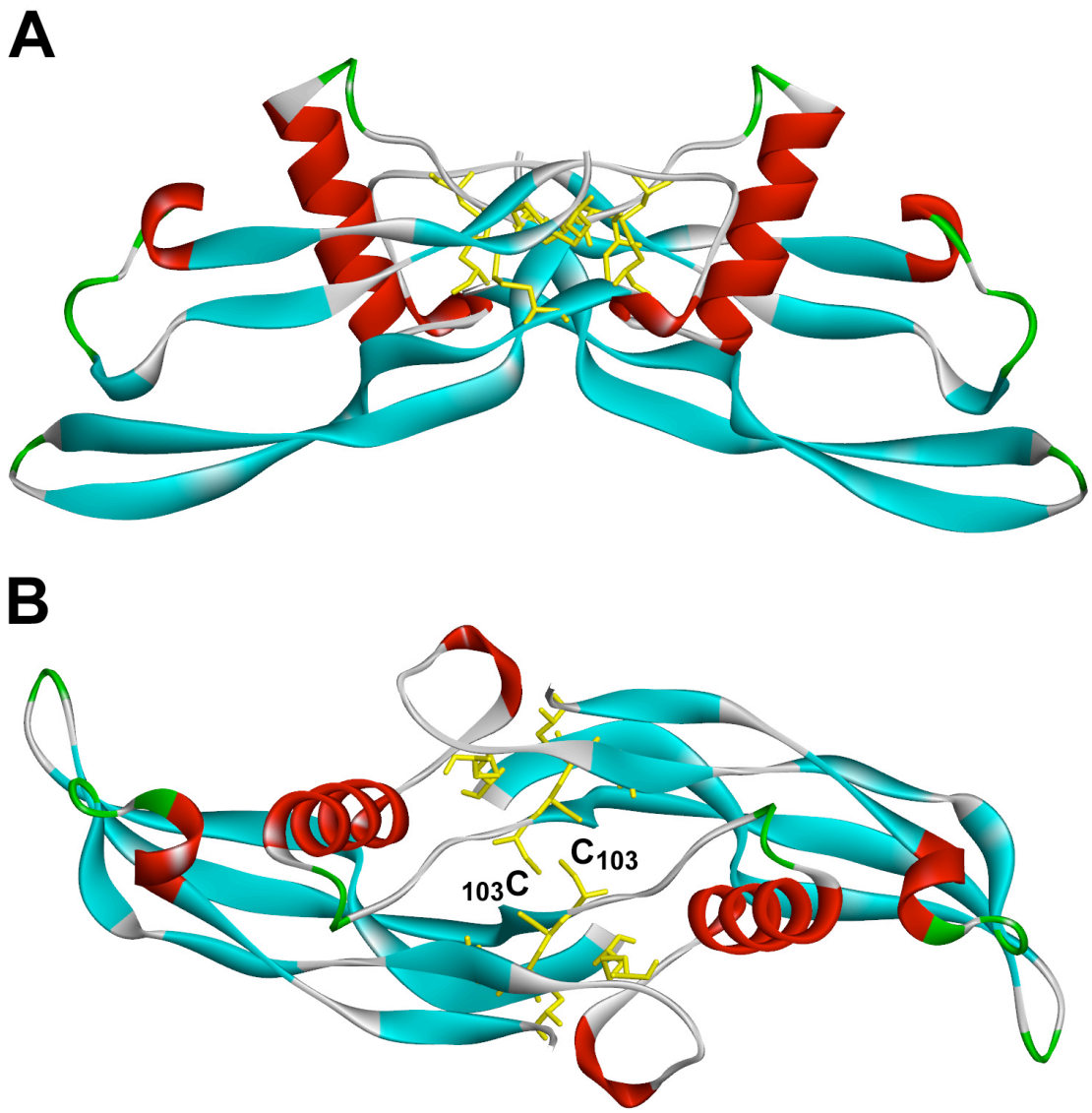

Figure 1.2 The BMP-7 dimer
Views of the BMP-7 dimer shown as ribbon representations from the front (A) and top (B). Upon dimerisation, the helix of one BMP monomer tucks into the concave face that is formed by the fingers of the other. A disulphide bond forms between the fourth conserved cysteine residue of each BMP monomer to link the two together covalently. In the case of BMP-7, this residue is cysteine 103 (labeled in B). The side chains of the cysteine residues that partake in forming the cystine-knot can be seen in yellow. Alpha helices are shown in red and beta sheets are shown in turquoise. The images seen in this figure were generated from the PDB file 1LXI using the Accelrys Discovery Studio software package.

1.1.5 Biological function and clinical applications

The hallmark of the BMPs is their striking ability to induce *de novo* bone formation in both orthotopic and ectopic sites *in vivo* by promoting osteoblast differentiation (Urist, 1965). This remarkable activity can also be demonstrated and measured *in vitro* with a bioassay that utilises the C2C12 myoblastic cell line (Katagiri *et al.*, 1994). Following stimulation with BMPs, these cells undergo a transformation, transdifferentiating from cells of a myogenic fate into cells with an osteogenic phenotype. As the cells transdifferentiate, the expression of muscle-type marker proteins such as muscle creatine kinase (MCK) is down-regulated whilst the expression of osteoblastic marker proteins such as alkaline phosphatase (ALP) and osteocalcin are up-regulated. Given the fact that members of the BMP family have such potent bone-inducing abilities (Sampath *et al.*, 1992), it is no surprise that the knockout of BMP genes in mice often results in skeletal abnormalities (Kingsley *et al.*, 1992). However, due to the level of functional redundancy that exists between the numerous members of the BMP family, these abnormalities are often relatively minor.

Since the discovery of the BMPs, their bone-inducing properties have been the subject of extensive research. Much of the research that has been carried out has been directed towards developing therapeutic strategies for the treatment of skeletal damage/loss that results from trauma, degenerative disease or ablative surgery (Warnke *et al.*, 2004). Clinical studies have provided supportive evidence for the use of BMPs -2 and -7 in spinal fusion and the treatment of difficult bone fractures, nonunions and delayed unions (reviewed by White *et al.*, 2007). A landmark in this research was the United States Food and Drug Administration (USFDA) approval being granted for the clinical use of BMP-7 (Stryker Corp., Kalamazoo, MI, 2001) and BMP-2 (Medtronic Sofamor Danek, Memphis, TN, 2002) for therapeutic applications like those described above (White *et al.*, 2007).

Despite the potent bone-inducing abilities of the BMPs, it has become apparent that the historical term ‘bone morphogenetic protein’ is now rather unsuitable and somewhat misleading. Although their name might suggest otherwise, extensive studies conducted since the BMPs gained their title have shown that BMP family members actually have a wide variety of pivotal roles outside skeletal tissue. These roles include the establishment of embryonic pattern formation and the

development and function of a number of organs (reviewed by Ducy and Karsenty, 2000). For example, it has been demonstrated that BMP-9 is a regulator of hepatic glucose homeostasis (Chen *et al.*, 2003), and that BMP-10 plays a crucial role in maintaining the proliferative activity of embryonic cardiomyocytes during the development of the heart (Chen *et al.*, 2004).

1.1.5.1 Bone morphogenetic protein-7 (BMP-7)

A particularly interesting member of this protein family is BMP-7, also known as osteogenic protein-1 (OP-1). BMP-7 is a 34-38 kDa disulphide-linked homodimeric protein. Each of its constituent monomeric units is initially synthesised as a 431 amino acid pre-pro-protein, which consists of a 29 residue signal peptide, a 263 residue pro-protein domain and a 139 residue mature protein domain. Once synthesised, this pre-pro-protein is cleaved between its signal peptide and pro-domain, glycosylated and dimerised. The mature BMP-7 protein is then liberated from its pro-domain by a second proteolytic cleavage step before being secreted (Jones *et al.*, 1994).

BMP-7 was initially discovered in bone matrix based on its bone-inducing properties (Celeste *et al.*, 1990; Ozkaynak *et al.*, 1990), but like many of the other BMPs it has since been found to be a multifunctional cytokine. The key extraskeletal roles of BMP-7 were elucidated using BMP-7-deficient knockout mice (Dudley *et al.*, 1995; Luo *et al.*, 1995). These studies have shown that the homozygous deletion of the BMP-7 gene results in perinatal lethality as a result of severe renal dysplasia, marked by the presence of small dysgenic kidneys that are almost completely absent of glomeruli (less than 3 glomeruli per histologic section compared with approximately 100 in normal mice). Although some functional redundancy is known to exist between members of the BMP family, this phenotype is not observed in other BMP knockouts. The same studies (Dudley *et al.*, 1995; Luo *et al.*, 1995) also revealed that BMP-7 function is essential for normal eye development, with BMP-7-deficient mice displaying eye defects that originate during lens induction.

Normal morphogenesis of the kidney is dependent on the specific interactions that take place between two early tissue components, known as the epithelial ureteric bud and the metanephric mesenchyme (Luo *et al.*, 1995). Further investigation of the observed kidney abnormalities in BMP-7-deficient mice revealed that the absence of

BMP-7 causes a defect in these interactions, which are associated with mesenchymal-to-epithelial transition (MET, Vukicevic *et al.*, 1996). As a consequence, the metanephric mesenchymal cells fail to differentiate and instead undergo cell death by apoptosis. Together, these findings demonstrate that BMP-7 plays a unique and critical role during kidney development, acting as a regulator of MET, an early inducer of glomeruli formation, and also a mediator of branching morphogenesis (Piscione *et al.*, 1997).

After fulfilling its indispensable role during nephrogenesis, BMP-7 expression and activity persists in the adult kidney (Zeisberg *et al.*, 2005; Wetzel *et al.*, 2006) where it continues to serve another important function: maintaining tubular homeostasis (Kopp, 2002; Kalluri and Zeisberg, 2003). It has long been known that TGF-β1 is a mediator of renal fibrosis and that its increased expression is associated with the progression of chronic renal disease (Border and Noble, 1994; Sharma *et al.*, 2000). TGF-β1 acts as the main inducer of epithelial-to-mesenchymal transition (EMT) in adult tubular epithelial cells (Zeisberg and Kalluri, 2004), which is a route by which fibroblasts may be derived (Iwano *et al.*, 2002). However, there is now evidence to suggest that BMP-7 acts as a physiological antagonist of this activity by stabilising the epithelial phenotype of tubular cells *in vivo* and *in vitro* (Simon *et al.*, 1999; Zeisberg, Hanai *et al.*, 2003; Wetzel *et al.*, 2006), and reversing TGF-β1-induced EMT (Zeisberg *et al.*, 2005).

As discussed previously, the use of BMPs in the treatment of skeletal conditions following injury or surgery is well documented (reviewed by Granjeiro *et al.*, 2005; White *et al.*, 2007). Of particular interest for the future is the therapeutic application of BMPs in the repair of other organs. Using animal models of both acute and chronic renal injury, it has been demonstrated that BMP-7 is a prime example of a BMP family member that has considerable extraskeletal regenerative potential. In these settings, the endogenous expression of BMP-7 is substantially decreased. However, studies have shown that administration of exogenous BMP-7 has a remarkable effect: enhancing the repair of tubular epithelial injury by inducing MET, and significantly improving renal function (Vukicevic *et al.*, 1998; Wang *et al.*, 2001; Morrissey *et al.*, 2002; Wang *et al.*, 2003; Zeisberg, Bottiglio *et al.*, 2003; Zeisberg, Hanai *et al.*, 2003). BMP-7 is therefore not only a key component of the mechanism that gives the adult kidney its intrinsic capacity to repair epithelial damage, but also

has the potential for use as a drug in cases where this repair mechanism has failed. Notably, at the present time it appears that recombinant BMP-7 is the only agent that is able to halt and possibly reverse fibrosis in animal models of chronic kidney disease.

1.1.6 Signaling

Members of the BMP family elicit their diverse range of signaling functions by forming complexes with various combinations of a type I activin receptor-like kinase receptor (ALKs -2 to -7) and a type II BMP or activin receptor (BMPRII; ActRIIA and ActRIIB) (reviewed by Shi and Massague, 2003; Mazerbourg and Hsueh, 2006). These structurally related dimeric receptors consist of an N-terminal extracellular ligand-binding domain, a transmembrane region, and a C-terminal intracellular serine/threonine kinase domain (Mathews and Vale, 1991; Greenwald *et al.*, 2003). Both the particular BMP ligand and the physiological context in which the complexes are formed dictate the combinations of type I and type II receptors that are engaged (Lin *et al.*, 2006; Mazerbourg and Hsueh, 2006). However, while there is some selectivity as to which receptor combinations individual BMPs will interact with, there is also evidence of promiscuity (Mazerbourg and Hsueh, 2006).

The structures of some of the BMP ligand-receptor complexes have been solved by X-ray crystallography and deposited in the RCSB PDB archive. The structures that are available at the present time include that of BMP-2 in complex with the extracellular domains of BMPRIA, also known as ALK-3 (Kirsch *et al.*, 2000) and BMP-7 in complex with the extracellular domains of ActRIIA (Figure 1.3, Greenwald *et al.*, 2003). These structural studies have revealed that the type I receptor chains interact with a number of amino acids in the wrist regions of the BMP dimers. These regions are situated close to the interfaces between the two constituent monomers, and each receptor chain can be seen to make contact with both monomers. The type II receptor chains each bind to a single BMP monomer, and interact with residues located in the knuckle regions on the convex faces of their finger-like protrusions (Figure 1.3). While the BMPs make extensive contacts with each of their individual receptors in the assembled ternary complexes, it has been shown that the extracellular

domains of the type I and type II receptors do not interact with each other (Kirsch *et al.*, 2000; Greenwald *et al.*, 2003).

Unlike the type I receptors, the serine/threonine kinase activity of the type II receptors is constitutively active (Wrana *et al.*, 1994; Attisano *et al.*, 1996). Upon binding a dimeric BMP ligand, the type II receptor trans-phosphorylates the type I receptor at a glycine- and serine-rich sequence (the GS domain) that lies just upstream of its C-terminal kinase domain (Wrana *et al.*, 1994). Once activated, the type I kinase phosphorylates and activates members of the Smad family of intracellular signal transducers, known as receptor-regulated Smad (R-Smad) proteins (Hoodless *et al.*, 1996; Liu *et al.*, 1996; Kretzschmar *et al.*, 1997; Massague and Wotton, 2000).

The R-Smad proteins are divided into two sub-sets based on their signaling specificities (Smads -1, -5 and -8; Smads -2 and -3) and each set counteracts the activities of the other (Shi and Massague, 2003). The particular type I receptor that is employed in the signaling complex determines which R-Smad protein is activated; ALKs -1, -2, -3 and -6 phosphorylate R-Smads -1, -5 and -8, whereas ALKs -4, -5 and -7 phosphorylate Smads -2 and -3 (Mazerbourg and Hsueh, 2006). Following activation, the R-Smads interact and form heteromeric complexes with Smad-4, which is a common-mediator Smad (Co-Smad) (Lagna *et al.*, 1996). These complexes translocate to the nucleus and regulate the transcription of target genes in conjunction with other nuclear transcription factors or co-activators (Chen *et al.*, 1996; Liu *et al.*, 1996; Kretzschmar *et al.*, 1997; Massague and Wotton, 2000).

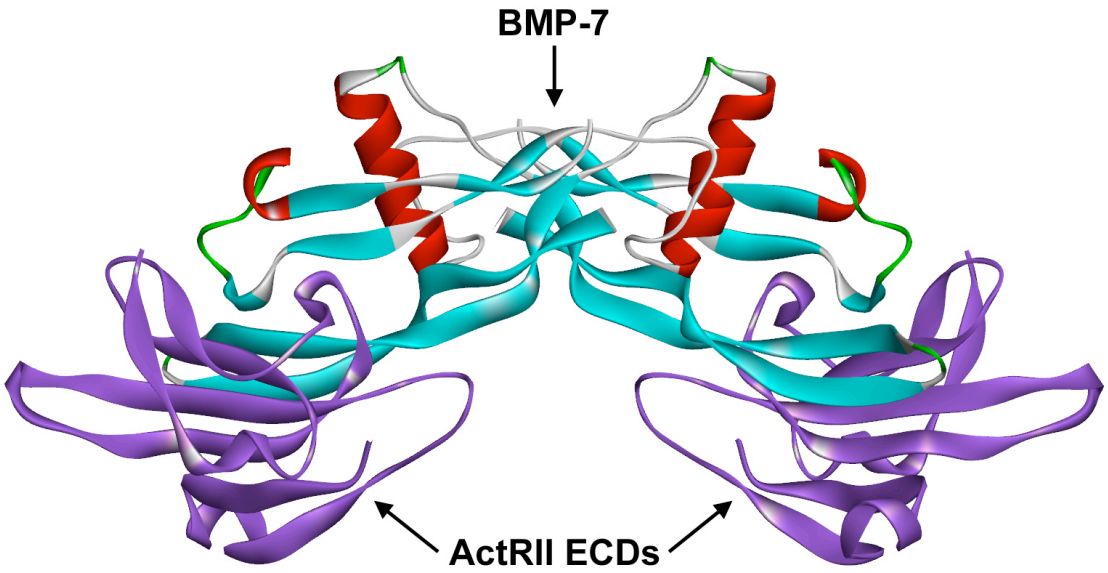

Figure 1.3 BMP-7 in complex with two ActRII extracellular domains
Each ActRII type II receptor extracellular domain (ECD, shown in purple) binds to a single BMP monomer (shown in red, turquoise and white), interacting with residues located in the knuckle and tip regions on the convex faces of their finger-like protrusions. This image was generated from the PDB file 1LX5 using the Accelrys Discovery Studio software package.

1.1.7 Regulation and localisation

There are a number of mechanisms in place to ensure that the BMPs act in a controlled manner during development and in adult tissues. Firstly, the expression of the BMPs and their individual receptors is strictly regulated both spatially and temporally. For example, the expression of GDF-9 and BMP-15 is restricted to male and female germ cells (McGrath *et al.*, 1995; Nicholls *et al.*, 2009). Secondly, several high affinity BMP antagonist proteins are known to exist, and their expression is also tightly regulated (Dionne *et al.*, 2001; Kim and Pleasure, 2003; Kusu *et al.*, 2003). The activity of a BMP within a particular tissue compartment is therefore not only dependent on its own expression and that of its receptors, but also the presence or absence of its specific antagonist(s).

Many of the BMP antagonists contain an identical or very similar cystine-knot structural motif to that found in their BMP ligands (Avsian-Kretchmer and Hsueh,

2006). They are therefore distant relatives of the TGF-β superfamily proteins and it has been suggested that the BMP ligands and such antagonists may have evolved from a common ancestor (Groppe *et al.*, 2002). An example of a cystine-knot-containing BMP antagonist protein is noggin (Smith and Harland, 1992). The X-ray crystal structure of noggin in complex with BMP-7 was the first of any of the antagonist structures to be solved (Groppe *et al.*, 2002). This structure revealed that noggin antagonises the activity of its BMP ligands by forming a clamp-like structure around them (Figure 1.4). In doing so, noggin masks both the type I and type II receptor-binding epitopes of its BMP ligands, and effectively mimics the binding mode of the heterotetrameric receptor assembly.

Another BMP antagonist protein is sclerostin (Balemans *et al.*, 2001). Interestingly, it has been reported that noggin and sclerostin are able to directly interact with high affinity and attenuate the BMP antagonistic abilities of each other (Winkler *et al.*, 2004). As a result, BMP activity is facilitated rather than being limited when these two antagonists are co-localised. This unexpected and remarkable finding adds yet another level of complexity to the way in which BMP-driven processes are finely controlled.

Finally, it has been observed that the BMPs function in a highly localised autocrine or paracrine manner (Grimsrud *et al.*, 1999; Miller *et al.*, 2000). However, after being liberated from their pro-domains by proteolytic cleavage and subsequently secreted, the mature BMP proteins are small, soluble and freely diffusible. This observation therefore raises a question as to how the distribution of these mature BMP proteins is so locally restricted. Because some of the BMPs have been found to bind to heparan sulphate (HS) and heparin (Ruppert *et al.*, 1996; Ohkawara *et al.*, 2002; Irie *et al.*, 2003; Takada *et al.*, 2003), one possible answer to this question is that the BMPs remain localised by interacting with these cell-surface and extracellular matrix glycosaminoglycans (GAGs) close to their sites of secretion.

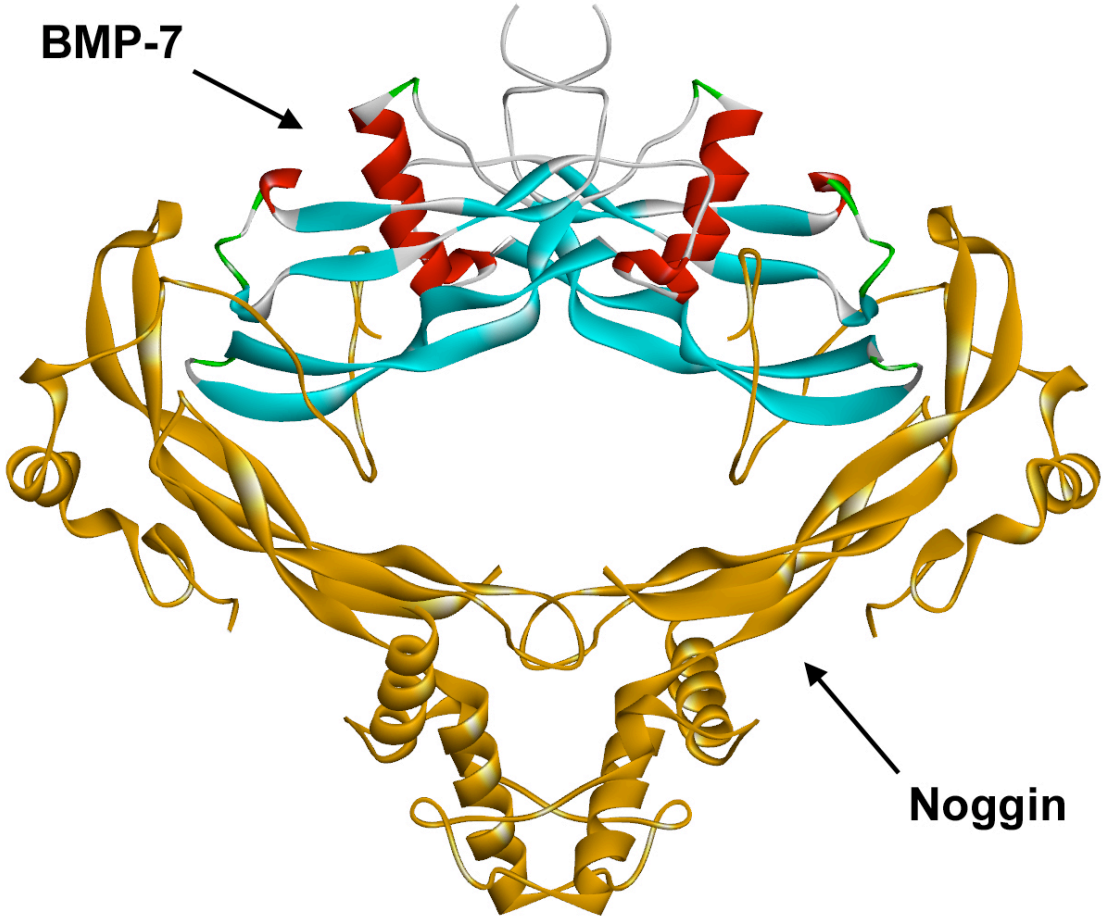

Figure 1.4 BMP-7 in complex with noggin
The X-ray crystal structure of BMP-7 (red, turquoise and white) in complex with its antagonist noggin (light brown) shows that noggin antagonises the activity of its BMP ligands by forming a clamp-like structure around them. In doing so, noggin masks both the type I and type II receptor-binding epitopes of its BMP ligands. Two short polyglycine loops (GGGGGAA) in the noggin structure, which link the clamp-like noggin dimer to two extended 'clip' segments, remain unresolved due to their flexibility (Groppe *et al.*, 2002). This image was generated from the PDB file 1M4U using the Accelrys Discovery Studio software package.

1.2 Heparan sulphate and heparin

1.2.1 What is heparan sulphate?

Heparan sulphate (HS) is a complex sulphated polysaccharide. It is produced by nearly every cell type in metazoan organisms and is found almost ubiquitously on cell surfaces and in the extracellular matrix (ECM) (Gallagher *et al.*, 1986; Esko and Selleck, 2002). HS is a member of the glycosaminoglycan (GAG) family of carbohydrates, which are long linear polysaccharides that are composed of a repeating disaccharide unit. As shown later in Figure 1.5, in HS, the disaccharide unit consists of a uronic acid residue [either β-D-glucuronic acid (GlcA), GlcA *O*-sulphated at C-2 (GlcA2S), α-L-iduronic acid (IdoA), or IdoA *O*-sulphated at C-2 (IdoA2S)] and a derivative of the amino sugar glucosamine [either *N*-acetyl-α-D-glucosamine (GlcNAc), *N*-sulphated-α-D-glucosamine (GlcNS) or unsubstituted α-D-glucosamine ($GlcNH_3$)] that is variably *O*-sulphated (comprehensively reviewed by Lindahl and Hook, 1978; Esko and Selleck, 2002).

1.2.2 Heparan sulphate biosynthesis and diversity

Unlike the synthesis of nucleic acids or proteins, the process by which HS chains are synthesised does not depend on a template macromolecule that codes for the exact sequence of building blocks in a new chain, and that is faithfully replicated to produce identical copies of that chain over and over again. Instead, the chains are generated by the concerted action of a large repertoire of biosynthetic enzymes whose presence and relative activities vary in a tissue-specific fashion (Esko and Lindahl, 2001). A brief overview of this process is provided below.

HS chains are assembled in the Golgi apparatus while attached to a proteoglycan (PG) core protein, yielding heparan sulphate proteoglycans (HSPGs) (Silbert, 1982; Stow *et al.*, 1985; Carlsson *et al.*, 2008). It is in this form that HS is found on cell surfaces and in the ECM. Proteoglycans are highly glycosylated glycoproteins that have one or more covalently attached GAG chains. A number of PG core proteins have been characterised. Amongst these proteins are the four members of the membrane-spanning syndecan family (Bernfield *et al.*, 1992), the six

members of the glycosylphosphatidylinositol (GPI)-linked glypican family (Filmus and Selleck , 2001) and the basement membrane PGs perlecan and agrin (Iozzo *et al.*, 1994; Cole and Halfter, 1996).

HS is initially synthesised as an unsulphated precursor polysaccharide known as heparan or *N*-acetylheparosan (Gallagher and Walker, 1985). The heparan chains are attached to specific serine residues at the GAG attachment sites on the core proteins via an *O*-linked tetrasaccharide linker (Esko and Zhang, 1996; Sugahara and Kitagawa, 2000). This linker is produced by the actions of various xylosyltransferase, galactosyltransferase and glucuronosyltransferase enzymes, and consists of a xylose residue, two galactose residues and a glucuronic acid residue (Ser-Xyl-Gal-Gal-GlcA) (Kitagawa *et al.*, 1998; Almeida *et al.*, 1999; Okajima *et al.*, 1999; Wei *et al.*, 1999; Gotting *et al.*, 2000; Bai *et al.*, 2001). Following the formation of the linker, a GlcNAc residue is added (Fritz *et al.*, 1994) and the heparan chains are elongated by the stepwise addition of alternating GlcA and GlcNAc residues to a final length that is generally between 40 and 160 disaccharides (Esko and Selleck, 2002). This chain polymerisation process depends on the actions of specific glycosyltransferase enzymes, which are members of the exostosin (EXT) family of tumour suppressors (McCormick *et al.*, 2000; Senay *et al.*, 2000; Kim *et al.*, 2001).

While the heparan chains are still undergoing chain extension, the incorporated disaccharide units are subjected to a sequential series of complex modification reactions. Firstly, the *N*-acetyl groups of GlcNAc residues may be replaced with *N*-sulphate groups (forming GlcNS) by dual-function *N*-acetylglucosamine *N*-deacetylase/*N*-sulfotransferase (NDST) enzymes (Brandan and Hirschberg, 1988; Hashimoto *et al.*, 1992; Wei *et al.*, 1993; Aikawa *et al.*, 2001). This modification not only marks the beginning of the transformation of heparan to HS, but also gives rise to the basic domain structure of HS (described in section 1.2.3 below). Secondly, glucuronic acid (GlcA) residues that are situated immediately adjacent to the reducing side of GlcNS moieties may be converted into iduronic acid (IdoA) (Jacobsson *et al.*, 1984). This epimerisation reaction is catalysed by the glucuronyl C5-epimerase enzyme (Malmstrom *et al.*, 1980; Campbell *et al.*, 1994). Thirdly, IdoA residues, and occasionally GlcA residues (Bienkowski and Conrad, 1985; Fedarko and Conrad, 1986), may be modified by sulphation at their C-2 position by heparan sulphate 2-*O*-sulphotransferase (HS2ST), producing IdoA2S and GlcA2S (Bai and Esko, 1996;

Kobayashi *et al.*, 1996; Kobayashi *et al.*, 1997). Finally, the disaccharides may also be sulphated at the C-6 position of the glucosamine residue by a heparan sulphate 6-*O*-sulphotransferase (HS6ST) variant (Habuchi *et al.*, 1995, 1998, 2000), and more rarely at the C-3 position of glucosamine by an isoform of heparan sulphate 3-*O*-sulphotransferase (HS3ST) (Liu *et al.*, 1996; Shworak *et al.*, 1997, 1999).

A fundamentally important point here is that the modifications described above are by no means comprehensive as the reactions do not go to completion (Lindahl and Hook, 1978; Kusche and Lindahl, 1990). Therefore, the extent to which individual disaccharide units within a HS chain are modified by any of the aforementioned enzymes is highly variable, and means that the disaccharides can be found in a number of partially modified states. As a result, HS chains exhibit a high degree of microsequence diversity. Overall, as many as 48 disaccharide combinations could potentially occur, but only 23 have been identified in nature to date (Figure 1.5, Esko and Selleck, 2002). It is thought that restrictions on the biosynthetic process may account for the absence of the remaining 25 theoretical combinations (Esko and Selleck, 2002). These restrictions include the substrate specificities of the biosynthetic enzymes and their differing spatial and temporal expression patterns (Esko and Lindahl, 2001). Also, all of the enzymes that play a part in HS GAG synthesis [with the exception of one intraluminal HS3ST isoenzyme (Shworak *et al.*, 1997)] are type II membrane proteins, which span the membranes of the Golgi apparatus (Pinhal *et al.*, 2001). This physical arrangement of the enzymes within the Golgi apparatus restricts their interactions to two dimensions within a lipid lattice.

Figure 1.5 Disaccharide subunits of HS/heparin
The 23 disaccharide units that have been identified in nature to date in HS/heparin. β-D-GlcA-containing disaccharides are shown on the left, and those containing α-L-IdoA are shown on the right. The C-4 hydroxyl groups of the uronic acid residues are not shown due to them normally being linked to C-1 of a derivative of α-D-glucosamine in the preceding disaccharide unit. X = H or SO_3^-. [Image taken from Esko and Selleck (2002)].

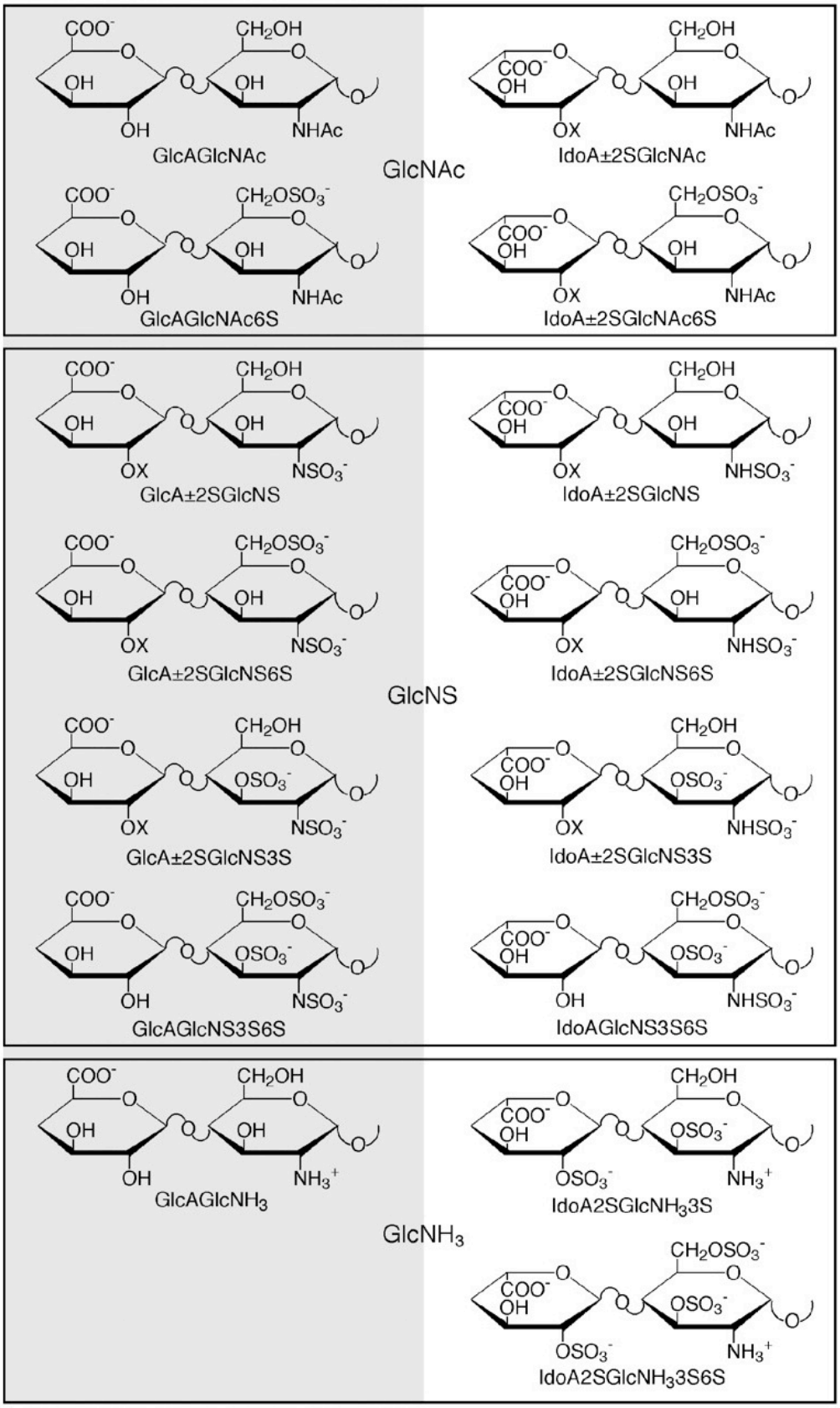

Figure 1.5 Disaccharide subunits of HS/heparin
Please refer to the figure legend on the opposite page.

1.2.3 Heparan sulphate domains

Typical HS chains contain relatively short but regularly spaced regions of high sulphation [known as *N*-sulphated (NS)- or S-domains] that are separated by longer regions of low modification [known as *N*-acetylated (NA)- or N-domains]. These N- and S-domains are linked by transition zones (T-zones), or NA/NS-domains (Turnbull and Gallagher, 1991; Murphy *et al.*, 2004), which are regions that contain a mixture of *N*-acetylated and *N*-sulphated disaccharide units. A simple representation of this domain structure is shown in Figure 1.6. In most variants of HS, the S-domains are between 2-9 disaccharide units in length and the stretches of unmodified and partly modified sequence that separate them average 16-18 disaccharide units in length (Lyon and Gallagher, 1998). In highly sulphated HS chains, the S-domains are longer and situated closer together than those that are found in chains containing lower levels of sulphate modification (Lyon *et al.*, 1994; Maccarana *et al.*, 1996; Lyon and Gallagher, 1998).

The combination of the variability in its domain organisation and the diversity of its disaccharide units results in HS being a highly structurally heterogenous GAG. Despite this heterogeneity, the existence of such well-ordered domain patterns suggests that the modification of heparan chains takes place in a manner that is at least partially organised rather than occurring randomly (Lindahl *et al.*, 1998).

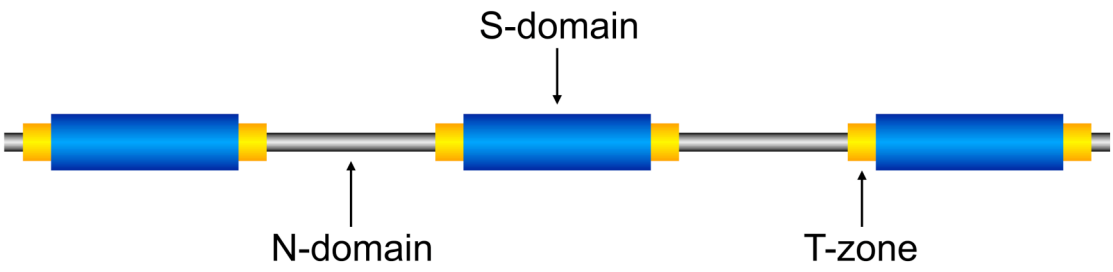

Figure 1.6 HS domain structure
HS chains contain regularly spaced regions of high sulphation (S-domains, blue) that are separated by regions of low sulphate modification (N-domains, silver). These N- and S-domains are linked by transition zones (T-zones, orange), which are regions that contain a mixture of *N*-acetylated and *N*-sulphated disaccharide units. This diagram is based on that presented by Murphy *et al.*, 2004.

1.2.4 Heparin

Heparin is a highly sulphated relative of HS that is primarily found in the granules of mast cells (Lindahl and Hook, 1978). Heparin chains are mainly composed of trisulphated IdoA2S-GlcNS6S disaccharide units (Dietrich *et al.*, 1973; Silva and Dietrich, 1975 and references within). This repeating unit is structurally similar to those found within the S-domains of HS chains, albeit with an even higher degree of sulphation. It can therefore be said that heparin chains resemble extensively modified, extended HS S-domains (Kreuger *et al.*, 2006). Because heparin is so rich in sulphate and carboxyl groups, it has the highest negative charge density of any known biological macromolecule (Salmivirta *et al.*, 1996).

The solution conformation of the main repeating structure that is found within heparin chains was characterised by Mulloy *et al.* (1993) using a combination of nuclear magnetic resonance (NMR) spectroscopy and molecular modelling techniques. This study demonstrated that heparin chains have a right-handed helical structure and that each turn of the helix contains approximately four residues. The sulphate groups of heparin chains are positioned in clusters on opposite faces of the helix in an offset manner (Figure 1.7), and with a periodicity of approximately 17 Å (1 Å = 0.1 nm). A consequence of the high density of negatively charged groups that are found along heparin chains is that intra-chain like-charge repulsions occur between them. Because of this, and due to the fact that heparin chains exhibit limited rotation about their glycosidic linkages (Mulloy *et al.*, 1994), the heparin helix is relatively rigid and straight, although a slight curve in the helical axis is apparent. In addition, the heparin helix is quite bulky due to its relatively large hydrodynamic volume. Because the S-domains of HS chains closely resemble heparin, it is likely that they also adopt a heparin-like structure. However, the unsulphated N-domains of HS differ in that they are more flexible and allow for some bending of the chains (Mobli *et al.*, 2008).

In typical heparin chains prepared from different sources, it has been demonstrated that between 70 % and 100 % of the GlcA moieties are converted to IdoA (Hook *et al.*, 1974; Rosenberg *et al.*, 1978; Sudo *et al.*, 2001). These IdoA residues (and their 2-*O*-sulphated IdoA2S counterparts) exhibit a remarkable conformational plasticity that is not found in GlcA residues. While the pyranose rings

of GlcA residues are stable in the $^4C_1$ chair conformation, those found in the IdoA residues of heparin chains (and presumably in the S-domains of HS chains) exist in a dynamic equilibrium between two solution conformations. These are the $^1C_4$ chair conformation and the $^2S_0$ skew-boat conformation (Ferro *et al.*, 1990). It can be seen in Figure 1.7 that this interconversion causes very little disturbance to the glycosidic linkages of neighbouring residues, and therefore the overall shape of the polysaccharide chain is not greatly affected (Mulloy *et al.*, 1993). However, it does add another level of variability and complexity to what are already structurally diverse biopolymers.

Heparin is widely utilised therapeutically as an anticoagulant and it is readily commercially available. Due to its resemblance to the S-domains of HS, and the ease with which it can be obtained in good quantities, heparin is often used as a model compound in both theoretical and experimental studies of interactions that would generally involve HS in a physiological context.

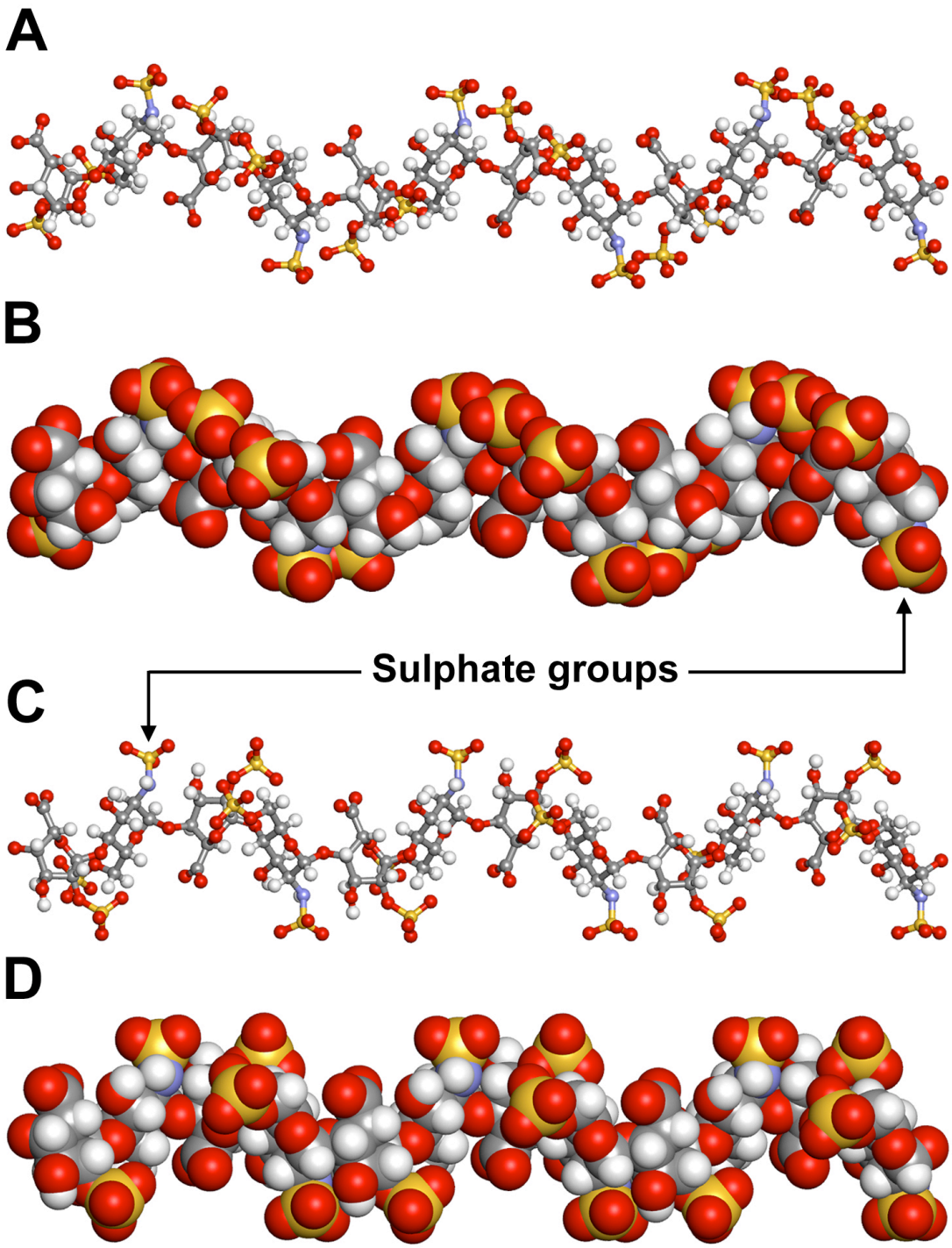

Figure 1.7 Heparin structure
Ball and stick (A and C) and space fill (B and D) representations of heparin dodecasaccharide NMR structures, in which all of the IdoA2S residues are in either the $^{1}C_{4}$ (A and B) or $^{2}S_{0}$ (C and D) conformations. It can be seen that heparin adopts a helical conformation and that its sulphate groups (sulphur atoms coloured yellow and oxygen atoms coloured red) are distributed along opposite faces of the helix in an offset manner. The images shown were generated from the PDB file 1HPN using the Accelrys Discovery Studio software package.

1.3 Heparan sulphate/heparin-protein interactions

1.3.1 Nature of the interactions

It is well documented that HS and heparin GAG chains have the ability to interact with a number of different proteins (Esko and Selleck, 2002). Such HS/heparin-protein binding interactions primarily utilise the most prominent feature of these GAG chains: their abundant sulphate groups. These highly acidic, negatively charged groups partake in ionic interactions with the side chains of positively charged, basic amino acid residues (arginine, lysine, and to a lesser extent, histidine) (Hileman *et al.*, 1998). As has already been established, the helices of heparin chains and the S-domains of HS chains are relatively bulky and rigid (Mulloy *et al.*, 1993). They are therefore unable to access crevices or pockets within protein structures. Consequently, for an interaction to occur, the basic side chains must be exposed prominently on the surface of the protein. They must also be suitably spaced and oriented to match the pattern of sulphate groups along the HS/heparin chain.

Because sulphate groups are present on opposite sides of the helices of heparin chains and the S-domains of HS chains, these structures have two faces that proteins can potentially bind to (Mulloy *et al.*, 1993). This may permit large protein complexes to form on relatively short polysaccharide sequence elements, as is the case in the X-ray crystal structure of two fibroblast growth factor-1 (FGF-1) ligands in complex with a heparin decasaccharide and two FGF receptor-2 (FGFR-2) ectodomains (Pellegrini *et al.*, 2000).

While it is clear that ionic bonds, which connect the sulphate groups of HS/heparin chains and the exposed basic side chains on protein surfaces, play an important part in HS/heparin-protein interactions, it should be noted that they are not the only contributors. In the case of the interaction between basic FGF (also known as bFGF or FGF-2) and heparin, Thompson *et al.* (1994) have demonstrated that a combination of hydrogen bonding, van der Waals forces and hydrophobic effects predominate, and that pure electrostatic interactions contribute only 30 % of the binding free energy.

1.3.2 HS/heparin-binding sites on protein surfaces

HS/heparin-binding sites on protein surfaces generally consist of a number of basic residues (typically 4-7) that are not interrupted by the presence of residues containing acidic side chains (Hileman *et al.*, 1998). These basic residues may form a single patch of positive charge or be arranged in a linear fashion along a face of the protein or one of its component structural elements, such as an α-helix. Where the former is true, the positively charged patch may be present either as a result of the basic residues being located in close proximity in the primary protein sequence, or due to them having been brought together as a result of folding in the three-dimensional tertiary structure of the protein (Hileman *et al.*, 1998 and references within).

For linear arrays of basic residues, it is particularly important that the side chains are in positions that are easily accessible to the sulphates of the GAG chain, and that the path of the chain across them is free from any obstruction. This is because heparin chains and the S-domains of HS chains are relatively straight and rigid, as explained earlier (section 1.2.4). They are therefore unable to bend into crevices or around obstacles such as protein surface protrusions, carbohydrate chains that are attached to the glycosylation sites of glycoproteins, or even acidic side chains. They are also unable to flex sufficiently to wrap around protein surfaces to accommodate interactions with basic residues that are situated on different sides of the structures.

While the S-domains of HS chains are relatively rigid, it was mentioned previously (section 1.2.4) that the unsulphated N-domains of HS GAGs offer these chains more flexibility and allow for some bending to occur. As noted by Gallagher (2001), it has been suggested that the flexibility of these *N*-acetyl-rich 'spacer' regions assists the simultaneous interaction of two S-domains within a single HS chain with dimeric proteins that possess a separate binding site on each of their subunits. Examples of proteins for which this is suggested to be the case include TGF-β (Lyon *et al.*, 1997), interferon gamma (IFN-γ; Lortat-Jacob *et al.*, 1995) and interleukin 8 (IL-8; Spillmann *et al.*, 1998). It has also been proposed that the flexibility of these *N*-acetylated regions permits two spaced S-domains on the same HS/heparin chain to simultaneously interact with two HS/heparin-binding sites that are situated on opposite faces of the platelet factor 4 (PF4) protein (Stringer and Gallagher, 1997).

1.3.3 Specificity of HS/heparin-protein interactions

Because heparin chains and the S-domains of HS chains are so negatively charged, one could assume that the interactions that take place between these GAGs and the exposed positively charged residues on protein surfaces occur simply as a result of structurally non-specific electrostatic encounters. While it is possible that this may be true in some instances, it is certainly not always the case. Indeed, for some proteins, high-affinity binding to HS/heparin GAGs is dependent on the presence of very specific saccharide sequences/structures within the chains. An example of such a protein is antithrombin III (ATIII), which requires a specific pentasaccharide that contains a central (and rare) 3-*O*-sulphate modification (Choay *et al.*, 1983; Lindahl *et al.*, 1984).

There are also proteins that do not stringently require the presence of a unique saccharide sequence in order to bind to HS/heparin but clearly do not interact with these GAGs in a non-specific manner. Instead, the binding of these proteins to HS/heparin chains is dependent on the occurrence of a limited set of specific structural features/modifications. For example, the minimum requirement for the interaction of FGF-2 with HS/heparin is a pentasaccharide sequence in which the glucosamine moieties are *N*-sulphated and at least one of the uronic acid entities is a 2-*O*-sulphated IdoA residue (Kreuger *et al.*, 2001 and references within). Based on these findings and those from other similar studies it is apparent that the degree of structural specificity varies considerably from one HS/heparin-protein interaction to another. Therefore, the minimal GAG sequences/modifications that different proteins require to be present for them to bind to HS/heparin chains needs to be determined on an individual basis.

1.3.4 Biological consequences of HS/heparin-protein interactions

The binding of a protein to HS/heparin GAG chains may serve a number of potential purposes. Firstly, such an interaction may protect a protein from proteolytic degradation. A fine example of a protein for which this is true is IFN-γ. Studies have shown that the carboxyl-terminal domain of IFN-γ is particularly susceptible to extensive proteolytic cleavage, and that this process results in the protein being

rapidly inactivated (Lortat-Jacob *et al.*, 1996). However, it has also been revealed that IFN-γ is able to bind to HS/heparin with high affinity through sequences within the same carboxyl-terminal domain (Lortat-Jacob *et al.*, 1991; Lortat-Jacob and Grimaud, 1992). Further investigation of these interactions has demonstrated that the binding of IFN-γ to HS/heparin serves to limit the extent to which the carboxyl-terminal domain of IFN-γ is degraded, which in turn results in a substantial increase in IFN-γ activity by as much as six-fold due to its prolonged circulatory half-life (Lortat-Jacob *et al.*, 1996).

Secondly, the interaction of a protein with HS/heparin GAGs may serve to restrict its diffusion following secretion. This is a particularly important function in the case of some small, soluble cytokines that would normally be readily diffusible but have a role that requires their distribution to be tightly controlled. A good example of such a protein is decapentaplegic (Dpp), the *Drosophila* morphogen that has close homology with BMPs -2 and -4. During development of the *Drosophila* wing, Dpp is produced by a stripe of cells along the anterior-posterior (A-P) compartment boundary (Posakony *et al.*, 1990; Capdevila and Guerrero, 1994). Following secretion, Dpp forms an extracellular concentration and activity gradient, which is required for it to direct the anteroposterior patterning of the wing in a concentration-dependent manner (Belenkaya *et al.*, 2004 and references within). Belenkaya *et al.* (2004) have provided evidence to support the idea that both the formation and maintenance of this gradient is dependent on the interaction of Dpp with dally and dally-like (dly), which are two *Drosophila* homologues of the glypican family of HS proteoglycans. They propose that Dpp moves across the cell surfaces by a process of restricted extracellular diffusion involving these glypican homologues.

Thirdly, HS/heparin GAGs may act as catalysts of protein-protein interactions. A notable example of an instance in which HS/heparin oligosaccharides serve such a purpose is during the binding of the serine protease inhibitor antithrombin III to factor Xa, which is an interaction that plays a key part in helping to maintain normal blood flow by inhibiting the coagulation cascade (Chuang *et al.*, 2001 and references within). Although antithrombin III circulates at a high concentration, it only becomes capable of efficiently antagonising the coagulating activity of factor Xa upon binding with high affinity to HS/heparin GAG chains that contain a specific pentasaccharide sequence (Choay *et al.*, 1983; Lindahl *et al.*, 1984). It has been demonstrated that

HS/heparin promotes this inhibition by inducing a conformational change in the structure of antithrombin III (Olson *et al.*, 1981; Gettins *et al.*, 1993). HS/heparin GAGs have also been shown to greatly enhance the rate at which antithrombin III inhibits the coagulating activity of thrombin by forming ternary complexes with these two proteins (Danielsson *et al.*, 1986; Li *et al.*, 2004). After promoting the initial encounter that takes place between antithrombin III and thrombin, the HS/heparin GAGs dissociate before the tightly bound inhibitor-protease complexes are rapidly cleared from circulation (Bourin and Lindahl, 1993; Kounnas *et al.*, 1996).

A different example of HS/heparin promoting protein-protein interactions arises from X-ray crystallographic studies that have been carried out on FGF-FGFR-heparin complexes (where FGF is fibroblast growth factor and FGFR is FGF receptor). These studies have provided evidence to suggest that HS/heparin chains assist with the assembly and/or stabilisation of FGF-FGFR signaling complexes. In the X-ray crystal structure of a 2:2:1 FGF-1-FGFR-2-heparin complex (Pellegrini *et al.*, 2000), one heparin decasaccharide links two FGF-1 ligands, each of which is bound to a FGFR-2 ectodomain. The FGF-1 ligands are shown to bind to opposite sides of the heparin oligosaccharide, highlighting the importance of the two-sided arrangement of the sulphate groups along the chain. While the heparin oligosaccharide can be seen to interact with both FGF-1 ligands, it only comes into contact with one of the FGFR-2 ectodomains due to its asymmetric arrangement within the core of the complex. Because there is little protein-protein interface between the two halves of the FGF-1-FGFR-2-heparin complex, Pellegrini *et al.* (2000) propose that the heparin oligosaccharide plays a critical role in FGF receptor dimerisation.

By carrying out high-resolution size-exclusion chromatography (SEC) studies on FGF-1-FGFR-2-heparin complexes in solution, Robinson *et al.* (2005) have shed some light on a potential mode of assembly for the structure resolved by Pellegrini *et al.* (2000). The findings of Robinson *et al.* (2005) suggest that the first step in the assembly process involves the cooperative binding of two FGF-1 molecules to a single heparin oligosaccharide to produce a FGF-1 dimer. Based on the X-ray crystal structure displayed in Pellegrini *et al.* (2000), it is likely that this FGF-1 dimer lacks any inter-molecule protein-protein contacts. Once dimerised, FGF-1 recruits two FGFR-2 ectodomains to form a stable signaling complex. In the absence of heparin, Robinson *et al.* (2005) demonstrated that FGF-1 had no detectable affinity for FGFR-

2. This may indicate that in addition to its role in dimerising FGF-1, heparin also induces a conformational change in FGF-1 that increases its affinity for FGFR-2 (Gallagher, 2006). From these studies, it appears that heparin-protein interactions play a critical role in dictating both the mode of assembly and overall arrangement of the FGF-1-FGFR-2-heparin signaling complex. It may therefore be said that HS/heparin GAGs have a co-receptor function in this context.

In an alternative X-ray crystallographic study, Schlessinger *et al.* (2000) resolved the structure of a 2:2:2 FGF-2-FGFR-1-heparin complex. This complex is symmetrical and consists of two identical 1:1:1 FGF-2-FGFR-1-heparin units. The two heparin decasaccharides are arranged non-reducing end to non-reducing end in a basic canyon that is situated at the membrane-distal end of the structure. Schlessinger *et al.* (2000) demonstrated that the heparin decasaccharides make numerous contacts with both FGF-2 and FGFR-1 within each 1:1:1 FGF-2-FGFR-1-heparin unit, and therefore augment the ligand-receptor interactions. They also showed that each heparin decasaccharide interacts with the FGFR-1 component of the adjoining 1:1:1 FGF-2-FGFR-1-heparin unit to promote FGFR-1 dimerisation. However, in contrast to the structure published by Pellegrini *et al.* (2000), the two halves of the Schlessinger structure are held together by a number of protein-protein contacts. It therefore appears that the heparin oligosaccharides play a part in stabilising the complex rather than dictating its arrangement or mode of assembly.

In the time since the two X-ray crystal structures described above were published (Pellegrini *et al.*, 2000; Schlessinger *et al.*, 2000), there has been much debate over which of them best represents the physiological FGF-FGFR-HS/heparin signaling complex. Although a considerable amount of time and effort has been invested in resolving this matter, there is still not a conclusive answer. Even so, it is clear that heparin-related GAGs play an important part in the FGF signaling process.

While the heparin-binding properties of a number of proteins have been well studied (including those discussed above), there are other proteins that have been shown to bind to HS/heparin but have received much less attention in this context. The role of HS/heparin-binding for these proteins therefore remains unclear. A large and interesting family of proteins for which this is particularly true is the BMPs.

1.4 HS/heparin-binding in the BMP family

The first indication that members of the BMP family may have HS/heparin-binding abilities came from the demonstration that both osteogenin (BMP-3) and BMP-2 bound to the heparin-affinity chromatography columns that were employed for their purification from demineralised bone matrix preparations (Sampath *et al.*, 1987; Wang *et al.*, 1990). Since this time, the heparin-binding properties of the BMPs have been investigated a little further, with a particular focus on the Dpp-type BMPs (BMPs -2 and -4). By conducting a series of biosensor experiments at physiological pH and salt concentration, Ruppert *et al.* (1996) confirmed the heparin-binding ability of recombinant BMP-2, showing that it binds to immobilised heparin chains (M_r of around 16,000) with a dissociation constant (K_d) of approximately 20 nM. Using an embryonic chicken limb bud cell system, Ruppert *et al.* (1996) also showed that the addition of exogenous heparin potentiated the activity of recombinant BMP-2 in a dose dependent manner.

Upon examining the effect that heparin and HS polysaccharides have on the activity of the BMPs in C2C12 mouse myoblast cells, Takada *et al.* (2003) reported similar findings to Ruppert *et al.* (1996). As discussed previously in section 1.1.5, the stimulation of C2C12 myoblast cells with BMPs causes them to transdifferentiate and begin to express osteoblastic markers such as alkaline phosphatase (Katagiri *et al.*, 1994). This is therefore an excellent *in vitro* cellular model system for the well-established *in vivo* activity of the BMPs, due to the fact that injection or implantation of BMPs into muscle results in the initiation of new bone formation (Urist, 1965). Takada *et al.* (2003) demonstrated that the addition of exogenous heparin dose-dependently potentiates the transdifferentiation of C2C12 cells when stimulated with BMPs -2 or -4. The same potentiating effect, albeit weaker, was observed when HS was used in place of heparin. However, chemically desulphated derivatives of heparin were shown to have lost their stimulatory capacity.

While the studies described above have provided evidence to support the idea that HS/heparin GAGs are able to bind to the Dpp-type BMP family members and enhance their biological activity, the exact role that these sulphated GAGs play in BMP-mediated processes *in vivo* remains unclear. To date, the best insight into the potential function of HS/heparin GAGs in these processes comes from the study of

Drosophila Dpp itself. As explained in more detail in section 1.3.4, the correct patterning of the *Drosophila* wing requires the establishment of an extracellular Dpp concentration and activity gradient. Belenkaya *et al.* (2004) demonstrated that the formation and maintenance of this gradient occurs via a process of restricted extracellular diffusion, which is dependent on the interaction of Dpp with two *Drosophila* homologues of the mammalian glypican family of HS proteoglycans (dally and dly). Due to the high degree of homology between Dpp and BMPs -2 and -4, it is possible that the patterning of vertebrate limbs and tissues by the Dpp-type BMPs is directed by a similar HS/heparin-dependent mechanism to that in *Drosophila*. Some early evidence to support this theory and suggest that the binding of the Dpp-type BMPs to HS/heparin may serve to restrict their diffusion *in vivo* can be found in a study published by Ohkawara *et al.* (2002). Ohkawara and colleagues demonstrated that in *Xenopus* embryos, a non-heparin-binding mutant of *Xenopus* BMP-4 exhibited a long-range signaling activity rather than the short-range action that was observed for the wildtype *Xenopus* BMP-4 protein.

Although the HS/heparin-binding properties of the Gbb-type BMPs (BMPs -5 to -8) have been little studied, work conducted in both our own laboratory (unpublished data) and that of Irie *et al.* (2003) has demonstrated that BMP-7 also has the ability to bind to HS/heparin GAGs. In addition to this, using rat osteosarcoma (ROS) 17/2.8 osteoblast-like cells, Irie *et al.* (2003) showed that the stripping of cell-surface HS by digestion with heparitinase markedly reduced the phosphorylation of the R-Smads (Smads -1, -5 and -8) in response to BMP-7 stimulation. They also found that inhibiting the sulphation of cell-surface HS chains by growing the cells in the presence of chlorate resulted in the same outcome, as did adding exogenous heparin to the cell culture media. The same pattern of results was obtained when a similar study was carried out in our own laboratory using mouse C2C12 myoblast cells (unpublished data). Together, these studies suggest that cell-surface HS chains also play an important part in BMP-7-mediated cellular processes, although their function is once again unclear. Because the Gbb-type BMPs share close homology with each other, it is likely that HS also plays a part in the cellular processes that take place under the direction of BMPs -5, -6 and -8.

Interestingly, in the functional studies described above, the addition of exogenous heparin to the cell culture media had the opposite effect on BMP-7 activity

to the effect it had on the activities of the Dpp-type BMPs at similar concentrations of GAG. In the cases of the Dpp-type BMPs, exogenous heparin potentiated their activity (Ruppert *et al.*, 1996; Takada *et al.*, 2003) whereas it was reported to decrease the activity of BMP-7 (Irie *et al.*, 2003). This finding opens up the possibility that the function of heparin-related GAGs in BMP-mediated processes may differ from one BMP sub-group to another.

Despite the present uncertainty surrounding the functional role that HS/heparin GAGs play in BMP-mediated processes, one thing that is now clear are the locations of the key HS/heparin-binding residues of BMPs -2 and -4. As shown in Figure 1.8, it has been demonstrated that these Dpp-type BMPs (and Dpp itself) bind to HS/heparin polysaccharides via a small cluster of basic arginine and lysine residues in their short N-terminal extensions, situated immediately upstream of the first of seven conserved cysteine residues that form their cystine-knot domains (Ruppert *et al.*, 1996; Ohkawara *et al.*, 2002; Akiyama *et al.*, 2008). Because the BMPs are homodimeric proteins, BMPs -2 and -4 both possess two of these key basic residue clusters, one on each monomer. As a result, these proteins may either contain two independent HS/heparin-binding sites, or the clusters on each of the constituent monomers may cooperate to bind a single sulphated GAG chain between them. However, at the present time it is not yet understood which of these two binding site configurations is adopted by BMPs -2 and -4.

It was mentioned briefly in section 1.1.2 that the most obvious difference between the Dpp-type and Gbb-type BMPs is in the length of their N-terminal extensions. At 36-37 residues in length, the N-terminal sequences of the Gbb-type BMPs are considerably longer than the 13-15 residue sequences that are found in their Dpp-type counterparts (Figure 1.8). However, an inspection of their protein sequences reveals that the distribution of basic residues also differs between the Dpp-type and Gbb-type BMPs (Figure 1.8). One notable difference is that unlike the Dpp-type BMPs, the Gbb-type BMPs exhibit an almost complete absence of basic amino acids in the region of their N-terminal extensions that lies immediately upstream of their first cysteine residue. As outlined above, the presence of a group of basic amino acids within this region of the protein has been shown to be an important requirement in order for HS/heparin-binding to take place in the cases of the Dpp-type BMPs. Regardless of the fact that BMP-7 is missing a number of key basic residues from this

particular section of its N-terminal extension, the aforementioned findings from the studies that were carried out in our own laboratory (unpublished data) and that of Irie *et al.* (2003) clearly show that it has the ability to interact with HS/heparin GAGs. This collection of observations and experimental findings therefore raises the question as to where the HS/heparin-binding site of BMP-7 is situated.

Figure 1.8 BMP N- and C-terminal sequences
A comparison of the N- and C-terminal mature protein sequences of human BMP-2, *Xenopus* BMP-4 and human BMP-7. It can be seen that BMP-7, a gbb-type BMP, has a considerably longer N-terminal extension than the dpp-type BMPs (BMPs -2 and -4). It is also apparent that the distribution of basic arginine and lysine residues differs between these two BMP sub-groups. Arginine and lysine residues that have been experimentally shown to play an important part in HS/heparin-binding in human BMP-2 and *Xenopus* BMP-4 are highlighted in red. Other arginine and lysine residues are highlighted in blue, and the conserved cysteine residues that form the cystine-knot are highlighted in yellow and numbered. The three basic residue clusters of BMP-7 are labeled accordingly.

Figure 1.8 BMP N- and C-terminal sequences
Please refer to the figure legend on the opposite page.

The mature human BMP-7 protein possesses a total of fifteen arginine and lysine residues. All but one of these basic residues lies within three short stretches of its amino acid sequence (Figure 1.8). The first stretch contains a cluster of six basic residues and can be found close to the beginning of the long N-terminal extension of BMP-7, upstream of the section of sequence that contains the key heparin-binding residues in BMPs -2 and -4. The second stretch contains a cluster of four basic residues and encompasses the region of sequence immediately upstream and downstream of the first cysteine residue. The third and final stretch contains a tight cluster of four basic residues and is located at the opposite end of the BMP-7 protein, in close proximity to its C-terminus. As can be seen in Figure 1.8, this C-terminal stretch of sequence is another example of a region in which the distribution of basic amino acids differs between BMP-7 and BMPs -2 and -4. Not only does BMP-7 contain an additional basic residue within this region, but the four basic residues it contains are also clustered tighter together. Like the other two clusters of basic residues described here, this C-terminal basic cluster is conserved throughout the Gbb-type BMP family. To date, there is no evidence to suggest that basic residues in the C-terminal ends of BMPs -2 and -4 are involved in the interaction of these proteins with HS/heparin. However, because both the number and arrangement of the basic residues within this region differs between the Dpp-type and Gbb-type BMPs, one cannot rule out the possibility that C-terminal arginine and lysine residues may play a part in the binding of BMP-7 to these sulphated GAGs.

Because the BMP-7 protein contains three basic residue clusters, there are a number of potential ways in which it may interact with HS/heparin GAGs. Firstly, any of the basic residue clusters described above could form a binding site on their own. Secondly, basic residues from different clusters on the same monomer may cooperate to form a binding site. Thirdly, basic residues from clusters in the same or different position on different covalently-linked monomers may cooperate to form a binding site. Due to the fact that these three options could potentially give rise to a multitude of different types of binding site, it is not possible to determine where the HS/heparin-binding site of BMP-7 is situated based only on primary sequence data or an inspection of the published BMP-7 X-ray crystal structures. Therefore, further investigation is required in order to resolve this matter, which brings us to the aim of this study.

1.5 Aim

The aim of this study is to determine the location of the HS/heparin-binding site of human BMP-7. To accomplish this goal, the locations of the key HS/heparin-binding residues will first be predicted by carrying out a series of computational molecular docking calculations using published BMP-7 and heparin structures. Based on the results that are obtained from these docking calculations, site-directed mutagenesis techniques will be employed to produce mutant BMP-7 DNA expression constructs in which the predicted key basic residues will be substituted for alanine residues. These DNA constructs will subsequently be transfected into cultured cells to express mutant BMP-7 proteins. Once expressed, the heparin-binding abilities of these mutant proteins will be determined by subjecting them to heparin-affinity chromatography. Mutants that are found to lack the ability to bind to heparin, or whose heparin-binding affinity has been markedly reduced compared to that of the wildtype protein, will indicate the location of the HS/heparin-binding site of BMP-7.

Comparison of the location of the HS/heparin-binding site of BMP-7 with that of BMPs -2 and -4 will provide insight into the extent to which members of the Gbb- and Dpp-type BMP sub-groups of this structurally homologous protein family differ in the way that they interact with HS/heparin. Moreover, any muteins that exhibit either a complete absence of or a marked reduction in heparin-binding affinity will be ideal for use in future functional studies to investigate the role that HS/heparin-binding plays in BMP mediated processes. With recombinant BMP-7 already being licensed for clinical use for the treatment of skeletal damage/loss, and with further potential clinical applications, such studies may provide information that could help to determine whether or not heparin mimetics would be a useful ancillary in therapeutic products containing recombinant BMP-7. These studies might also help to determine whether heparin mimetics could be utilised to create an optimal extracellular environment for endogenous BMP-7 to function, thereby potentially avoiding the necessity to use exogenous BMP-7.

Chapter 2: Materials and methods

2.1 Molecular docking studies

Molecular docking studies were carried out according to the method described in Forster and Mulloy (2006) and Mulloy and Forster (2008). A brief outline of this method can be found below, with a more detailed account being provided in section 3.2.1.

Coordinates for the experimentally determined protein and oligosaccharide structures were derived from PDB files deposited in the Research Collaboratory for Structural Bioinformatics (RCSB) Protein Data Bank (PDB) archive (http://www.rcsb.org/pdb). The structural coordinates for the human BMP-7 protein monomer and dimer were taken from the files 1LXI (Greenwald *et al.*, 2003) and 1M4U (Groppe *et al.*, 2002) respectively. Three heparin oligosaccharide ligands were used, one of which was an endecasaccharide [(GlcNS6S-IdoA2S)$_5$-GlcNS6S] whilst the other two were pentasaccharides. As explained in section 3.2.1, the two iduronate residues in one of these pentasaccharides were both fixed in the $^1C_4$ conformation. For the other, they were both fixed in the $^2S_0$ conformation. All of the heparin ligands were derived from the PDB file 1HPN (Mulloy *et al.*, 1993).

The docking of heparin oligosaccharide ligand models to human BMP-7 protein structures was performed in an 84 x 84 x 84 Å grid using Autodock version 2.4 (Morris *et al.*, 1996). The Autodock version of the AMBER force field was used to provide partial charges for protein atoms (Weiner *et al.*, 1984). To generate models of mutant BMP-7 proteins, *in silico* amino acid substitution mutations were introduced using the Biopolymer module of the Insight II software package (Accelrys, San Diego, CA, USA) on a 300 MHz SGI Octane workstation running the IRIX operating system (Silicon Graphics Inc, Fremont, CA, USA). Protein structural coordinates were visualised and figures were prepared using The PyMOL Molecular Graphics System (DeLano Scientific LLC, San Carlos, CA, USA) and the Accelrys Insight II and Discovery Studio software packages.

2.2 BMP-7 cDNA clone

A 1814 base pair complementary deoxyribonucleic acid (cDNA) clone containing the complete coding sequence of *Homo sapiens* BMP-7 (I.M.A.G.E ID: 4183402, GenBank accession: BC008584) was purchased as a stab colony from Geneservice Limited (Cambridge, UK). This clone was handled as advised in the documentation provided by the supplier.

2.3 Plasmid DNA extraction and purification

2.3.1 Plasmid DNA miniprep

A 5 ml volume of Luria-Bertani (LB) medium [1 % (w/v) bacto-tryptone, 0.5 % (w/v) yeast extract, 171 mM NaCl, pH 7.2] containing an appropriate selective antibiotic was inoculated with a single colony from an agar plate of *E. coli* cells that had been transformed with a DNA plasmid of interest. The culture was grown by shaking at 225 rpm in a 37 °C incubator overnight (approximately 16 hours). A 1.5 ml aliquot of the culture was transferred to a microcentrifuge tube and the cells were pelletted by centrifugation at 10,000 rpm for 3 minutes in a MiniSpin microcentrifuge (Eppendorf, Hamburg, Germany). The supernatant was removed and this step was repeated once more before the DNA was extracted using the QIAprep Spin Miniprep Kit (Qiagen Inc, Valencia, CA, USA) according to the manufacturers instructions. Purified plasmid DNA was eluted from the silica membrane of the supplied QIAprep spin column with 50 µl of sterile distilled water.

2.3.2 Endotoxin-free plasmid DNA maxiprep

A starter culture was prepared by inoculating a 2 ml volume of LB medium containing an appropriate selective antibiotic with a single colony from an agar plate of *E. coli* cells transformed with a DNA plasmid of interest. The culture was grown by shaking at 225 rpm in a 37 °C incubator for approximately 8 hours. The starter culture was then diluted 1:500 in a 100 ml volume of selective LB medium, and this culture was grown overnight in a 37 ºC incubator while shaking at 225 rpm. Following this,

the cells were pelletted by centrifugation at 6000 x g for 15 minutes at 4 ºC before DNA was extracted using the EndoFree Plasmid Maxi Kit (Qiagen) according to the manufacturers instructions.

2.3.3 DNA clean-up following modification, restriction digestion and polymerase chain reaction (PCR)

Following restriction digests and PCR reactions, DNA clean-up and concentration was performed using the QIAquick PCR Purification Kit (Qiagen) according to the supplied protocol. The purified DNA was eluted from the silica membrane of the supplied QIAquick spin column with 30 µl of sterile distilled water.

2.3.4 Extraction and purification of DNA from agarose gels

An ultraviolet (UV) light box was used to visualise DNA bands on agarose gels, and a sterile scalpel was used to quickly but carefully excise bands and trim off excess agarose. DNA bands were purified from the gel slice using the QIAquick Gel Extraction Kit (Qiagen) according to the supplied protocol. The purified DNA was eluted from the silica membrane of the supplied QIAquick spin column with 30 µl of sterile distilled water.

2.4 Quantification of DNA and RNA

The quantification of DNA and RNA was carried out using a SmartSpec 3000 spectrophotometer (Bio-Rad Laboratories, Hercules, CA, USA), and absorbance readings were carried out using the pre-programmed methods according to the manufacturers instructions.

2.5 DNA sequencing

DNA sequencing was performed by The Sequencing Service (College of Life Sciences, University of Dundee, Scotland, http://www.dnaseq.co.uk) using Applied

Biosystems Big-Dye Ver 3.1 chemistry, on an Applied Biosystems model 3730 automated capillary DNA sequencer.

2.6 Digestion of DNA with restriction endonuclease (RE) enzymes

Restriction endonucleases and their accompanying buffers were purchased from either Promega Corporation (Madison, WI, USA) or Fermentas International Inc (Burlington, Ontario, Canada). Digestion mixtures were set-up in 0.5 ml thin-walled Eppendorf PCR tubes containing the following components:

1x final concentration of the appropriate reaction buffer (supplied)
1-4 µg DNA
2 µg acetylated bovine serum albumin (BSA)
5-10 units of each restriction enzyme
Sterile distilled water to a suitable reaction volume (typically 20 µl)

Mixtures were incubated in a water bath at the appropriate temperature (as indicated by the enclosed data sheet and generally 37 ºC) for 2 hours. When carrying out tandem digestions with restriction enzymes that required buffers that were incompatible with one another, and there was no suitable alternative, the reactions were carried out in two stages to optimise enzyme activity. Following the first digestion, the mixture was diluted 1:1 with sterile distilled water and a suitable volume of the second supplied 10x buffer and restriction enzyme were added prior to a further 2 hour incubation.

2.7 DNA PCR primers

DNA oligonucleotide primers for PCR were designed according to requirements and purchased from Invitrogen (Carlsbad, CA, USA). Upon receipt, the lyophilised primers were resuspended in sterile distilled water to a stock concentration of 100 µM. The sequences of the primers that were used during this study can be found in Table 2.1.

Primer name	Primer sequence (5' to 3')
BMP7WT1-S	ATAGGATCCGCCCGGAGCCCGGAGCCCGGGTAC
BMP7WT2-S	ATAGGATCCGCCGCCACCATGGACGTGCGCTCACTGCGAGCT
BMP7WT-A	ATTGGATCCCTAGTGGCAGCCACAGGCCCG
BMP7K419A/R421A-S	CTCCAACGTCATCCTGAAGGCATACGCAAACATGGTGGTCCGGGCC
BMP7K419A/R421A-A	GGCCCGGACCACCATGTTTGCGTATGCCTTCAGGATGACGTTGGAG
BMP7ΔS296-R327-S	TTCCGCAGCATCCGGTCCACGGGGCAGGCCTGTAAGAAGCACGAGCTG
BMP7ΔS296-R327-A	CAGCTCGTGCTTCTTACAGGCCTGCCCCGTGGACCGGATGCTGCGGAA
pIRESbla-S	CGACTCACTATAGGGAGACC
pIRESbla-A	CTGACAATCTTAGCGCAGAAGTC
T7	TAATACGACTCACTATAGGG
SP6	AGCTATTTAGGTGACACTATAG
pFastBac1-S	TATTCCGGATTATTCATACCGTC
pFastBac1-A	GTATGGCTGATTATGATCCTC
Actin-S	GGCCACGGCTGCTTC
Actin-A	GTTGGCGTACAGGTCTTTGC

Table 2.1 PCR primers
The names and sequences, in the 5' to 3' orientation, of the DNA PCR primers that were used during this study. All primers were purchased from Invitrogen.

2.8 Polymerase chain reaction (PCR)

2.8.1 PCR using Platinum *Pfx* DNA Polymerase

For applications that required PCR products with high fidelity, such as cloning, PCR amplifications were carried out using Platinum *Pfx* DNA Polymerase (Invitrogen). Unlike *Taq* polymerase, this recombinant polymerase (derived from *Thermococcus* sp. strain KOD) possesses a proofreading 3' to 5' exonuclease activity. This enables it to correct nucleotide mis-incorporation errors. Reaction mixtures were assembled on ice as follows in 0.5 ml thin-walled Eppendorf PCR tubes:

1x final concentration of *Pfx* Amplification Buffer (supplied)
Deoxynucleotide triphosphate (dNTP) mixture (0.3 mM each)
1 mM $MgSO_4$
0.3 µM 5' sense primer
0.3 µM 3' antisense primer
20-50 ng template DNA
1 unit Platinum *Pfx* DNA Polymerase
Sterile distilled water to a final volume of 50 µl

The components were mixed well and centrifuged briefly to collect the contents at the bottom of the tubes before cycling using the following parameters in a Progene thermal cycler (Techne Ltd, Cambridge, UK):

Initial denaturation:	94 ºC	2 minutes	
Denaturation:	94 ºC	30 seconds	30 cycles
Annealing:	55 ºC	30 seconds	
Extension:	68 ºC	1 minute per kb	
Final extension:	68 ºC	5 minutes	

PCR products were stored at -20 ºC.

2.8.2 PCR using BIOTAQ DNA Polymerase

For routine PCR applications where the fidelity of the PCR product was less important, amplifications were carried out using BIOTAQ DNA Polymerase (Bioline Ltd, London, UK), which is a purified enzyme from *Thermus aquaticus*. Reaction mixtures were assembled on ice in 0.5 ml thin-walled Eppendorf PCR tubes containing the following components:

1x final concentration of NH_4 Buffer (supplied)
dNTP mixture (0.3 mM each)
1.5 mM $MgCl_2$
0.3 µM 5' sense primer
0.3 µM 3' antisense primer
20-50 ng template DNA
1 unit BIOTAQ DNA Polymerase
Sterile distilled water to a final volume of 50 µl

The components were mixed well and centrifuged briefly to collect the contents at the bottom of the tubes before cycling using the following parameters in a Progene thermal cycler (Techne):

Initial denaturation:	94 ºC	2 minutes	
Denaturation:	94 ºC	30 seconds	30 cycles
Annealing:	55 ºC	30 seconds	
Extension:	72 ºC	1 minute per kb	
Final extension:	72 ºC	5 minutes	

PCR products were stored at -20 ºC.

2.8.3 Colony PCR

Colony PCR was carried out according to the protocol described in section 2.8.2 above with one amendment. Colonies were picked carefully using a sterile pipette tip and re-streaked on to a divided and labelled fresh LB-agar plate containing an appropriate selective antibiotic. The remainder of the colony was added to 10 µl sterile distilled water, mixed well by pipetting, and 1 µl of this solution was added to the PCR reaction mixture in place of the template DNA. PCR products were analysed on agarose gels.

2.9 Agarose gel electrophoresis

DNA size analysis was carried out on 1 % (w/v) agarose gels, which were prepared by melting molecular biology grade agarose (Helena BioSciences Europe, Tyne & Wear, UK) in Tris-acetate-EDTA (TAE) buffer [40 mM Tris-acetate, 1 mM ethylenediaminetetraacetic acid (EDTA)]. The solution was heated until the agarose had completely dissolved using a microwave oven on the low power setting. Once the agarose solution had cooled, 0.5 μg/ml ethidium bromide was added and the solution was poured into a gel-tray. A comb was placed in the tray to form wells and the gel was allowed to set at room temperature. The gel was then placed in a horizontal electrophoresis tank (Bio-Rad) filled with TAE buffer. The DNA samples were mixed with an appropriate volume of 5x DNA loading buffer (Bioline), and were loaded into the wells alongside a DNA molecular weight marker that contained bands of a suitable size range, typically HyperLadder I (Bioline). Gel electrophoresis was performed at 80 V for an appropriate time for the size of gel being used, and DNA bands were visualised using a Doc-It UV transilluminator and camera (UVP, Upland, CA, USA).

2.10 Cloning PCR products using the pGEM-T vector system

The pGEM-T vector system (Promega) provides a convenient way to clone PCR products. The vectors are prepared by cutting with EcoRV, a blunt cutter, and adding a 3' terminal thymidine to both ends of the insertion site. The single 3'-T overhangs improve the efficiency of ligation by providing a compatible overhang for PCR products generated using some thermostable polymerases that add a single 3'-A overhang. However, proofreading thermostable DNA polymerases generate blunt-ended PCR fragments, and 3'-A overhangs must be added to these fragments prior to them being ligated in to the pGEM-T vector.

2.10.1 Addition of 3'-A overhangs to PCR fragments

3'-A overhangs were added to purified PCR fragments using GoTaq DNA Polymerase (Promega). Mixtures were set up containing the following components:

1x final concentration of GoTaq reaction buffer with $MgCl_2$ (supplied)

1-6 µl of purified blunt-ended PCR fragment (0.5-1.0 µg total amount)

0.2 mM dATP

5 units GoTaq DNA Polymerase

Sterile deionised water to a final reaction volume of 10 µl

Mixtures were incubated at 72 ºC for 30 minutes in a Progene thermal cycler (Techne), and 1-2 µl of the mixture was then used in a ligation reaction with the pGEM-T vector according to the supplied instructions.

2.11 Transformation of competent *E. coli* cells with plasmid DNA

Library Efficiency competent DH5α *E. coli* cells, MAX Efficiency competent DH10Bac *E. coli* cells (both Invitrogen) and XL-1 Blue supercompetent *E.coli* cells (Stratagene, La Jolla, CA, USA) were stored at -80 °C, and were thawed on ice immediately before use. A 100 µl aliquot of cells was transferred to a chilled 14 ml BD Falcon polypropylene round-bottom tube (BD Biosciences, San Jose, CA, USA) containing 1-5 µl of DNA, mixed very gently by swirling, and incubated for 30 minutes on ice. The cells were then heat-shocked in a water bath at 42 ºC for 45 seconds before a further 2 minute incubation on ice. 0.9 ml room temperature Super optimal broth with catabolite repression (SOC) medium [2 % (w/v) bacto-tryptone, 0.5 % (w/v) yeast extract, 8.56 mM NaCl, 2.5 mM KCl, 10 mM $MgCl_2$, 20 mM glucose, pH 7.0] was added to the solution of cells and DNA, mixed gently by swirling, and incubated at 37 °C whilst shaking vigorously at 225 rpm for 1 hour. A suitable volume of the culture was then spread out on to pre-warmed LB-agar plates containing the appropriate antibiotic for selection (generally 50 µg/ml ampicillin), with 80 µg/ml X-gal (5-bromo-4-chloro-3-indolyl-beta-D-galactopyranoside) and 20 mM IPTG (Isopropyl-β-D-1-thiogalactopyranoside) where required. Plates were incubated at 37 °C overnight.

2.12 pIRESbla vector

The pIRESbla mammalian expression vector was a kind gift received from Chris Ball at the National Institute for Biological Standards and Control (NIBSC), Potters Bar, Herts, UK. The vector was produced at NIBSC (Thorpe *et al.*, 2008) as a modification of the pIRESneo vector (Clontech Laboratories Inc, Mountain View, CA, USA). Briefly, the neomycin phosphotransferase (NPT II) gene and the bovine growth hormone polyadenylation signal were removed from pIRESneo, and replaced with the Blasticidin resistance gene (Bsd^r) and SV40 early polyadenylation signal from the pcDNA 6.2/V5-DEST vector (Invitrogen). This enabled stable cell lines to be selected using Blasticidin S HCl.

2.13 Alkaline phosphatase treatment of DNA

When being digested prior to use in a ligation reaction, vector DNA was treated with Shrimp alkaline phosphatase (SAP, Promega) to remove 5' phosphates, therefore preventing recircularisation and religation of the linearised DNA. 10 units SAP / µg vector DNA was added in a final volume of 30-50 µl, and incubated at 37 ºC in a water bath for 15 minutes. SAP was then heat-inactivated at 65 ºC for 15 minutes.

2.14 DNA ligation

DNA ligation reactions were carried out using T4 DNA Ligase (Promega). Ligation mixtures were set up on ice in 0.5 ml thin-walled Eppendorf PCR tubes containing the following components:

1x final concentration of ligation buffer (supplied)
50-100 ng vector
An appropriate quantity of insert DNA to give either a 1:1 or 3:1 insert:vector molar ratio
1 unit T4 DNA Ligase
Sterile distilled water to a total volume of 20 µl

Ligation mixtures were incubated overnight at 16 ºC in a Progene thermal cycler (Techne), and 5 µl was then used to transform competent *E. coli* cells.

2.15 Site-directed mutagenesis

Site-directed mutagenesis was carried out using the QuikChange II Site-Directed Mutagenesis Kit (Stratagene), generally according to the enclosed instructions and including the appropriate controls. The double-stranded plasmid template DNA used in the experiments was purified from Library Efficiency DH5α cells (Invitrogen) by carrying out a DNA miniprep or maxiprep. Mutagenic primers were designed using Stratagene's web-based QuikChange Primer Design Program.

2.15.1 Mutant strand synthesis reaction

Mutant DNA strands were synthesised in reactions containing the following components in 0.5 ml thin-walled Eppendorf PCR tubes:

5 µl of 10x reaction buffer
20 ng of double stranded DNA template
125 ng of oligonucleotide primer #1
125 ng of oligonucleotide primer #2
1 µl of supplied dNTP mix
Distilled water to a final volume of 50 µl
1 µl of PfuUltra HF DNA polymerase (2.5 U/µl)

The components were mixed well and centrifuged briefly to collect the contents at the bottom of the tubes before cycling using the following parameters in a Progene thermal cycler (Techne):

Initial denaturation:	95 ºC	30 seconds	
Denaturation:	95 ºC	30 seconds	18 cycles
Annealing:	55 ºC	1 minute	
Extension:	68 ºC	1 minute / kb of plasmid length	

Following temperature cycling, tubes were placed on ice for 2-3 minutes to cool reactions to ≤37 °C.

2.15.2 DpnI digestion of template plasmid DNA

Following the synthesis of mutant DNA strands, the restriction enzyme DpnI was used to digest the parental (i.e. non-mutated) template DNA. DpnI cleaves only when its recognition sites are methylated, which is the case when the template DNA is purified from a *dam*$^+$ *E. coli* strain such as DH5α (a requirement of the procedure). Because the newly-synthesised mutant strands are not methylated, the enzyme can distinguish between the two DNA forms and leave the mutant strands intact.

1 µl of the supplied DpnI restriction enzyme (10 units/µl) was added directly to each mutant strand synthesis reaction, and the contents of the tubes were mixed gently but thoroughly by pipetting up and down several times. The reaction mixtures were spun down briefly in a microcentrifuge and immediately incubated in a water bath at 37 ºC for 2 hours to digest the parental DNA. Following this, 1-2 µl of the mixture (containing mutated plasmid DNA) was used to transform the supplied XL-1 Blue supercompetent cells according to the method described in section 2.11. Single colonies were picked from transformation plates, and plasmid DNA was isolated by carrying out DNA minipreps (section 2.3.1). The presence of the desired mutations was confirmed by sending purified plasmid DNA for sequencing (section 2.5).

2.16 Detection of BMP-7 by enzyme-linked immunosorbent assay (ELISA)

Detection of the BMP-7 protein in samples by ELISA was carried out using the human BMP-7 DuoSet sandwich ELISA development kit (R&D Systems Inc,

Minneapolis, MN, USA). Wells of a Nunc Maxisorp 96-well plate (Fisher Scientific UK Ltd, Loughborough, Leics, UK) were coated overnight at room temperature with 100 µl phosphate buffered saline (PBS, 137 mM NaCl, 2.7 mM KCl, 10 mM Na_2HPO_4, 1.76 mM KH_2PO_4, pH 7.4) containing 2 µg/ml of mouse anti-human BMP-7 monoclonal capture antibody. The wells were then washed three times by filling with 400 µl PBS containing 0.05 % (v/v) Tween 20 (PBS-Tween 20). The wells were blocked for 1 hour at room temperature on a rotating platform, with 300 µl PBS containing 1 % (w/v) Probumin Diagnostic Grade Bovine Serum Albumin (BSA) (Millipore UK Ltd, Watford, Herts, UK), before washing three times with PBS-Tween 20. 100 µl volumes of samples, or recombinant human BMP-7 standards (R&D Systems) diluted in PBS containing 1 % (w/v) BSA, were added to the wells and incubated at room temperature for 2 hours. After washing the wells three times with PBS-Tween 20, 100 µl of biotinylated mouse anti-human BMP-7 monoclonal detection antibody was added at a concentration of 0.5 µg/ml diluted in PBS / 1 % (w/v) BSA, and incubated at room temperature for 2 hours. Following this, the wells were washed three times with PBS-Tween 20, and 100 µl PBS / 1 % (w/v) BSA containing 1:200 diluted streptavidin-horseradish peroxidase (HRP) conjugate was added. After 20 minutes at room temperature, the wells were washed three times with PBS-Tween 20. 100 µl of substrate solution [1:1 mixture of Colour Reagent A (H_2O_2) and Colour Reagent B (Tetramethylbenzidine), R&D Systems] was added to each well, and after allowing a further 20 minutes in the dark at room temperature for colour development, 50 µl of stop solution (2 N H_2SO_4) was added. The optical density of each well was determined immediately using an Emax plate reader (Molecular Devices, Sunnyvale, CA, USA) set to 450 nm, with wavelength correction set at 595 nm to correct for any optical imperfections in the plate.

2.17 Sample preparation

2.17.1 Preparation of supernatant samples for sodium dodecyl sulphate polyacrylamide gel electrophoresis (SDS-PAGE)

Laemmli sample buffer [62.5 mM Tris-HCl pH 6.8, containing 20 % (v/v) glycerol, 2 % (v/v) ß-mercaptoethanol and 2 % (w/v) SDS] was added to each sample

at a 1:1 ratio as described by Laemmli (1970), to give a final concentration of 1 % (v/v) ß-mercaptoethanol and 1 % (w/v) SDS. In addition, 5 µl of bromophenol blue [0.1 % (w/v) in 10 mM Tris] was added per 100 µl of sample to enable visualisation of the dye front during protein separation. Samples were boiled for 5 minutes in a 100 ºC water bath to denature the proteins prior to loading on polyacrylamide gels.

2.17.2 Preparation of whole cell lysates for SDS-PAGE and ELISA

Cells were pelleted by centrifugation at 1000 x g for 5 minutes, the supernatant was aspirated completely and the pellet was washed once gently with PBS. For SDS-PAGE, the pellets were resuspended in 200 µl of Laemmli sample buffer, and boiled for 5 minutes in a 100 ºC water bath to denature the proteins. For use in ELISA, the pellets were resuspended in 200 µl of PBS, frozen in a dry ice and isopropanol bath for 10 minutes, and the suspension was thawed in a 37 ºC water bath. This freeze/thaw cycle was repeated 3 times.

2.18 SDS-PAGE and Western blotting

2.18.1 SDS-PAGE

SDS-polyacrylamide gel electrophoresis was carried out as described by Laemmli (1970) using the Bio-Rad Mini-PROTEAN III mini-gel apparatus, according to the manufacturers instructions. 1 mm thick 15 % (w/v) polyacrylamide gels were used, which were cast using the same apparatus and were made up with 3.6 ml of deionised water, 3.75 ml of 1.5 M Tris-HCl pH 8.8, 150 µl of 10 % SDS and 7.5 ml of 30 % (w/v) acrylamide solution containing 0.8 % (w/v) bis-acrylamide (BDH Scientific, VWR International, Dublin, Ireland), with 150 µl 10 % (w/v) ammonium persulphate (APS) and 10 µl tetramethylethylenediamine (TEMED) to catalyse polymerisation. The stacking gel [5.5 % (w/v) acrylamide] contained 2.9 ml of deionised water, 1.25 ml of 0.5 M Tris-HCl pH 6.8, 0.95 ml of 30 % (w/v) acrylamide solution containing 0.8 % (w/v) bis-acrylamide and 50 µl of 10 % SDS, with 31.5 µl 10 % (w/v) APS and 7.5 µl TEMED.

Gels were clamped in to the tank and the inner chamber was filled to the top (above the level of the gel) with reservoir buffer [25 mM Tris, 192 mM glycine, 0.1 % (w/v) SDS, pH 8.3]. The buffer was also used to fill the outer chamber of the tank to a depth of approximately 5 centimetres. Protein samples were prepared as stated in section 2.17 above, and were loaded in 5 mm wide tracks. Gels were run at 200 V constant voltage until the dye front reached the end of the gel (approximately 45 minutes). Pre-stained molecular weight markers (SeeBlue Plus2, Invitrogen) were used on all gels.

2.18.2 Western blotting

Following gel electrophoresis, the proteins separated by SDS-PAGE were transferred onto a nitrocellulose transfer membrane with a pore size of 0.45 μm (Schleicher & Schuell Protran, Whatman plc, Maidstone, Kent, UK). A wet Western blotting technique was developed (modified from Towbin *et al.*, 1979) using the Bio-Rad Mini Trans-Blot cell in combination with the Mini-PROTEAN III electrophoresis system. The nitrocellulose membrane was pre-equilibrated in blotting buffer [25 mM Tris, 192 mM glycine, 20 % (v/v) methanol, 0.1 % (w/v) SDS, pH 8.3] for 1 hour prior to blotting, and electrophoretic transfer was carried out in the same buffer for 1 hour at 100 V constant voltage.

2.18.3 Development of Western blots

Following Western blotting, membranes were washed three times for 15 minutes each on a rotating platform with Tris buffered saline (TBS, 50 mM Tris, 150 mM NaCl, pH 7.6) containing 0.05 % (v/v) Tween 20 (TBS-Tween 20), and blocked for 1 hour in blocking solution [5 % (w/v) Marvel low fat milk powder in TBS-Tween 20]. The blots were then incubated overnight with primary antibody dissolved in blocking solution (0.5 μg/ml goat polyclonal anti-human BMP-7, R&D Systems) on a rotating platform at 4˚C. Following this, membranes were washed three times for 15 mins with TBS-Tween 20, before a 1 hour incubation at room temperature with secondary antibody [horseradish peroxidase (HRP) conjugated rabbit anti-goat IgG (Sigma-Aldrich Company Ltd, Dorset, UK)] at a dilution of 1:2000 in blocking

solution. After washing three times for 5 minutes each, blots were developed using SuperSignal West Pico or Femto Chemiluminescent Substrate (Pierce Biotechnology Inc, Rockford, IL, USA) according to the manufacturers instructions. An appropriately sized piece of photographic film (Hyperfilm ECL, GE Healthcare UK Ltd, Chalfont St Giles, Bucks, UK) was placed over blots wrapped in cling-film and exposed for a suitable amount of time (initially 20 seconds but varied depending on the intensity of chemiluminescence). After exposure, the film was placed in developer for 1-2 minutes, rinsed thoroughly with water, and placed in fixer for 2 minutes.

2.19 Cell culture

2.19.1 Adherent Chinese Hamster Ovary-K1 (CHO-K1) cells

CHO-K1 cells were purchased from the European Collection of Cell Cultures (ECACC, Health Protection Agency, Salisbury, UK) and were cultured as a monolayer in a 37 ºC incubator with 5 % CO_2 and 95 % relative humidity. The cells were routinely maintained in 25 cm^2 flasks with vented caps (Orange Scientific, B-1420 Braine-l'Alleud, Belgium), and were seeded at a density of 0.25 x 10^6 cells/25 cm^2 flask in a total volume of 8 ml F-12 Nutrient Mixture (Ham) containing 2 mM L-glutamine and 10 % (v/v) foetal bovine serum (FBS) (both Gibco, Invitrogen). Once the cells reached 70-80 % confluence, the maintenance media was aspirated and the monolayer was washed briefly with 2 ml 0.25 % Trypsin-EDTA solution (Sigma), which was then removed. The cells were detached from the flask by adding 0.5 ml of fresh 0.25 % Trypsin-EDTA solution, incubating the flask at 37 ºC for 1 minute and gently tapping the sides of the flask. Once detached, the cell suspension was diluted by adding 9.5 ml of maintenance media to the flask, and pipetted up and down with a 10 ml pipette to break up cell clumps. Before re-seeding, the cells were counted using an Improved Neubauer Hemocytometer, and their viability was determined by carrying out a Trypan Blue dye exclusion assay (section 2.20). When scaling-up was required, the cells were cultured in 75 cm^2 or 150 cm^2 flasks. The cell numbers and all volumes stated above were increased proportionally to the surface area of the flask.

2.19.2 Adherent *Spodoptera frugiperda* (Sf9) insect cells

Spodoptera frugiperda (Sf9) insect cells were purchased from Invitrogen for use with the Bac-to-Bac Baculovirus Expression System, and were cultured as a monolayer in a 27 ºC incubator according to the supplied manual. Sf9 cells were routinely maintained in Supplemented Grace's Insect Medium (Gibco, Invitrogen) containing 10 % FBS.

2.19.3 Suspension FreeStyle Chinese Hamster Ovary (CHO-S) cells

FreeStyle CHO-S cells were purchased from Invitrogen as part of the FreeStyle MAX CHO Expression System. FreeStyle CHO-S cells are derived from the CHO cell line, and are adapted to suspension culture in FreeStyle CHO Expression Medium supplemented with 8 mM L-glutamine. The cells were cultured as described in the supplied manual in 125 ml, 250 ml or 1 litre polycarbonate sterile Erlenmeyer shaker flasks with vented caps (VWR International, Dublin, Ireland). Cells were grown in a 37 ºC incubator containing a humidified atmosphere of 8 % CO_2 in air on an orbital shaker platform rotating at 135 rpm.

2.20 Trypan Blue dye exclusion assay for determining cell viability

A 5 µl volume of 0.4 % Trypan Blue dye solution (Sigma) was added to 95 µl cell suspension and mixed thoroughly. 20 µl of this solution was applied to each side of an Improved Neubauer Hemocytometer by allowing drops held at the end of a pipette tip to be taken under the coverslip by capillary action. The percentage cell viability was determined by comparing the number of unstained viable cells to the number of dead cells that stained blue.

2.21 Transfection of cells

2.21.1 Stable transfection of adherent CHO-K1 cells

Prior to being used in transfections, the CHO-K1 cells were grown in 25 cm^2 or 75 cm^2 flasks until they reached approximately 90 % confluency. They were then trypsinised, counted, and their viability was determined (as described in section 2.20) to ensure that they were >95 % viable and therefore in optimum condition to be transfected.

Approximately 24 hours before transfection, the cells were seeded in to 6-well plates (Orange Scientific) at a density of 3 x 10^5 cells/well in 3 ml maintenance medium. Duplicate wells were prepared for each plasmid to be transfected, and the necessary control transfections (vector only and a sham transfection without DNA). Plates were placed in a 37 ºC incubator containing 5 % CO_2 overnight. The next day, the following components were assembled in a sterile 1.5 ml tube:

100 µl F-12 Nutrient Mixture (no FBS)
3 µl GeneJuice Transfection Reagent (Novagen, Merck Chemicals Ltd, Notts, UK)

The contents of the tube were mixed well by vortexing and incubated for 5 minutes at room temperature. Following this, 1 µl of endotoxin-free plasmid DNA (1 mg/ml) was added to the mixture, mixed by gently pipetting, and incubated at room temperature for 15 minutes. The plasmid DNA / GeneJuice mixture was then added to the plated cells dropwise in different areas of the well and the plate was rocked gently from side to side before being incubated for approximately 24 hours at 37 ºC with 5 % CO_2.

The day after transfection when the cells were approximately 90 % confluent, stably transfected cells were selected for resistance to the antibiotic Blasticidin S HCl (Invitrogen). The media was aspirated from the wells and the cell monolayer was washed with 1 ml 0.25 % Trypsin-EDTA solution. After this solution was removed, another 0.25 ml of the same solution was used to detach the cells from the surface of the wells. The detached cells were resuspended in 2 ml transfection medium

(maintenance medium containing 10 µg/ml Blasticidin S HCl) and added to 23 ml transfection medium in 75 cm^2 flasks. The flasks were incubated at 37 ºC with 5 % CO_2 and the transfection medium was replaced every 3-4 days until the cells were 80-90 % confluent and required passaging (approximately 7-10 days). The same procedure was followed for the control transfections.

2.21.2 Transfection of Sf9 insect cells

In each well of a 6-well plate, 9 x 10^5 Sf9 cells were seeded in 2 ml of growth medium and allowed to attach at 27 ºC for 1 hour. For each transfection, 1 µg of purified bacmid DNA was diluted in 100 µl of unsupplemented Grace's Medium (Invitrogen). 6 µl of Cellfectin transfection reagent (Invitrogen) was also diluted in 100 µl of unsupplemented Grace's Medium. The diluted bacmid DNA was then combined with the diluted Cellfectin reagent, mixed gently, and incubated at room temperature for 45 minutes. The media was removed from the cells and the cells were washed once with 2 ml of unsupplemented Grace's Medium, which was then removed. 0.8 ml of unsupplemented Grace's Medium was added to each tube containing the DNA-Cellfectin complexes and mixed gently before being added to each well containing the cells to be transfected. The cells were then incubated at 27 ºC for 5 hours, after which time the media containing the DNA-Cellfectin complexes was removed and replaced with 2 ml of fresh growth media. The cells were once again incubated in a 27 ºC humidified incubator for approximately 72 hours until signs of viral infection were seen. After this time, the medium containing the P1 baculoviral stock was collected from each well, clarified by centrifugation at 500 x g for 5 minutes and stored at 4 ºC protected from light.

2.21.3 Transfection of FreeStyle CHO-S cells

Approximately 24 hours before transfection, FreeStyle CHO-S cells (Invitrogen) were passaged at 5 x 10^5 cells/ml, and placed on an orbital shaker platform rotating at 135 rpm in a 37 ºC incubator containing 8 % CO_2. On the day of transfection, the cells were counted and their viability was determined to ensure that they were >95 % viable, and therefore in optimum condition for transfection. The

cells were then diluted to a density of 1 x 10^6 cells/ml in FreeStyle CHO Expression Medium (Invitrogen) and 30 ml of cell suspension was transferred into each 125 ml shake flask (VWR) ready for transfection. 37.5 µg of plasmid DNA was diluted into OptiPro SFM (Invitrogen) to a total volume of 600 µl and mixed. In another tube, 37.5 µl of FreeStyle MAX Transfection Reagent (Invitrogen) was also diluted in OptiPro SFM to a total volume of 600 µl, and mixed gently by inverting the tube. The diluted FreeStyle MAX Transfection Reagent was then immediately added to the diluted DNA solution, and the 1.2 ml total volume was mixed gently and incubated at room temperature for 10 minutes to allow DNA-FreeStyle MAX Reagent complexes to form. After this time, the 1.2 ml volume containing the DNA-FreeStyle MAX complex was slowly added into the 125 ml flask containing FreeStyle CHO-S cells while slowly swirling the flask. Transfected cell cultures were incubated at 37 ºC with 8 % CO_2 on an orbital shaker platform rotating at 135 rpm.

2.21.4 Transfection of adherent CHO-K1 cells with the Centocor mutant DNA constructs

Approximately 24 hours prior to transfection, CHO-K1 cells were seeded in to 150 cm^2 flasks (Orange Scientific) at a density of 1 x 10^7 cells/flask in 30 ml maintenance medium (DMEM/F-12 containing 10 % FBS). The flasks were placed in a 37 ºC incubator containing 5 % CO_2 overnight. The next day, for each transfection, 1 ml of Opti-MEM (Invitrogen) was added to each of two sterile 15 ml tubes. To one of these tubes, 30 µg of plasmid DNA was added. To the other, 90 µl of Lipofectamine 2000 transfection reagent (Invitrogen) was added. The tubes were incubated at room temperature for 5 minutes, before the contents of the tubes were combined and mixed gently. Following a further 20 minute incubation at room temperature, the 2 ml mixtures were added directly to the flasks containing cells and the culture media was gently swirled. The flasks were again incubated at 37 ºC overnight. Approximately 24 hours later, the media containing the DNA complex was aspirated from the flasks and the cell monolayer was washed with PBS. 30 ml of fresh CD CHO medium containing 4 mM L-glutamine and 5 mM sodium butyrate (all Invitrogen) was then added to each flask, and the flasks were incubated at 37 ºC for 4

days. After this time, the conditioned supernatants were collected from the transfected cells, clarified by centrifugation and assayed for BMP-7 content by ELISA.

2.22 Viral plaque assay

Viral plaque assays to determine the titer of baculoviral stocks were carried out as described in Invitrogen's Bac to Bac Baculovirus Expression System manual, in a 6-well plate format. Briefly, on the day of infection the Sf9 cells were harvested and a cell suspension was prepared at 5 x 10^5 cells/ml in Sf-900 II SFM medium (Invitrogen). 2 ml of the cell suspension was aliquoted into each well, and the cells were allowed to settle and attach to the bottom of the plate for 1 hour at room temperature. After this time, an 8-log serial dilution (10^{-1} to 10^{-8}) of the baculoviral stock was prepared in Sf-900 II SFM medium. The medium was removed from each well and immediately replaced with 1 ml of the appropriate virus dilution. The cells were then incubated with the virus for 1 hour at room temperature, after which time the virus-containing medium was removed and replaced with 2 ml of Sf-900 plaquing medium (60 ml of Sf-900 medium (1.3X) plus 20 ml of 4 % melted agarose gel solution). The agarose gel overlay was allowed to set for 20 minutes at room temperature, and the cells were placed in a 27 ºC humidified incubator for 7 days until plaques were visible and ready to count after staining with neutral red.

2.23 Clarification of cell culture supernatants

After harvesting cell culture supernatants, cell debris was removed by centrifugation at 4500 x g for 5 minutes.

2.24 Protease inhibitors

A cocktail of protease inhibitors for general use (Sigma) was added to harvested cell culture supernatants and cell lysates from a 100x concentrated stock, which was prepared as described in the included datasheet.

2.25 Protein concentration

Protein concentration was carried out using Vivaspin 2 sample concentrators with a 10 kDa molecular weight cut-off (GE Healthcare UK Ltd) according to the manufacturers instructions.

2.26 Protein assay

Samples were assayed to determine their total protein concentration using the Bio-Rad Protein Assay Dye Reagent Concentrate kit, according to the microtitre plate protocol in the enclosed manual. Briefly, the dye reagent was prepared by diluting 1 part Dye Reagent Concentrate with 4 parts distilled and deionised water, and the BSA protein standard and samples were diluted as appropriate. 10 µl of each standard or sample solution were pipetted into separate wells of a 96-well microtitre plate, and 200 µl of diluted dye reagent was added per well. The sample and reagent were mixed thoroughly using a Wellwarm 1 microplate mixer (Labsystems, Cambridge, UK), incubated for 5 minutes at room temperature, and the absorbance was measured at 595 nm using an Emax plate reader (Molecular Devices).

2.27 Ion exchange chromatography

2.27.1 Cation exchange chromatography

Cation exchange chromatography was carried out mainly according to the method described by Sampath *et al.* (1992). Briefly, conditioned supernatants were clarified and dialysed against 20 mM HEPES buffer pH 7.0, containing 20 mM NaCl. Volumes of the dialysed supernatants (20-100 ml) were then applied at a flow rate of 5 ml/hour to columns containing a 2 ml bed volume of SP-Trisacryl beads (Sigma), which had been equilibrated in the same buffer and packed according to the manufacturers instructions. Columns were washed with 5 bed volumes of buffer, and a 16 ml linear gradient of NaCl, up to a final concentration of 1.3 M, was applied at the same flow rate. The column pass-through was pooled and 1 ml fractions were

collected throughout the wash and NaCl gradient steps. This entire procedure was carried out at 4 ºC. Fractions were assayed for BMP-7 content by ELISA.

2.27.2 Anion exchange chromatography

Anion exchange chromatography was carried out as described for cation exchange chromatography except that 20 mM Tris-Cl pH 8.5 containing 100 mM NaCl was used as the buffer, and Q-Sepharose beads (GE Healthcare UK Ltd) as the column matrix.

2.28 RNA extraction and purification

CHO-K1 cells were grown in 75 cm^2 flasks until 80-90 % confluent and harvested as described in section 2.19.1. 7.5 x 10^6 cells were pelleted by centrifugation at 300 x g for 5 minutes in 15 ml RNase-free polypropylene tubes (BD Biosciences). The cell culture medium was completely aspirated, and RNA was extracted and purified using the RNeasy Mini Kit (Qiagen) according to the supplied protocol for the purification of total RNA from animal cells. During the RNA purification process, any residual genomic DNA was eliminated by carrying out an on-column DNase digestion using the RNase-Free DNase Set (Qiagen) containing DNase I. Purified RNA was eluted from the silica membrane of the supplied RNeasy spin column in two steps with 30 µl volumes of the supplied RNase-free water.

2.29 Reverse transcription polymerase chain reaction (RT-PCR)

cDNA was synthesised from purified total RNA by carrying out reverse transcription using SuperScript II Reverse Transcriptase (Invitrogen). Reaction mixtures were set up as follows in 0.5 ml thin-walled PCR tubes:

150 ng random primers (Invitrogen)
1 µg purified total RNA
1 µl dNTP mix (10 mM each)
Sterile distilled water to a final volume of 12 µl

The mixture was heated to 65 ºC for 5 minutes in a thermal cycler, and quickly chilled on ice. The contents of the tubes were collected by briefly centrifuging, and the following components were added:

4 µl 5x first-strand buffer (supplied)
2 µl 0.1 M 1,4-Dithiothreitol (DTT)
1 µl RNaseOUT (40 units /µl, Invitrogen)

The contents of the tubes were mixed gently and incubated at 25 ºC for 2 minutes. 1 µl (200 units) of SuperScript II Reverse Transcriptase was added, mixed gently by pipetting up and down, and the tubes were incubated at 25 ºC for a further 10 minutes. cDNA first strand synthesis was carried out by incubating the tubes at 42 ºC for 50 minutes, before the reaction was inactivated by heating at 70 ºC for 15 minutes. Newly synthesised cDNA was used as a template for PCR amplification as described in section 2.8.2.

2.30 Heparin affinity chromatography

Clarified cell culture supernatants containing recombinant BMP-7 proteins were dialysed against 100 volumes of PBS for 4 hours at 4 ºC. Prior to sample application, 1 ml Heparin HiTrap HP columns (GE Healthcare UK Ltd) were equilibrated with 20 ml PBS. Unless otherwise stated, a volume of dialysed supernatant containing 500 ng of BMP-7 protein (approximately 5 - 8 ml determined by ELISA) was applied to the columns at a flow rate of 0.5 ml/min using a peristaltic pump. After columns were washed with 5 ml of PBS containing 25 µg/ml BSA, a 20 ml linear gradient of NaCl in PBS was applied at the same flow rate up to a final concentration of 1.5 M, also containing 25 µg/ml BSA. The whole procedure was carried out at 4 ºC and 1 ml fractions were collected throughout. The NaCl

concentration of the fractions was determined by carrying out conductivity measurements and standardising against a series of solutions of known concentration.

2.31 Digestion of BMP-7 with Endoproteinase Lys-C

Reaction mixtures containing 50 ng of recombinant human BMP-7 (R&D Systems) in 25 µl volumes of 100 mM Tris-Cl pH 8.5, in the presence and absence of 5 µg/ml heparin (Sigma), were assembled in thin-walled 0.5 ml PCR tubes on ice. The mixtures were incubated for 30 minutes at room temperature before 1 ng Endoproteinase Lys-C (Sigma) was added to each tube with the exception of the zero time samples, to which Laemmli sample buffer was added and the tubes contents were immediately boiled for 5 minutes in a 100 ºC water bath. The remaining digestion mixtures were incubated in a 37 ºC water bath for the specified time, after which Laemmli sample buffer was added and they were also boiled immediately for 5 minutes in a 100 ºC water bath. Following digestion, samples were stored at -20 ºC until they were analysed by carrying out SDS-PAGE and Western blotting (section 2.18).

Chapter 3: Molecular docking calculations

3.1 Introduction

During the drug discovery process, high throughput computer-based simulation techniques, known as docking calculations, are widely used to identify small molecule drug candidates that will interact with a specific protein target (Kitchen *et al.*, 2004). Using high-resolution experimental structural information, these docking calculations can be used to predict the optimal way to accommodate a particular ligand in the binding site of the protein. The most favourable mutual orientation of the protein and its ligand in the theoretical complex is that with the lowest interaction energy, which is used as a scoring function.

Since the solution conformation of the main repeating structure in the heparin polysaccharide was characterised (Mulloy *et al.*, 1993), it has been possible to apply similar methods to those described above for the prediction of heparin/HS-binding sites on proteins. However, before doing so, some modification of the methods was required. This is because in general, the nature of protein-heparin/HS interactions differs from other protein-ligand binding interactions. Firstly, due to the level of structural complexity and heterogeneity, no single structure of heparin/HS exists (section 1.2.2). Secondly, rather than binding tightly to deep clefts in the structure of the protein, HS and heparin bind primarily electrostatically to sites on the surfaces of proteins (sections 1.3.1 and 1.3.2). Although the above complications exist, the nature of the binding interactions - being dependent on a combination of charge and geometry - make them particularly suitable for modeling using adapted docking calculation techniques. Therefore, similar equally successful methods were simultaneously but independently developed and validated by Forster and Mulloy (described in Forster and Mulloy, 2006; Mulloy and Forster, 2008) and by Bitomsky and Wade (1999) to enable such studies to be carried out. Since then, another alternative approach has also been successfully implemented (Ricard-Blum *et al.*, 2004). As outlined in this chapter, the strategy that was adopted for use in this investigation was that of Forster and Mulloy. Docking calculations were performed to

predict the location of potential HS/heparin-binding sites on the surface of the BMP-7 protein, and the results of these calculations were used to assist in the design of the site-directed mutagenesis experiments described in Chapter 4.

3.2 Results and discussion

3.2.1 The Forster and Mulloy docking strategy

As mentioned above, the docking calculations carried out in this chapter to predict the location of the BMP-7 HS/heparin-binding site were conducted using a method developed by Forster and Mulloy. A full detailed explanation of this strategy is provided in Forster and Mulloy (2006) and Mulloy and Forster (2008), but what follows is a summary account covering the key aspects.

The method that was developed is a relatively simple one, which utilises a software application called Autodock, version 2.4 (Morris *et al.*, 1996). This software enables the automated docking of heparin oligosaccharide ligands to experimentally derived protein structures. In this particular scenario, Autodock achieves this by screening the entire protein surface for clusters of basic residues that have suitable shape and charge profiles to complement the pattern of acidic sulphate groups along the heparin chain. The coordinates for these structures are obtained from PDB files deposited in the Research Collaboratory for Structural Bioinformatics (RCSB) Protein Data Bank (PDB) archive (http://www.rcsb.org/pdb). The Autodock version of the AMBER force field (Weiner *et al.*, 1984) is used to provide the required partial charges for protein atoms, whilst the Jaguar program (Schrodinger, Portland, OR, USA) is used to provide the partial atomic charges for the heparin oligosaccharide ligands, based on *ab initio* calculations using 1-OMe, 4-OMe substituted monosaccharides.

Using this strategy, the calculation of probe atom interaction energies is carried out on a grid of 120 x 120 x 120 points. A central grid point is also added, and the grid is centred on the mean of the coordinates of the protein. A grid spacing of 0.7 Å (1 Å = 0.1 nm) is used, producing a total grid size of 84 x 84 x 84 Å. Consequently, this is also the maximum size of protein that can be studied using this method. Docking is performed using a Monte Carlo simulated annealing procedure (128 runs

of 300 cycles are generally performed), in which the protein remains stationary while the oligosaccharide ligand performs a random walk in space around it. In doing so, the position, orientation and allowed rotatable torsion angles of the ligand structure are optimised to find the fit with the lowest intermolecular interaction energy. The five or ten lowest energy coordinate sets can then be extracted and visualized using a suitable molecular graphics viewer, such as the Discovery Studio software package (Accelrys, San Diego, CA, USA). In these coordinate sets, the amino acid residues that contain atoms that lie within 3.5 Å of the oligosaccharide ligand are generally recorded.

Although the accurate computation of interaction energies is not the focus of this method, complexes with predicted energies of less than -1000 kcal/mol are considered to have the potential to represent a feasible protein-heparin interaction. Where the predicted interaction energy is greater than zero, the protein is regarded as having no ability to bind heparin. The reported energies are the result of a scoring function only, and have no significance in absolute terms. The reason for this is that the predictions made by the docking calculations are based upon a simulation of binding in a hard vacuum rather than in aqueous solution. As a result, the docking calculations exaggerate binding affinity, and the predicted interaction energies that result from these calculations are therefore larger than would be expected in aqueous solution.

Three different heparin oligosaccharide model ligands are commonly used, which are all derived from the NMR structure of the disaccharide repeat of heparin, named 1HPN (Mulloy *et al.*, 1993). These ligands include two pentasaccharide structures that both contain three GlcNS6S (*N*-sulpho-D-glucosamine 6-*O*-sulphate) residues, separated by IdoA2S (L-iduronic acid 2-*O*-sulphate) residues. This results in sequences of OMe-GlcNS6S-IdoA2S-GlcNS6S-IdoA2S-GlcNS6S-OMe. However, because the IdoA2S residues are able to adopt two different ring formations, the two pentasaccharides differ in that one of them contains all of the IdoA2S residues in the $^{1}C_{4}$ conformation, whilst in the other they are all in the $^{2}S_{0}$ conformation. Although this a simplistic way of incorporating conformational mobility of the IdoA2S residue, there have been no previous cases in which the difference between the two conformations has produced considerably different predictions. The remaining heparin model ligand that is often used is an endecasaccharide [$(GlcNS6S\text{-}IdoA2S)_5$-GlcNS6S].

During the docking process, Autodock conducts a docking approximation that treats the protein entity as a rigid body. Although this results in a decrease in the calculation time, it prevents the successful modelling of interactions in which the conformation of the protein is changed to achieve a fit. However, some oligosaccharide ligand flexibility is permitted but is limited by Autodock, which allows a maximum of 32 rotatable bonds. For the pentasaccharide ligand structures, this means that all of the exocyclic torsion angles can be flexible with the exception of the glycosidic linkages. For the larger endecasaccharide model ligand, all bonds have fixed torsion angles. The results from docking calculations carried out using the small pentasaccharide ligands (with their flexible sulphate groups) can be useful for predicting the location of the core of the heparin-binding site of a protein. Use of the longer and completely rigid endecasaccharide ligand in such calculations can assist in confirming the location of the predicted heparin-binding site. It may also give an indication of extensions to the binding site and the preferred orientation of the bound heparin fragment.

Although the Forster and Mulloy method is an effective one for generating predictions and aiding the design of site-directed mutagenesis experiments, it does have certain limitations in addition to those mentioned above. For example, it does not provide any details of interactions that may occur between specific atoms in either the protein or oligosaccharide ligand structures, or give any information about the mode of binding. Furthermore, the specific sulphate groups that play a key role in a particular interaction cannot be precisely identified. This method is also unable to determine the preferred direction, if any, of the bound heparin chain. This is due to the fact that the pattern of sulphates along a fully sulphated heparin chain appears very similar in either direction, irrespective of the directionality of the carbohydrate backbone.

3.2.2 Human BMP-7 X-ray crystal structures

To date, four human BMP-7 X-ray crystal structures have been published and their coordinates have been deposited as pdb files in the RCSB protein data bank (http://www.rcsb.org/pdb). These structures are identified as 1BMP (Griffith *et al.*, 1996), 1M4U (Groppe *et al.*, 2002), 1LXI (Greenwald *et al.*, 2003) and 1LX5

(Greenwald *et al.*, 2003). Whilst the pdb files for 1BMP and the higher resolution 1LXI contain the coordinates for the BMP-7 protein structure alone, the other two available files contain the coordinates for the BMP-7 protein in complex with either its antagonist Noggin (1M4U), or the extracellular domain of its receptor ActRII (1LX5).

The availability of these structures enabled docking calculations to be performed to predict the location of the HS/heparin-binding site of BMP-7 prior to conducting site-directed mutagenesis experiments. However, an important limitation of all the structures is that they are missing the first 27 to 35 amino acids out of a total of 37 residues in their N-terminal extensions, upstream of the first cysteine residue. As a result, either 6 or 7 (depending on the structure used) of the 15 basic residues found within the mature BMP-7 protein are absent from these structures. It is likely that this region of the protein remains unresolved as a result of it being disordered (Griffith *et al.*, 1996; Greenwald *et al.*, 2003).

Before carrying out any docking calculations, close attention was paid to ensuring that suitable BMP-7 structures were selected for study, using files that contained the appropriate coordinates for either the BMP-7 monomer or dimer. The required coordinates were extracted and the structures were checked to ensure that there were no missing atoms or residues, other than those that were situated in the unresolved N-terminal region. Docking calculations based on the BMP-7 monomer and dimer were conducted using the 1LXI and 1M4U structures respectively.

3.2.3 Prediction of the heparin-binding site of human BMP-7 using molecular docking calculations

As mentioned previously, BMP-7 is a homodimeric protein. Because of this, it was unclear whether it possesses two independent heparin-binding sites - one on each monomer - or a single cooperative binding site that requires the involvement of both its constituent monomers. It was therefore necessary to conduct any docking calculations to predict the heparin-binding site of human BMP-7 using both monomeric and dimeric BMP-7 structures. It was thought that a comparison of the resulting predictions might provide some insight into the nature of the binding interaction.

3.2.3.1 Docking of the heparin pentasaccharide ligands to the BMP-7 protein monomer

When the heparin pentasaccharides were docked to the BMP-7 monomer, the resulting predictions were almost identical to one another. This was expected as fixing all the IdoA2S residues in either the $^{1}C_{4}$ or $^{2}S_{0}$ conformation has never previously produced considerably different predictions (Forster and Mulloy, 2006). As displayed in Figure 3.1 and summarised in Table 3.1, the pentasaccharide structures docked very consistently across the lower face of a region of the BMP-7 protein known as finger 2. This region of the protein lies close to the C-terminus of BMP-7 and consists of two antiparallel beta-sheets, formed by two pairs of antiparallel beta-strands (β5 and β8, β6 and β7) (Griffith *et al.*, 1996).

More specifically, the docking calculations that were performed predicted that the core of the heparin-binding site of BMP-7 may be localised to a small C-terminal cluster of basic amino acids situated in beta-strands 7 and 8, and the connecting region between them. In total, three basic residues were in close contact (≤ 3.5 Å) with the heparin ligands and therefore predicted to be involved in the interaction. These residues were lysine 419, arginine 421 and arginine 426 (coloured purple in Figure 3.1 and labeled in the absence of any heparin ligands for clarity in Figure 3.2B). Although lysine 418 is also present in this region (coloured purple in Figure 3.1 and labeled in Figure 3.2B), the orientation of its basic side chain was not conducive to its participation in the interaction. Another three residues upstream of the basic cluster were also predicted to come into close contact with the heparin ligands. These were asparagine 402, alanine 403 and serine 405, which are located at the C-terminal end of beta-strand 5, the region between beta-strands 5 and 6, and in beta-strand 6 respectively. However, as these residues are all neutral at physiological pH, it is likely that they would play a lesser role in any interaction of the protein with heparin. For example, the polar side chains of asparagine 402 and serine 405 could assist in stabilising the complex by forming hydrogen bonds with the heparin chain. More importantly, the close proximity of these residues would not destabilise the complex like the presence of a negatively charged aspartic or glutamic acidic residue might do via like-charge repulsion.

It can be seen in Figure 3.1A that when overlaid, the five lowest energy arrangements for the docked IdoA2S $^{1}C_{4}$ heparin pentasaccharide were in very close

agreement. This is a good indication that Autodock has been able to positively discriminate between a region that it considers to possess the theoretical characteristics of a suitable heparin-binding site, and other regions that do not. A very small amount of variation was observed in the predicted orientations of the IdoA2S $^{2}S_{0}$ pentasaccharide (Figure 3.1B). However, this variation did not alter the protein region or particular selection of amino acid residues that came into close contact with the oligosaccharide.

The lowest predicted intermolecular interaction energies calculated for the two heparin pentasaccharide ligands were very similar. Values of -1098.04 kcal/mol (IdoA2S $^{1}C_{4}$) and -1055.62 kcal/mol (IdoA2S $^{2}S_{0}$) were reported. Both of these values were slightly below the -1000 kcal/mol threshold that is generally regarded as being indicative of a protein that has the capacity to bind heparin. Therefore, it can be said that these docking outcomes have the potential to be representative of physiologically possible BMP-7-heparin complexes. Even still, the results of any docking calculations may be taken only as predictions. This is especially true in this case and it is not only due to the limitation of the unresolved N-terminus. It is also because these predictions were based on a BMP-7 monomer, which is not the physiological state of the protein.

Figure 3.1 Molecular docking of two heparin pentasaccharides to a BMP-7 monomer

Molecular docking calculations were performed using Autodock (version 2.4) to determine if/how two different heparin pentasaccharide ligands would interact with a BMP-7 monomer. In these ligands, all of the IdoA2S residues were fixed in either the $^{1}C_{4}$ conformation (A) or the $^{2}S_{0}$ conformation (B). It can be seen that the heparin pentasaccharides both docked across the bottom face of finger 2 on the BMP-7 monomer, coming into close contact with K419, R421 and R426. The side chains of these residues (and K418) are shown in stick form and coloured purple. For clarity, they have also been shown and labeled in Figure 3.2B in the absence of any heparin ligands. In each case, the five lowest energy arrangements of the heparin ligands are overlaid and are in close agreement with each other, with the exception of one IdoA2S $^{2}S_{0}$ pentasaccharide ligand shown in (B). The N-linked glycan stub (containing two GlcNAc residues) that is present in the BMP-7 structure is represented in stick form and is also labeled 'Carb.' in Figure 3.2B.

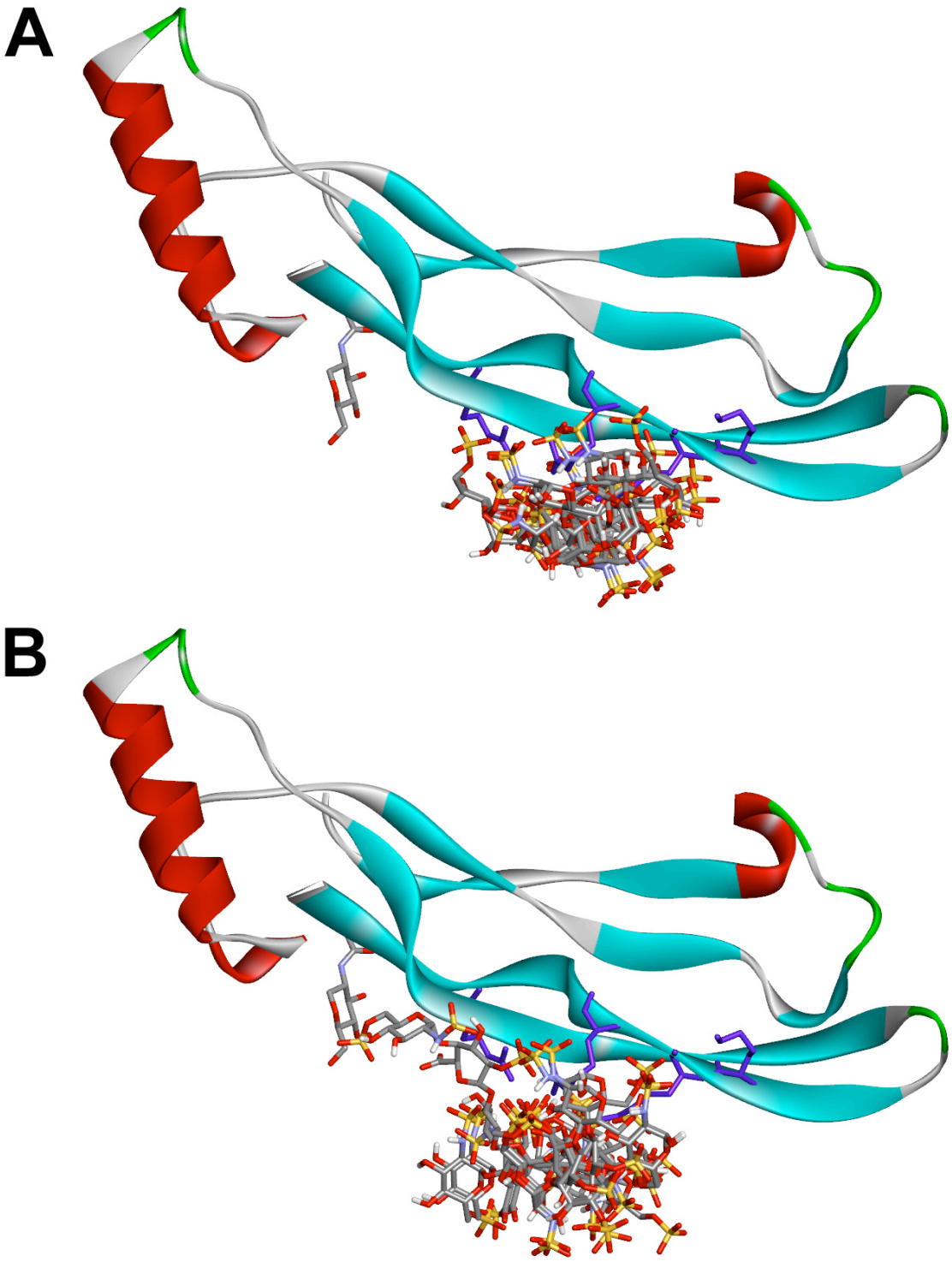

Figure 3.1 Molecular docking of two heparin pentasaccharides to a BMP-7 monomer
Please refer to the figure legend on the opposite page.

3.2.3.2 Docking of the heparin endecasaccharide ligand to the BMP-7 protein monomer

When the heparin endecasaccharide ligand was docked to the BMP-7 monomer, the prediction of the protein contact site made by Autodock firmly supported those obtained for the pentasaccharide ligands. It can be seen in Figure 3.2A that the endecasaccharide model ligand docked diagonally across the same region in finger 2 of the monomeric BMP-7 protein that the pentasaccharides had before. As a result, the individual amino acid residues that were pinpointed as being in close proximity of the heparin chain were also largely the same. Asparagine 402, lysine 419, arginine 421 and arginine 426 once again contained atoms that were located within 3.5 Å of the ligand structure. In addition to these previously mentioned residues, the increased length of the endecasaccharide ligand compared to the two pentasaccharides also brought it in to close contact with lysine 332, glutamine 400 and alanine 427 (Table 3.1).

A consequence of the electrostatic attraction of the heparin endecasaccharide to lysine 332 was that it docked across the only N-linked glycosylation site that is utilised out of the three potential sites located within the mature BMP-7 protein (Jones *et al.*, 1994). Two GlcNAc residues from the N-linked glycan chain that is attached to asparagine 372 of BMP-7 are visible in the available BMP-7 X-ray crystal structures and can be seen in Figure 3.2A and B. Due to the steric obstruction that would most likely be caused by the presence of the carbohydrate entity in this particular region, it is doubtful that this complex arrangement would be feasible. It also remained to be seen if this type of arrangement would be favoured, or even possible, when the BMP-7 protein was in its physiological dimeric form.

Figure 3.2A shows that the five lowest energy orientations of the docked endecasaccharide were again in very close agreement. The predicted intermolecular interaction energy for the best-fit arrangement was -1362.17 kcal/mol. Although no flexibility was allowed for in the heparin endecasaccharide ligand structure, this value was lower than those reported for the pentasaccharides. Theoretically, the BMP-7 monomer therefore interacted more favourably with the longer heparin endecasaccharide than with the pentasaccharides. However, it is possible that this reduction in energy occurred largely as a result of the additional basic residue contact with lysine 332. Because the described arrrangement of the BMP-7 monomer-

endecasaccharide complex would be unlikely to assemble in practice, such a comparison in interaction energies has little value in this instance.

As previously discussed, it is the basic lysine and arginine residues that are generally of particular interest when investigating the location of the heparin-binding site of any given protein. All of the docking calculations to this point supported each another in suggesting that the C-terminal residues lysine 419, arginine 421 and arginine 426 might all be of key importance for the binding of BMP-7 to heparin. Although the particular complex arrangement that is displayed in Figure 3.2A appeared to be unfeasible, the close proximity of lysine 332 to the endecasaccharide ligand also provoked some thought into the possibility that the N- and C-termini of the BMP-7 protein could perhaps form a cooperative heparin-binding site. The major component of the N-terminus of BMP-7 is likely to be flexible, intimated by the fact that it is unresolved in the available crystal structures. Therefore, one can imagine that a number of additional N-terminal residues might also have the capacity to be appropriately oriented to interact with a heparin chain. Unfortunately, the absence of the N-terminus in the available crystal structures prevented further investigation of this possibility using these methods.

Figure 3.2 Molecular docking of a heparin endecasaccharide to a BMP-7 monomer

A molecular docking calculation was performed using Autodock (version 2.4) to determine if/how a heparin endecasaccharide ligand would interact with a BMP-7 monomer. (A) It can be seen that the heparin endecasaccharide docked across the bottom face of finger 2 on the BMP-7 monomer, coming into close contact with K419, R421 and R426. The side chains of these residues (and K418) are shown in stick form, coloured purple, and have been labeled in (B) in the absence of any heparin ligands for clarity. The five lowest energy arrangements of the heparin ligand are overlaid and are in close agreement with each other. The N-linked glycan stub (containing two GlcNAc residues) that is present in the BMP-7 structure is represented in stick form and labeled 'Carb.' in (B).

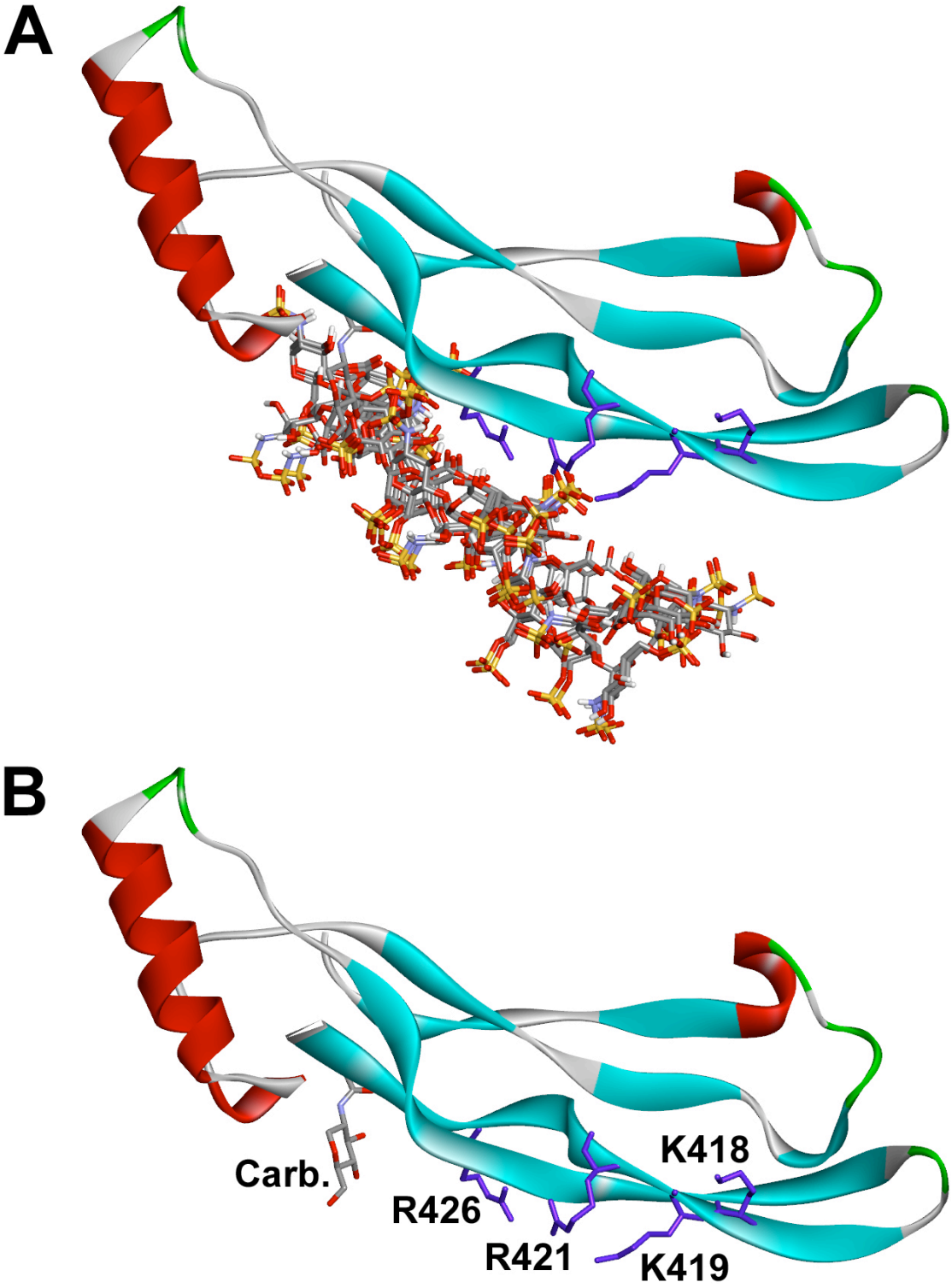

Figure 3.2 Molecular docking of a heparin endecasaccharide to a BMP-7 monomer
Please refer to the figure legend on the opposite page.

3.2.3.3 Docking of the heparin pentasaccharide ligands to the BMP-7 protein dimer

It can be seen in Figure 3.3 (and Table 3.1) that when the IdoA2S $^{1}C_{4}$ and $^{2}S_{0}$ heparin pentasaccharide structures were independently docked to the BMP-7 protein dimer, amino acid residues in the same region of finger 2 as found for the BMP-7 monomer before (section 3.2.3.1) were once again consistently predicted to be important for heparin-binding. However, due to the presence of both overlapping BMP-7 monomers, the results of the docking calculations differed from those seen before. Rather than docking across the lower face of a single monomer, both of the pentasaccharide ligands were predicted to bridge between the lower faces of the two disulphide-linked monomeric structures. In doing so, the ligands came in to contact with amino acids lying within the same region on both monomers.

As before, the results from both docking calculations predicted the involvement of the basic residues lysine 419, arginine 421 and arginine 426 in the heparin-binding site of BMP-7 (coloured purple in Figure 3.3 and labeled in the absence of any heparin ligands for clarity in Figure 3.4B). The contact of the heparin ligands with these residues also brought them into close proximity with a small number of additional amino acids, which were located in the same protein region. In the case of the IdoA2S $^{1}C_{4}$ pentasaccharide, these additional residues were asparagine 402 and alanine 403. As well as these two residues, the IdoA2S $^{2}S_{0}$ pentasaccharide also came into contact with threonine 399, glutamine 400, leucine 401 and asparagine 422.

The interaction energies that were reported for the lowest energy arrangements of the BMP-7 dimer-pentasaccharide complexes were -1142.32 kcal/mol (IdoA2S $^{1}C_{4}$) and -1148.03 kcal/mol (IdoA2S $^{2}S_{0}$). It can be seen in Table 3.1 that these values were slightly lower than those obtained for the monomer-pentasaccharide complexes, which were -1098.04 kcal/mol (IdoA2S $^{1}C_{4}$) and -1055.62 kcal/mol (IdoA2S $^{2}S_{0}$). As explained previously, this docking method places no emphasis on the accurate calculation of interaction energies. Despite this, relative to each other these results would appear to suggest that the docking of the pentasaccharide ligands between the two monomers of the BMP-7 dimer would be a little more energetically favourable.

The bridged dimer-pentasaccharide arrangements shown in Figure 3.3 had the potential to allow for twice the number of basic residue-heparin contacts that the

monomer-pentasaccharide complexes did. Therefore, one might have expected the dimer-pentasaccharide complexes to have been greatly preferred, and that this would have been demonstrated by these particular complex arrangements having considerably lower theoretical interaction energies than the monomer-pentasaccharide complexes. However, this was not the case as the energies reported were in fact quite similar.

Upon inspection of the docking calculation predictions, the likely reasons for the lack of a considerable difference between the interaction energies of the BMP-7 dimer-pentasaccharide and monomer-pentasaccharide complexes became apparent. Due to the limited length of the two pentasaccharide ligands employed, neither ligand was able to make contact with all of the previously mentioned predicted key basic residues on both monomers at the same time. Therefore, a preference was still displayed for making a greater number of contacts with one of the monomers than the other. This resulted in fewer basic residue-pentasaccharide contacts being made overall than it would first appear. Also, to accommodate the interaction with the additional BMP-7 monomer, the orientation of the docked pentasaccharides was altered from that preferred previously in the monomer-pentasaccharide complexes. Any considerable reduction in the theoretical interaction energy, which might have resulted from docking the pentasaccharide ligands to basic residues on both of the consituent monomers of BMP-7, may have been counteracted by this change in orientation.

Figure 3.3 Molecular docking of two heparin pentasaccharides to a BMP-7 dimer
Molecular docking calculations were performed using Autodock (version 2.4) to determine if/how two different heparin pentasaccharide ligands would interact with a BMP-7 dimer. In these ligands, all of the IdoA2S residues were fixed in either the $^{1}C_{4}$ conformation (A) or the $^{2}S_{0}$ conformation (B). It can be seen that the heparin pentasaccharides both docked between the bottom faces of the two constituent BMP-7 monomers, coming into close contact with K419, R421 and R426 on each subunit. The side chains of these residues (and K418) are shown in stick form and coloured purple. For clarity, they have also been shown and labeled in Figure 3.4B in the absence of any heparin ligands. In each case, the five lowest energy arrangements of the heparin ligands are overlaid and are in close agreement with each other, with the exception of one IdoA2S $^{2}S_{0}$ pentasaccharide ligand shown in (B). The N-linked glycan stub (containing two GlcNAc residues) that is present in the BMP-7 structure is represented in stick form and is also labeled 'Carb.' in Figure 3.4B.

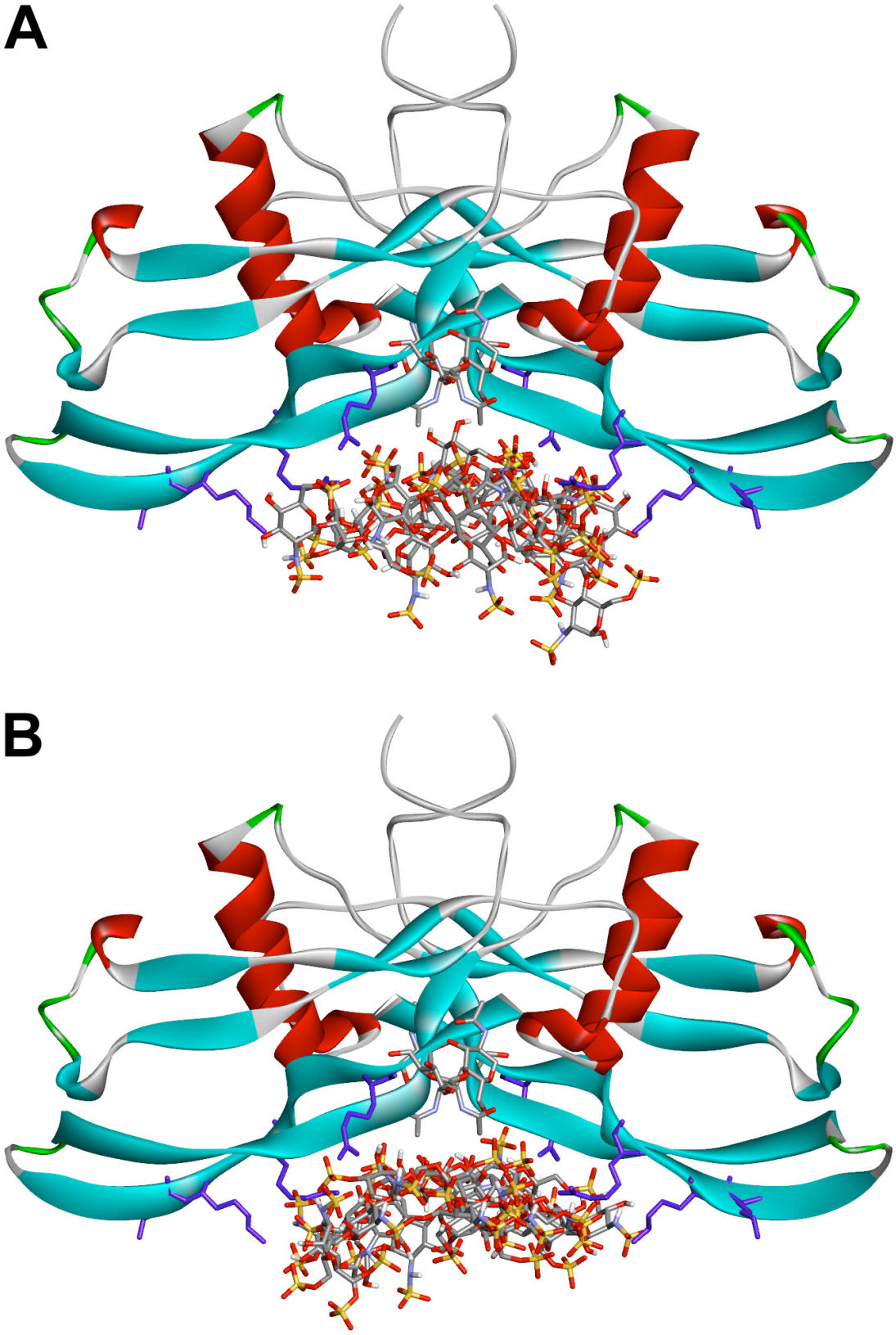

Figure 3.3 Molecular docking of two heparin pentasaccharides to a BMP-7 dimer
Please refer to the figure legend on the opposite page.

3.2.3.4 Docking of the heparin endecasaccharide ligand to the BMP-7 protein dimer

When the heparin endecasaccharide ligand was docked to the BMP-7 protein dimer, the heparin-binding site of BMP-7 was once again predicted to be localised to the same specific region of finger 2 that was described in section 3.2.3.1. In support of all three of the previous docking calculations, lysine 419, arginine 421 and arginine 426 were also predicted to be the key contributors of the basic charges that are necessary for binding to heparin/HS. Table 3.1 shows that in addition to these three basic residues, the orientation of the docked endecasaccharide ligand also brought it into close proximity with asparagine 402, alanine 403 and serine 405.

It can be seen in Figure 3.4A that the heparin endecasaccharide consistently docked to identical sites on both constituent monomers of the BMP-7 dimer, forming a bridge between them. As explained before in section 3.2.3.3, this was also the case when the pentasaccharide ligands were docked to the BMP-7 protein in its native dimeric form. However, unlike the pentasaccharide ligand structures, the heparin endecasaccharide was not so restricted in its chain length. Therefore, a single chain was able to make contact with most of the amino acid residues mentioned above on both monomers at the same time. As a result, the predicted interaction energy for the best-fit BMP-7 dimer-endecasaccharide complex arrangement, at -1925.43 kcal/mol, was substantially lower than those of the dimer-pentasaccharide complexes, which were -1142.32 kcal/mol (IdoA2S $^{1}C_{4}$) and -1148.03 kcal/mol (IdoA2S $^{2}S_{0}$).

In the predicted BMP-7 dimer-heparin endecasaccharide complex shown in Figure 3.4A, the heparin ligand docked across the lower face of the BMP-7 protein dimer in such a way that it passed through the middle of the two occupied glycosylation sites. The two present N-linked glycan stubs (each consisting of two GlcNAc residues) extended outwards and away from the docked ligand from opposite sides of the structure. Therefore, it would appear from this prediction that such a complex would be both energetically and sterically feasible, and that the presence of the attached glycan chains would not provide an obstruction and prevent its formation.

Overall, the docking calculations described in this chapter predicted that the C-terminal basic residues lysine 419, arginine 421 and arginine 426 would be most likely to form the core component of the heparin-binding site of BMP-7. This suggested that these residues would be ideal initial targets for mutagenesis

experiments. The docking calculations also suggested that the dimer-endecasaccharide complex shown in Figure 3.4A, in which the two monomers formed a cooperative heparin-binding site, would be the most energetically favourable BMP-7-heparin ligand arrangement.

Figure 3.4 Molecular docking of a heparin endecasaccharide to a BMP-7 dimer
A molecular docking calculation was performed using Autodock (version 2.4) to determine if/how a heparin endecasaccharide ligand would interact with a BMP-7 dimer. (A) It can be seen that the heparin endecasaccharide docked across the bottom faces of the two constituent BMP-7 monomers, coming into close contact with K419, R421 and R426 on each subunit. The side chains of these residues (and K418) are shown in stick form, coloured purple, and have been labeled in (B) in the absence of any heparin ligands for clarity. The five lowest energy arrangements of the heparin ligand are overlaid and are in close agreement with each other. The N-linked glycan stub (containing two GlcNAc residues) that is present in the BMP-7 structure is represented in stick form and labeled 'Carb.' in (B).

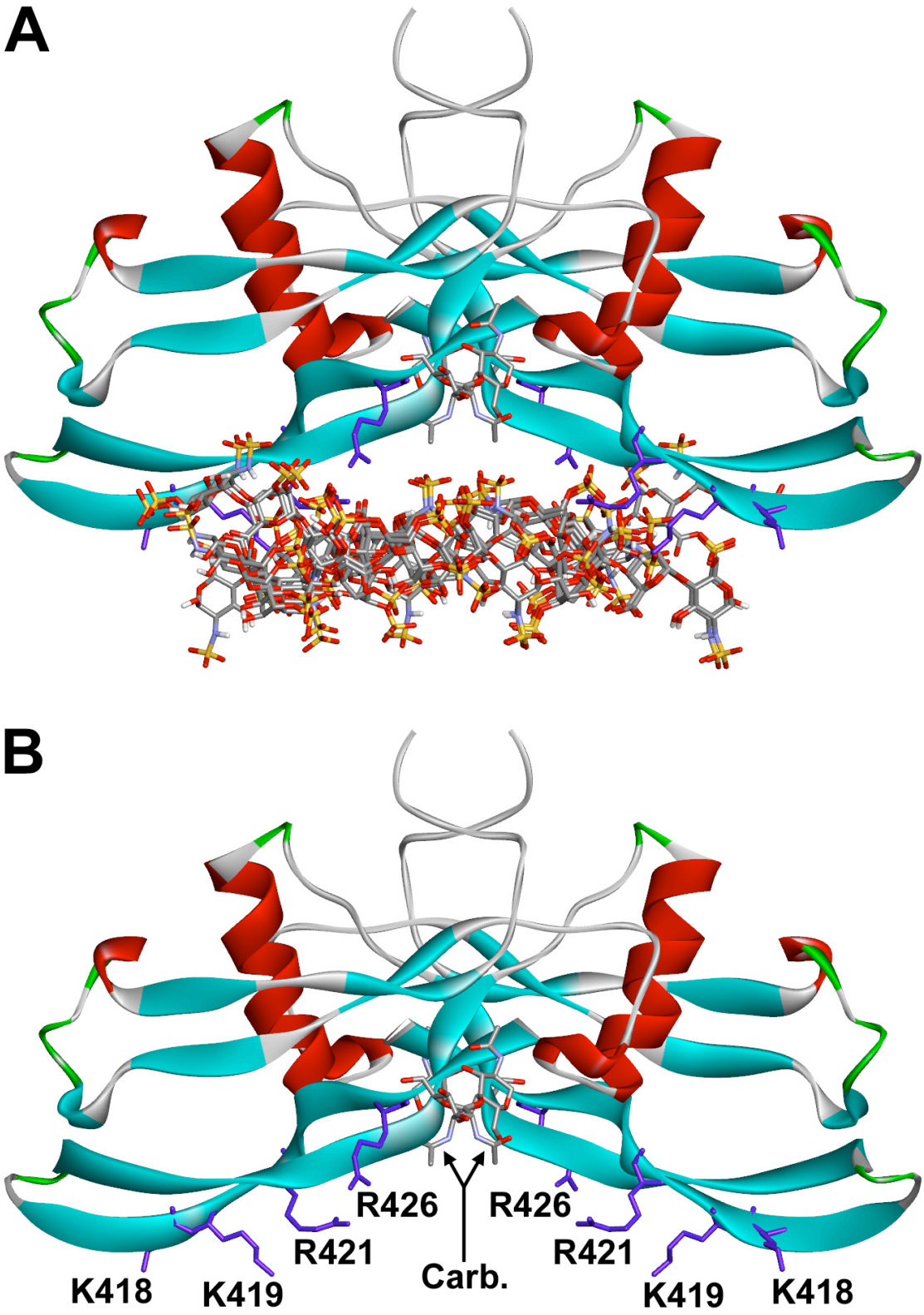

Figure 3.4 Molecular docking of a heparin endecasaccharide to a BMP-7 dimer
Please refer to the figure legend on the opposite page.

3.2.3.5 Docking of the heparin endecasaccharide ligand to a BMP-7 mutant protein created *in silico*

As mentioned above in section 3.2.3.4, the docking calculations that were previously carried out pinpointed lysine 419, arginine 421 and arginine 426 as being ideal targets for site-directed mutagenesis experiments. Prior to carrying out such experiments, docking calculations were performed to predict the effect that substituting these C-terminal basic residues, which are situated in finger 2 of BMP-7, would have on its heparin-binding ability. However, before doing so, it was first necessary to plan and create a suitable BMP-7 mutant protein *in silico*.

The predictions that were made by the previous docking calculations suggested that as many as 6 basic residues (3 on each monomer) might take part in the binding interaction between BMP-7 and heparin/HS. To maximise the chance of reducing the heparin/HS-binding affinity of BMP-7, whilst hopefully maintaining the structural integrity of the protein, the decision was made to make substitutions of these predicted key residues in pairs. This would result in a reduction of the number of predicted basic contact residues in the C-terminal region by two-thirds. Only one of the predicted key basic residues would remain on each monomer, which would be insufficient to form a heparin/HS-binding site even if the protein monomers were to bind cooperatively to a single oligosaccharide chain. Alanine residues were selected as replacement residues due to them possessing small methyl groups as side chains, which are both structurally and chemically simple. With such properties, it was thought that the introduction of these residues would not disrupt the BMP-7 protein structure, which is constrained by three intra-chain disulphide bridges. The docking calculations described previously suggested that atoms from lysine 419 and arginine 421 would make the highest number of contacts with the heparin oligosaccharide ligands (data not shown). Therefore, this was the first pair of basic amino acids selected for substitution to alanine both theoretically and experimentally. These amino acid substitutions were made in the human BMP-7 structure 1M4U (Groppe *et al.*, 2002), using the Biopolymer module of the Insight II software package (Accelrys, San Diego, CA, USA).

Having produced the BMP-7 K419A/R421A mutant protein *in silico*, the heparin endecasaccharide ligand was docked to it to predict the effect that the double substitution would have on the heparin-binding ability of BMP-7. The protein-

oligosaccharide complex that resulted from this docking calculation is shown in Figure 3.5A. It can be seen that the heparin endecasaccharide consistently docked to and formed a bridge between identical regions of finger 2 on each monomer. This was also true when the same ligand was docked to the wildtype BMP-7 protein dimer (section 3.2.3.4). However, due to the absence of lysine 419 and arginine 421 from the mutant protein, arginine 426 was the only suitably oriented basic contact residue on each monomer. As a consequence, the angle of the docked endecasaccharide ligand was altered to enable close contact to be made with both of the available basic arginine 426 residues. The orientation of the docked ligand also brought it into close proximity with glutamine 400, leucine 401 and asparagine 402. More importantly, the reduction in the number of basic residues by two-thirds resulted in a substantial increase in the value of the predicted interaction energy for the best-fit complex arrangement, from the previous -1925.43 kcal/mol to +273.73 kcal/mol. As the interaction energy of this complex was predicted to be greater than zero kcal/mol, its formation would be highly unfavourable. The results that were obtained when the heparin pentasaccharide ligands were docked to the same BMP-7 mutant structure were also very similar (data not shown). Based on these predictions, it would appear unlikely that a BMP-7 K419A/R421A mutant protein would be capable of binding to heparin/HS. Therefore, lysine 419 and arginine 421 were deemed to be suitable initial targets for substitution in experimental site-directed mutagenesis studies.

Figure 3.5 Molecular docking of a heparin endecasaccharide to a BMP-7 K419A/R421A mutant dimer

To predict the effect that the removal of K419 and R421 would have on the HS/heparin-binding ability of BMP-7, a mutant BMP-7 protein was produced *in silico* using the Biopolymer module of the Accelyrys Insight II software package. In this mutant, the K419 and R421 residues on each monomer were substituted for alanine residues. A molecular docking calculation was then performed using Autodock (version 2.4) to determine if/how a heparin endecasaccharide ligand would interact with the BMP-7 K419A/R421A mutant dimer. (A) It can be seen that despite the absence of K419 and R421, the heparin endecasaccharide continued to dock across the bottom faces of the two constituent mutant BMP-7 monomers, albeit in a different orientation in order to accommodate contact with R426 on each subunit. Even so, the results from the docking calculation suggest such an interaction would be energetically unfavourable. The five lowest energy arrangements of the heparin ligand are overlaid and are in close agreement with each other. The side chains of K418 and R426 are shown in stick form and coloured purple. The side chains of A419 and A421 are shown in stick form and coloured pink. For clarity, these residues have also been labeled in (B) in the absence of any heparin ligands.

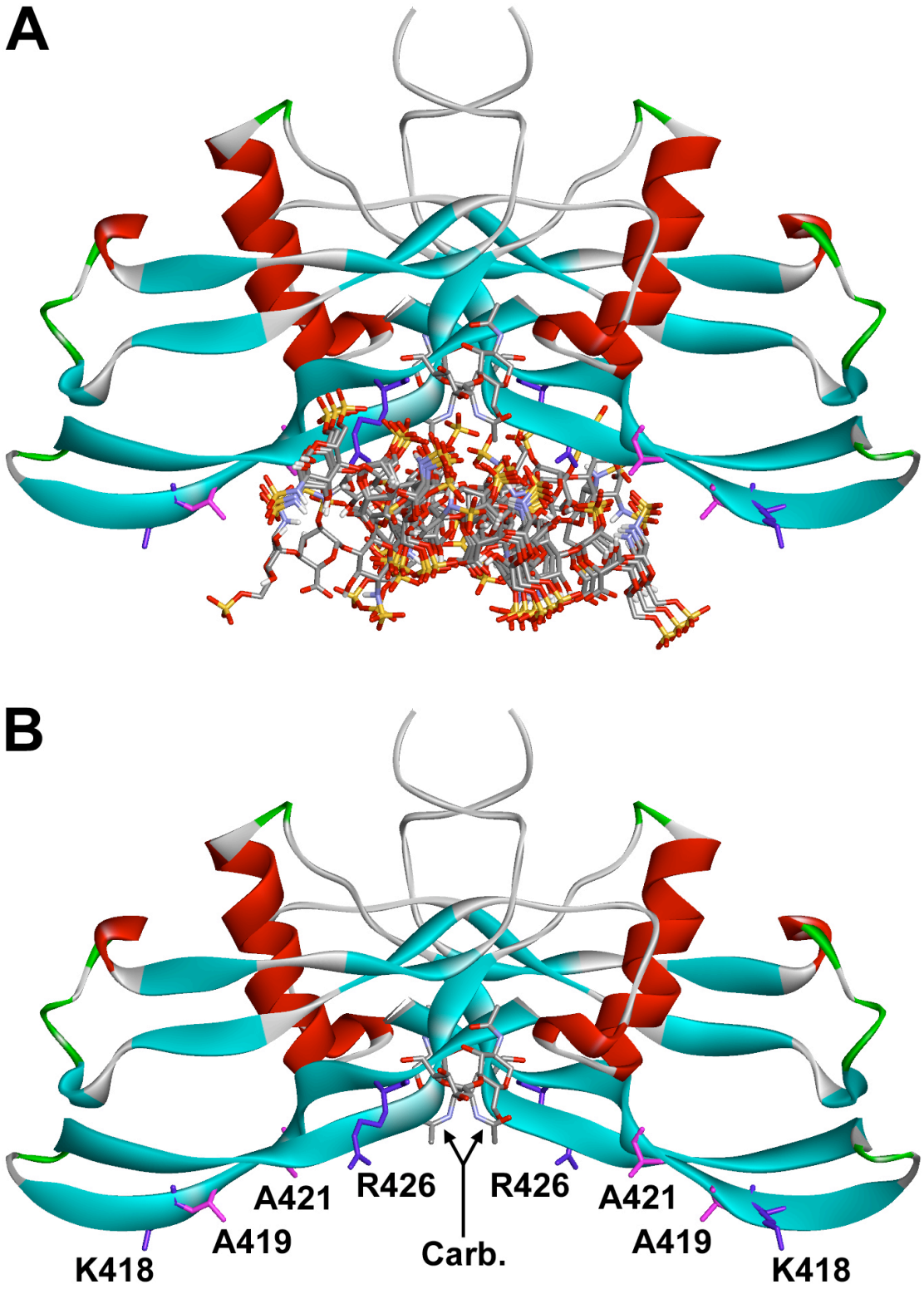

Figure 3.5 Molecular docking of a heparin endecasaccharide to a BMP-7 K419A/R421A mutant dimer
Please refer to the figure legend on the opposite page.

Table 3.1 Docking calculation summary
A summary of the residues on monomeric and dimeric BMP-7 protein structures that were predicted to come into closest contact with the heparin pentasaccharide and endecasaccharide ligands. The predicted interaction energies are also provided.

BMP-7 PDB structure (monomer or dimer)	BMP-7 residues predicted to lie within 3.5 Å of the docked heparin ligand			Lowest predicted intermolecular interaction energies (kcal/mol)		
	Heparin pentasaccharide		Heparin endecasaccharide	Heparin pentasaccharide		Heparin endecasaccharide
	IdoA2S $^1C_4$	IdoA2S $^2S_0$		IdoA2S $^1C_4$	IdoA2S $^2S_0$	
1LXI (monomer)	ASN 402 ALA 403 SER 405 **LYS 419** **ARG 421** **ARG 426**	ASN 402 ALA 403 **LYS 419** **ARG 421** **ARG 426**	**LYS 332** GLN 400 ASN 402 **LYS 419** **ARG 421** **ARG 426** ALA 427	-1098.04	-1055.62	-1362.17
1M4U (dimer)	ASN 402 ALA 403 **LYS 419** **ARG 421** **ARG 426**	THR 399 GLN 400 LEU 401 ASN 402 ALA 403 **LYS 419** **ARG 421** ASN 422 **ARG 426**	ASN 402 ALA 403 SER 405 **LYS 419** **ARG 421** **ARG 426**	-1142.32	-1148.03	-1925.43

Table 3.1 Docking calculation summary
Please refer to the table legend on the opposite page.

Overall, the results obtained from this predictive study suggested that a C-terminal cluster of basic lysine 419, argine 421 and argine 426 residues in each monomeric unit of the BMP-7 protein may play a key part in its interaction with HS/heparin. These results also suggested that in the absence of some of these basic residues, the mature BMP-7 protein does not contain any alternative residue clusters with the necessary characteristics to bind heparin/HS. However, there is an important caveat to this conclusion. As mentioned previously, the N-terminal extension of the mature BMP-7 protein was unresolved in all of the available X-ray crystal structures. Consequently, this protein region and the cluster of basic residues located within it (Figure 1.8) were absent from the structures that were used to carry out the docking calculations. This was a limitation of all the predictive calculations that were conducted. Therefore, the possibility that the unresolved N-terminal region may also have the capacity to bind heparin/HS could not be disregarded based on the outcome of docking calculations alone and required experimental investigation.

Chapter 4: The expression of recombinant human BMP-7 and mutant variants thereof

4.1 Introduction

The results obtained from the molecular docking calculations that were discussed in Chapter 3 predicted that BMP-7 binds to HS/heparin GAGs through three basic residues that are situated close to the C-terminal ends of each of its constituent monomers (K419, R421 and R426). These docking calculations also predicted that BMP-7 would not be able to bind to HS/heparin in the absence of both K419 and R421. In order to test the validity of these predictions experimentally using a site-directed mutagenesis approach, it was necessary to express mutant BMP-7 variants. However, despite the wildtype BMP-7 protein being commercially available, the decision was made to express this protein first to optimise the expression conditions. It was also thought that expressing the wildtype BMP-7 protein as a control alongside mutant variants would provide an indication as to whether or not the mutations that were made had any effect on the expression levels of these proteins. Such insight can be especially informative in the event that difficulties are encountered when attempting to express particular muteins.

Prior to commencing these expression experiments, it was necessary to select a suitable cell line to use to express the required recombinant BMP-7 proteins. In previous studies, much success was had when the wildtype BMP-7 protein was expressed in stably transfected Chinese hamster ovary (CHO) cells (Sampath *et al.*, 1992; Jones *et al.*, 1994). Upon characterising the expressed BMP-7 protein, it was found that it was glycosylated, dimerised, processed and secreted correctly. The protein was also demonstrated to be functional and was consequently deemed to be correctly folded. This has since been confirmed by X-ray crystallography (Griffith *et al.*, 1996; Groppe *et al.*, 2002; Greenwald *et al.*, 2003). Therefore, it was decided that the same cell line and expression approach would be adopted for use during this investigation. Once this decision had been made, a BMP-7 cDNA clone was sourced

and inserted into an appropriate mammalian expression vector using PCR (polymerase chain reaction) and a number of DNA manipulation techniques. This newly constructed expression cassette was then transfected into CHO cells to express the recombinant wildtype BMP-7 protein. To produce mutant BMP-7 variants, the BMP-7 cDNA sequence was modified accordingly. A detailed account of this work and the procedures involved is provided within this Chapter.

4.2 Results and discussion

4.2.1 Commercial BMP-7 cDNA clone

A 1814 base pair (bp) cDNA clone of human BMP-7 (I.M.A.G.E ID: 4183402, GenBank accession: BC008584), was purchased from Geneservice Limited (Cambridge, UK). This cDNA clone contained the complete coding sequence of human BMP-7 (1296 bp), along with a 41 bp untranslated region upstream (5' UTR) of the start codon and a 477 bp untranslated region downstream (3' UTR) of the stop codon (Figure 4.1). The clone was provided as a 5'-SalI / 3'-NotI oriented insert in the 4396 bp pCMV-SPORT6 vector (Invitrogen, Figure 4.3), in the form of a bacterial stab culture. Upon receipt, the culture was streaked onto a fresh agar plate containing ampicillin and incubated overnight at 37 ºC to obtain single colonies. A colony was picked, grown up as a liquid culture, and the DNA was isolated and purified by carrying out a DNA maxi-prep.

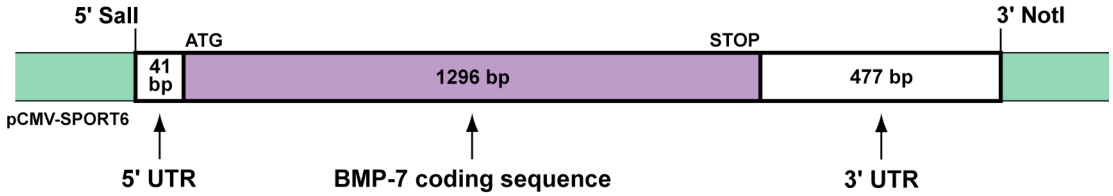

Figure 4.1 Commercial BMP-7 cDNA clone
A BMP-7 cDNA clone (GenBank accession: BC008584) was purchased from Geneservice Limited containing the full coding sequence of human BMP-7 (1296 bp), a 41 bp 5' UTR and a 477 bp 3' UTR. The cDNA was provided in the pCMV-SPORT6 vector, inserted via the SalI (5') and NotI (3') restriction sites in its multiple cloning site.

4.2.2 Characterisation of the BMP-7 cDNA clone

To confirm that the purchased BMP-7 cDNA clone was the correct size, 1 µg of the maxi-prep DNA was tandem digested with the restriction enzymes NotI and SalI. Agarose gel electrophoresis of the digestion products revealed that the liberated BMP-7 cDNA clone was of the expected 1814 bp size, with the 4396 bp pCMV-SPORT6 vector band also present in the expected size region (Figure 4.2).

The purchased construct was also sent for DNA sequence analysis using T7 and SP6 primers (all primer sequences provided in Chapter 2, Table 2.1) that annealed to promoter sequences found within the pCMV-SPORT6 vector. A ClustalW sequence alignment was then carried out to compare the sequencing results against a human BMP-7 cDNA reference sequence (GenBank accession: NM_001719). This confirmed that the supplied BMP-7 cDNA was identical to the reference sequence and was therefore absent of any errors.

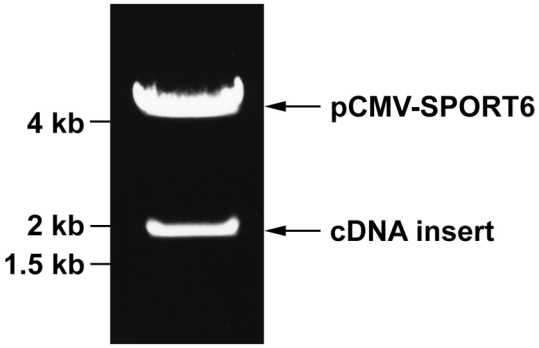

Figure 4.2 Restriction digestion of the BMP-7 cDNA clone
1 µg of the plasmid maxi-prep DNA, containing the human BMP-7 cDNA clone in the pCMV-SPORT6 vector, was restriction digested with the NotI and SalI enzymes. The digestion products were analysed by agarose gel electrophoresis, revealing two bands of the appropriate size corresponding to the 1814 bp cDNA insert and 4396 bp pCMV-SPORT6 vector.

4.2.3 Cloning strategy

The purchased BMP-7 cDNA was provided in the pCMV-SPORT6 mammalian expression vector (Figure 4.3A). This vector does not contain an

antibiotic resistance gene that could be used for the selection of mammalian cells following transfection, therefore making it unsuitable for the generation of stable cell lines. In order to confer antibiotic resistance to cells expressing the BMP-7 protein, the cDNA was cloned into pIRESbla (Figure 4.3B) using the procedures described below. pIRESbla is a mammalian expression vector that contains the gene for blasticidin resistance. pIRESbla also contains an internal ribosome entry site (IRES) sequence from the Encephalomyocarditis virus (ECMV). This allows the ribosomes to initiate translation in the middle of a bicistronic messenger RNA (mRNA) sequence during protein synthesis, rather than just at the 5' end where 5' cap recognition is usually required. This has the benefit of permitting the translation of two open reading frames from a single mRNA sequence. In this case, it enabled the expression of both the inserted cDNA and the resistance gene to be driven from the same constitutively active human cytomegalovirus (CMV) major immediate-early promoter/enhancer sequence. Having both genes present on the same mRNA transcript allows the antibiotic to exert selective pressure on the whole expression cassette. Therefore, a high dose of antibiotic will select only the cells that are expressing a high level of the gene of interest. This helps to ensure that nearly all of the surviving cells will stably express the BMP-7 gene following selection with blasticidin without having to isolate and characterise clonal cell lines.

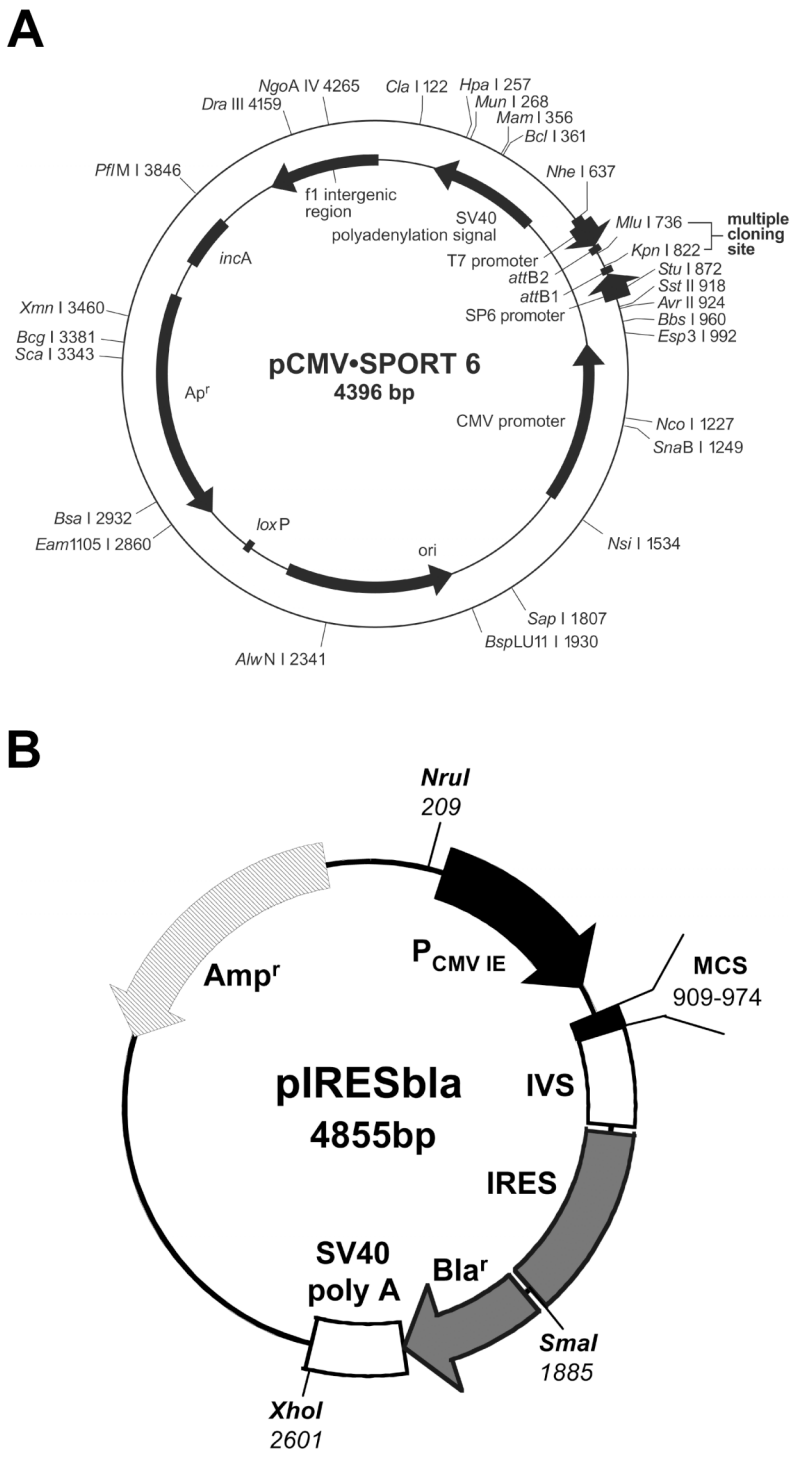

Figure 4.3 pCMV-SPORT6 and pIRESbla expression vectors
pCMV-SPORT6 (A) and pIRESbla (B) both contain multiple cloning sites (MCS) into which cDNA coding sequences can be inserted to express proteins under the control of the CMV promoter, as well as a gene encoding for ampicillin resistance for the selection of bacterial transformants. pIRESbla also contains a blasticidin resistance gene to enable the generation of stable mammalian cell lines. (pCMV-SPORT6 image taken from the Invitrogen pCMV-SPORT6 product manual, pIRESbla image adapted from a vector map produced by Chris Ball, NIBSC).

4.2.3.1 PCR amplification of the BMP-7 cDNA

The first cloning step entailed PCR amplifying the required regions of the BMP-7 cDNA, including the full 1296 bp coding sequence and the 41 bp 5' untranslated region (5' UTR). The 5' UTR was included as it contains the native ribosomal binding site immediately upstream of the start codon, which is required for the initiation of protein translation. The 3' UTR was excluded as these regions often contain regulatory sequences (Mazumder *et al.*, 2003; Sampath *et al.*, 2003) that could function to counteract efforts to overexpress the BMP-7 protein. 3' UTRs also have a role in mRNA stability and contain polyadenylation signals. However, the pIRESbla vector already has an incorporated synthetic intron that is known to enhance mRNA stability, and it also includes the Simian vacuolating virus 40 (SV40) polyadenylation signal. Therefore, it was not necessary to include these components in the amplified and cloned cDNA insert.

As shown in Figure 4.4, the BMP-7 cDNA was PCR amplified with the BMP7WT1-S and BMP7WT-A sense and antisense primers respectively. This amplification was performed using the proofreading Platinum *Pfx* DNA polymerase (Invitrogen) to ensure that high sequence fidelity was obtained in the amplification product. To facilitate the insertion of the amplified cDNA sequence into the multiple cloning site of the pIRESbla vector, BamHI restriction sites were included in short non-annealing sequences at the 5' ends of the primers. Agarose gel electrophoresis of the PCR product showed that the amplification was successful, producing a single band in the region of 1.35 kilobase (kb) pairs in size as expected (Figure 4.4). This product was purified using a PCR product purification kit (Qiagen).

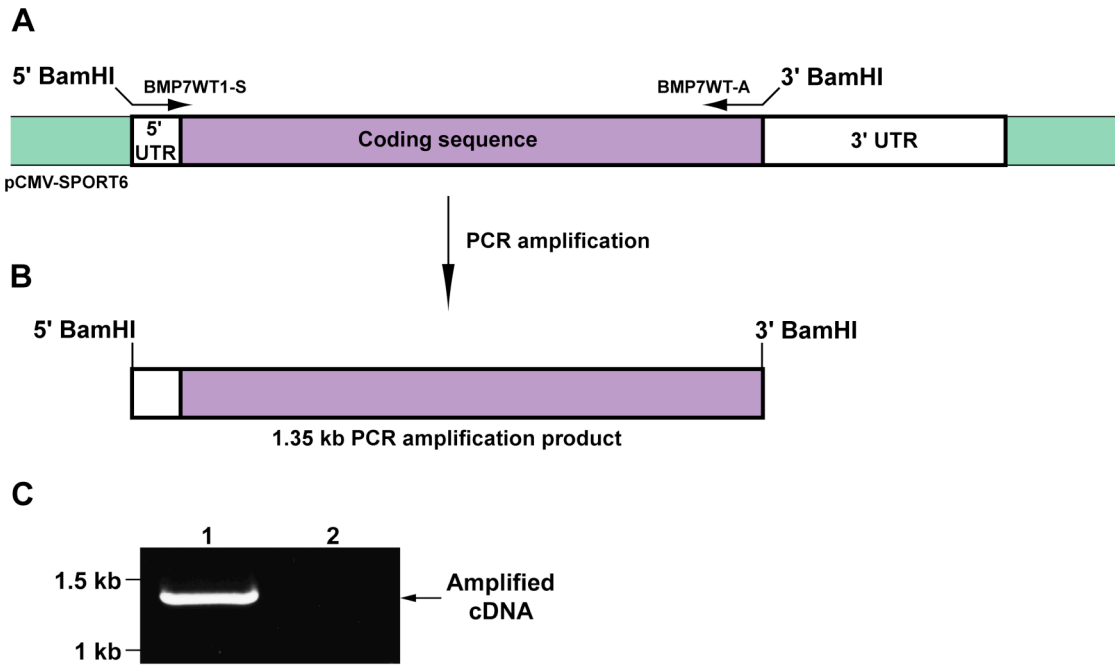

Figure 4.4 PCR amplification of the BMP-7 cDNA
The 1296 bp coding sequence and 41 bp of the 5' UTR of human BMP-7 were PCR amplified using the BMP7WT1-S and BMP7WT-A primers (A), to produce a 1.35 kb PCR amplification product, with BamHI sites introduced by the primers at both the 5' and 3' ends (B). (C) Agarose gel electrophoresis of the PCR product confirmed that the amplification was successful, producing a single band in the region of 1.35 kb in size (lane 1). In the absence of template DNA, no band was produced in the negative control reaction (lane 2).

4.2.3.2 Cloning PCR products using the pGEM-T Vector System

As restriction endonuclease enzymes generally cut PCR products directly with low efficiency when their specific recognition sites are located close to the termini of the DNA sequences, the newly synthesised DNA was sub-cloned using the pGEM-T Vector System (Promega, Figure 4.5) prior to being ligated into the pIRESbla vector. Inserting PCR products into the pGEM-T vector serves to increase the efficiency of digestion and also provides a convenient way to sequence the PCR product, and to grow it up if required at a later date without risking the introduction of PCR errors.

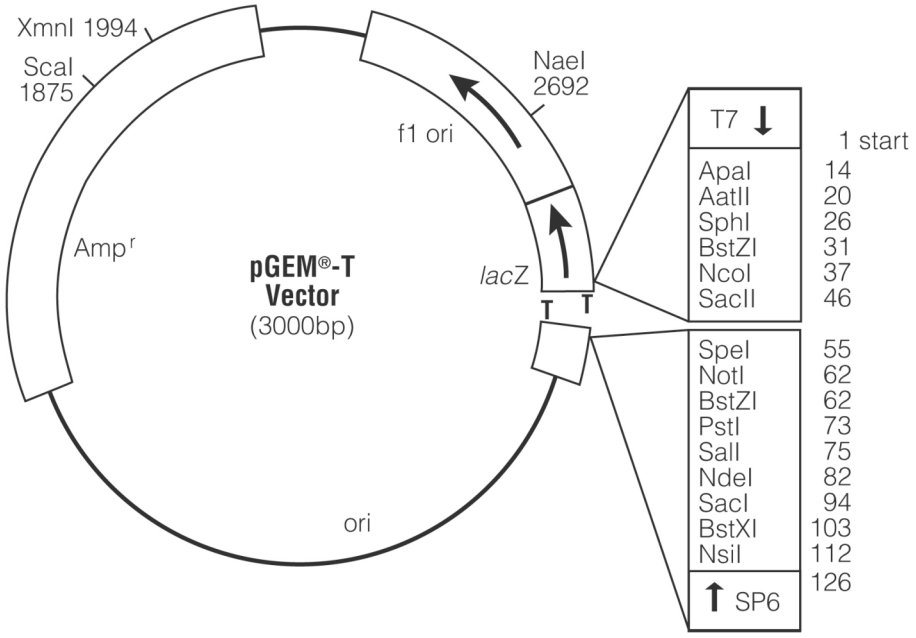

Figure 4.5 pGEM-T sub-cloning vector
With its single 3'-T overhangs, the pGEM-T vector provides a convenient way to sub-clone PCR products that possess a compatible 3'-A overhang. (Image taken from the Promega pGEM-T product manual).

The 3 kb pGEM-T vector is supplied linearised, with 3' terminal thymidines added to each end. The single 3'-T overhangs at the DNA insertion site provide a compatible overhang for the ligation of PCR products generated using DNA polymerases that add a single 3' deoxyadenosine in a template-independent manner. However, because the BMP-7 cDNA was amplified using a proofreading DNA polymerase, which produce blunt-ended PCR fragments without the required 3'-A overhangs, these overhangs were added in another reaction using GoTaq DNA Polymerase (Promega) and dATP. The PCR product was then ligated into the pGEM-T vector (Figure 4.6) and transformed into competent DH5α E. coli cells. Four white colonies were picked from the agar plate, grown up in liquid cultures, and recombinant plasmid DNA was isolated by carrying out DNA mini-preps. To confirm the presence of the BMP-7 cDNA insert, the purified plasmid DNA from each of the four liquid cultures was digested with BamHI and analysed by carrying out agarose gel electrophoresis (Figure 4.7). The presence of both a 3 kb vector band and a 1.35 kb insert band was indicative of a successful ligation. The recombinant pGEM-T

plasmid DNA containing the BMP-7 insert was sent for sequence verification using its incorporated T7 and SP6 primer sites, which confirmed that the insert was absent of any sequence errors.

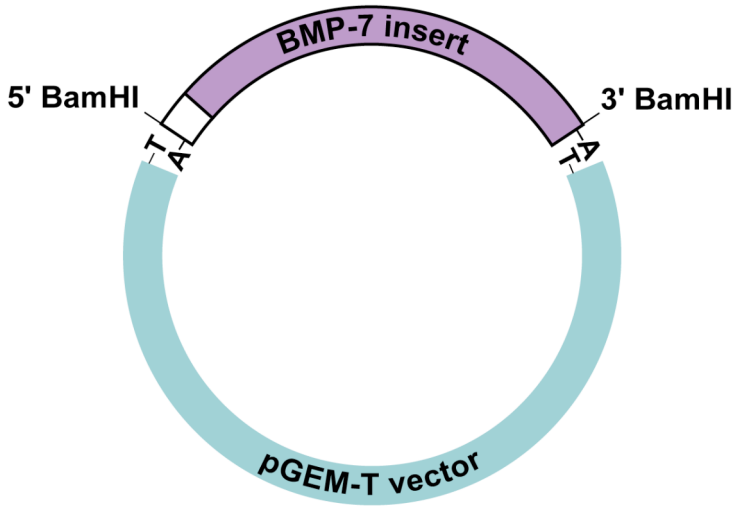

Figure 4.6 Cloning the BMP-7 cDNA into pGEM-T
A-overhangs were added to the 3' ends of the amplified BMP-7 cDNA, and a ligation reaction was carried out to insert the BMP-7 cDNA into the pGEM-T vector via its single T-overhangs.

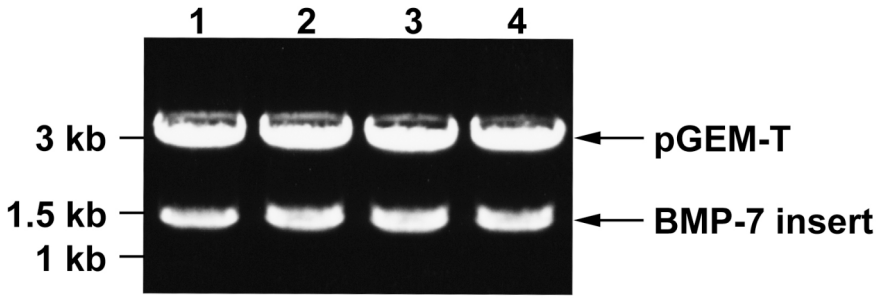

Figure 4.7 Confirming the presence of the BMP-7 cDNA insert in pGEM-T
2 µg of mini-prep DNA from each of four liquid DH5α *E. coli* cultures was digested with BamHI to confirm the presence of a BMP-7 cDNA insert within the pGEM-T vector. The digestion products were analysed by agarose gel electrophoresis (lanes 1-4). The presence of two bands at 3 kb and 1.35 kb in size in each lane, corresponding to the pGEM-T vector and BMP-7 insert respectively, indicated that the ligation was successful with each clone containing the BMP-7 cDNA.

4.2.3.3 Cloning the BMP-7 cDNA into pIRESbla

The amplified BMP-7 cDNA insert was released from the pGEM-T vector by carrying out a restriction digestion with the enzyme BamHI, utilising the sites that had been introduced in the PCR primers at both the 5' and 3' ends of the sequence (Figure 4.8). The pIRESbla vector was linearised by digestion in the same way to create a compatible site for ligation, and both digestion products were electrophoresed in separate tracks of an agarose gel. The 1.35 kb BMP-7 insert band and the 4.85 kb pIRESbla vector band were then carefully excised from the gel and purified from the gel slice using a QIAquick Gel Extraction Kit (Qiagen). To prevent the BamHI digested vector from recircularising in the absence of a DNA insert, the vector was treated with alkaline phosphatase. After quantifying the DNA, a ligation reaction was carried out to insert the BMP-7 cDNA fragment into the prepared pIRESbla vector, via the BamHI site within its multiple cloning site. 1 µl of the ligation reaction mixture was transformed into competent DH5α *E. coli* cells and six colonies were picked from the agar plate and grown up in 5 ml liquid cultures. Recombinant plasmid DNA was isolated by carrying out DNA mini-preps, and a BamHI digestion was carried out, which confirmed the presence of a BMP-7 insert in the plasmid DNA isolated from each of the six clones of transformed cells (data not shown).

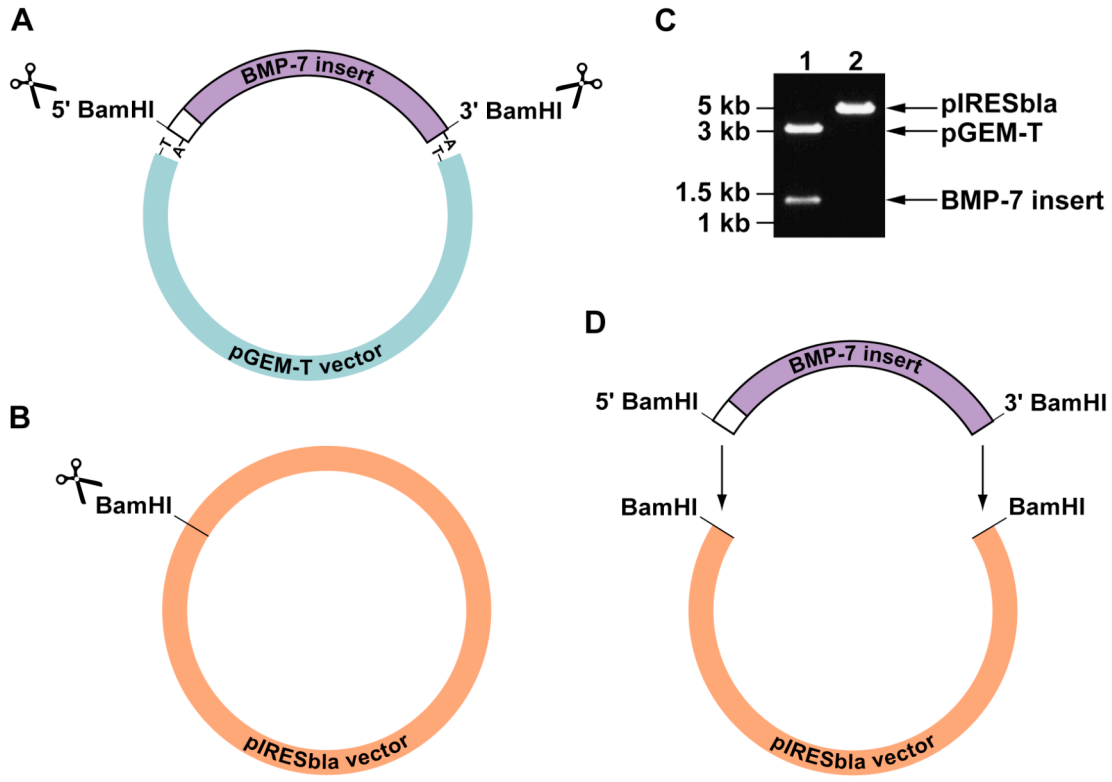

Figure 4.8 Cloning the BMP-7 cDNA into pIRESbla
(A) The BMP-7 cDNA insert was released from the pGEM-T vector by carrying out a digestion with the BamHI restriction enzyme. (B) The pIRESbla expression vector was also digested with BamHI within its multiple cloning site, to produce compatible ends for ligation with the digested BMP-7 cDNA. (C) The digestion products were run on a 1 % agarose gel in separate tracks. Digestion of the pGEM-T vector that contained the BMP-7 insert produced two bands of 3 kb and 1.35 kb in size respectively (lane 1). Digestion of the pIRESbla vector via its single BamHI site resulted in a band of 4.85 kb in size (lane 2). (D) A ligation reaction was carried out to insert the BMP-7 cDNA into the pIRESbla vector via the prepared BamHI sites.

4.2.3.3.1 Confirming the orientation of the BMP-7 insert

Because the BMP-7 cDNA was inserted into the pIRESbla vector non-directionally using a BamHI site at both the 5' and 3' ends, it was possible for the insert to ligate in either the correct 5'-3' orientation or the reverse 3'-5' orientation. The CMV promoter drives expression in the pIRESbla vector in a directional manner, requiring the ATG start codon at the 5' end of the sense strand of the inserted cDNA to be downstream of the promoter sequence in order for expression to occur.

Therefore, it was important to ensure that the BMP-7 cDNA insert was not only present in the pIRESbla vector, but also in the correct orientation.

This was accomplished using a PCR-based approach, where the sense primer (pIRESbla-S) was located outside of the BMP-7 insert, adjacent to the 5' end of the multiple cloning site of the pIRESbla vector and directed towards the insert. The antisense primer (BMP7WT-A) was located within the BMP-7 cDNA insert, at the 3' terminal end (Figure 4.9). Purified mini-prep DNA isolated from the transformed DH5α *E. coli* cells was used as a template, and the PCR reaction products were electrophoresed on 1 % agarose gels (Figure 4.9C). In the case that the BMP-7 cDNA insert had ligated into the pIRESbla vector in the correct 5'-3' orientation, the PCR reaction yielded a product of 1.4 kb in size. However, if the insert was in the reverse orientation, no amplification product would be produced from the reaction as a result of the primers being directed the same way rather than towards each other. Figure 4.9C shows that both clones 2 and 3 contained a BMP-7 cDNA insert in the correct orientation, indicated by the presence of a 1.4 kb PCR product. The plasmid DNA from clone 2 was scaled-up in preparation for transfection by carrying out an endotoxin-free DNA maxi-prep, and was sent for sequencing using the pIRESbla-S and pIRESbla-A primers, which confirmed that the insert DNA was absent of any errors.

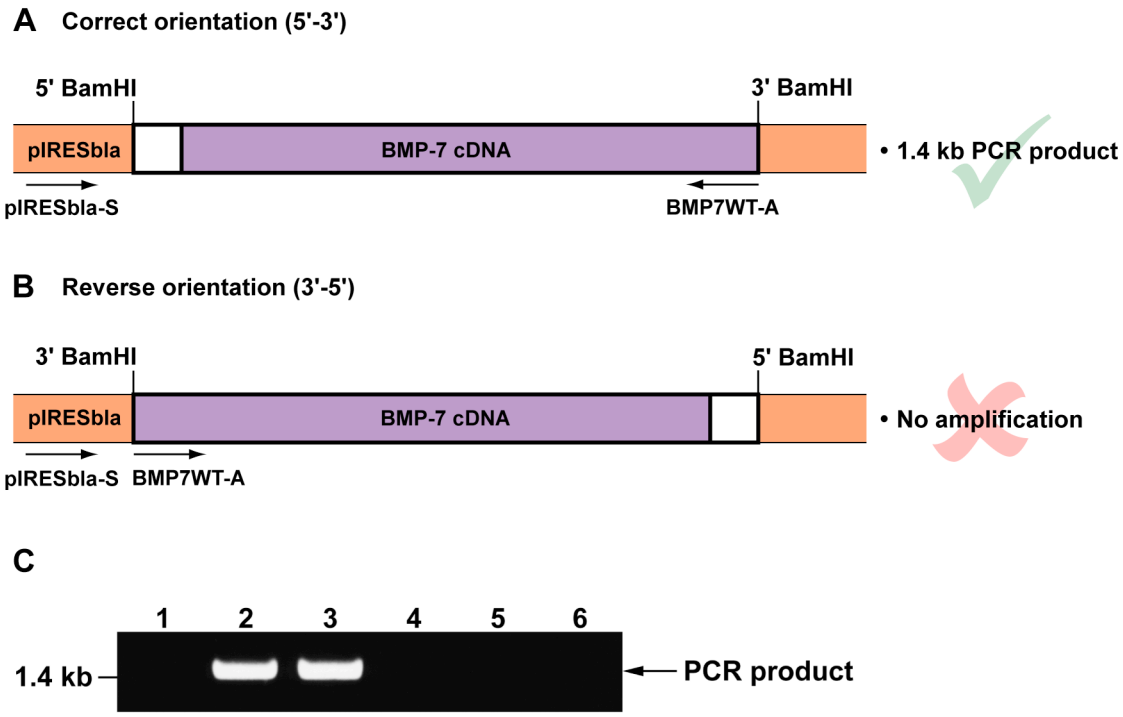

Figure 4.9 Determining the BMP-7 cDNA orientation within pIRESbla
A PCR reaction was carried out on the plasmid DNA from six clones of transformed cells, to determine the orientation that the BMP-7 cDNA insert had ligated into the pIRESbla vector. The pIRESbla-S and BMP-7WT-A primers were used, annealing to sequences within the pIRESbla vector and BMP-7 insert respectively. (A) The BMP-7 cDNA insert ligated into the pIRESbla vector in the correct orientation, with the primers directed towards each other, produced a 1.4 kb amplification product. (B) The BMP-7 cDNA insert ligated into the pIRESbla vector in the reverse orientation, with the primers directed the same way, produced no amplification product. (C) Agarose gel electrophoresis of the PCR products showed that clones 2 and 3 both contained a BMP-7 insert in the correct orientation, producing an appropriately sized 1.4 kb band.

4.2.4 Detection of the BMP-7 protein by ELISA

When carrying out studies that involve the expression of recombinant proteins, it is important that suitable methods are in place to detect the presence and determine the quantity of the expressed protein of interest. Therefore, the human BMP-7 DuoSet ELISA kit (R&D Systems) was utilised for the detection of the BMP-7 protein in cell culture supernatants and cell lysates following transfection experiments. This assay was calibrated using highly purified recombinant human BMP-7 produced in CHO cells by R&D Systems. To determine the sensitivity of the assay, a standard curve was

produced using a range of BMP-7 concentrations from 0 to 1000 pg/ml, with each standard loaded in duplicate. Figure 4.10 shows that the assay remained sensitive in detecting BMP-7 at concentrations as low as 31.25 pg/ml, and that the background absorbance was minimal.

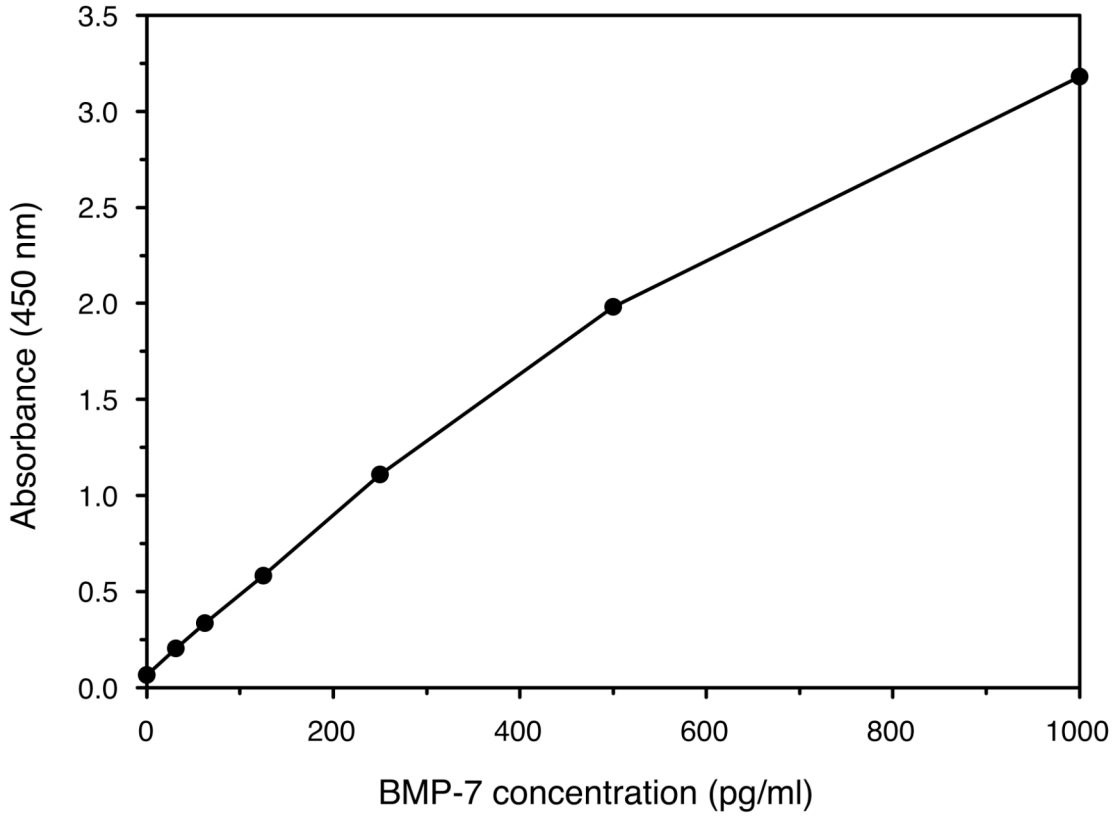

Figure 4.10 BMP-7 ELISA standard curve
A standard curve of recombinant human BMP-7 concentrations, from 0 to 1000 pg/ml, was produced to determine the sensitivity of the R&D Systems BMP-7 DuoSet ELISA assay. The assay sensitively detected the BMP-7 at concentrations as low as 31.25 pg/ml. A minimal amount of background absorbance was seen, and the result shown remained consistent throughout.

4.2.5 Stable transfection of CHO-K1 cells with the pIRESbla/BMP-7 vector

Adherent CHO-K1 cells were transfected with the pIRESbla expression vector containing the cloned BMP-7 cDNA insert (pIRESbla/BMP-7). At the same time,

control transfections were also carried out. These were an empty pIRESbla vector only transfection without insert DNA, and a sham transfection using the transfection reagent alone in the absence of any DNA. Approximately 24 hours post-transfection, the stably transfected cells were selected for resistance to the antibiotic blasticidin at a concentration of 10 μg/ml. In the presence of blasticidin in the culture media, all of the sham transfected cells died within 24-48 hours of its addition, due to the absence of the blasticidin resistance gene. However, cells transfected with the pIRESbla/BMP-7 vector or the pIRESbla vector alone, which both contained the blasticidin resistance gene, survived and began to divide. This indicated that the CHO-K1 cells had been successfully transfected.

Once the transfected cells were growing consistently after passaging and considered to be established, 25 cm^2 and 75 cm^2 flasks were seeded with 0.25 x 10^6 cells and 0.75 x 10^6 cells respectively. After 3 days, when the cells were approximately 80 % confluent, the media was aspirated and replaced with fresh media containing blasticidin. To determine the time at which expression of the BMP-7 protein was optimal, 0.5 ml (25 cm^2 flasks) or 1 ml (75 cm^2 flasks) samples of the cell culture supernatants were taken daily for 14 days. A cocktail of protease inhibitors was added to the samples immediately after collection, and the supernatants were clarified by centrifugation to remove whole detached cells and cell debris, before being stored at -20 ºC prior to analysis. To ensure that the total volume in the flask remained the same throughout the 14-day time period, a volume of fresh media equal to that of the sample removed was added each day.

Although the stably transfected cells were blasticidin-resistant, and therefore expressing the blasticidin S deaminase gene transcript and translating its protein product, analysis of the collected supernatant samples by ELISA and Western blotting showed that they were not producing and secreting detectable levels of the BMP-7 protein into the cell culture media at any time during the 14 days. There were no discernible differences between the ELISA background absorbance readings and those that were obtained from the supernatants of cells transfected with the pIRESbla/BMP-7 vector or the pIRESbla vector alone. The BMP-7 protein was still undetectable after carrying out a twenty-fold concentration of the supernatants using Vivaspin sample concentrators (GE Healthcare UK Ltd), and increasing the concentration of blasticidin in the media to 20 μg/ml over the same 14-day time course also had no effect.

Therefore, cell lysates were prepared to check if the BMP-7 protein was being produced but retained within the cell rather than secreted. However, the BMP-7 protein still remained undetectable, either because it was not being produced, or because it was present at levels so low that it fell below the detectable threshold of the assays used.

4.2.6 Expression of the BMP-7 protein using adherent *Spodoptera frugiperda* (Sf9) insect cells

Our laboratory had previously successfully expressed glial cell line-derived neurotrophic factor (GDNF) using the Invitrogen Bac-to-Bac Baculovirus Expression System (detailed in Alfano *et al.*, 2007). As GDNF is another TGF-ß superfamily member that possesses the characteristic cystine-knot motif, and is therefore structurally similar to BMP-7, an attempt was made to express the human BMP-7 protein using this system.

The Bac-to-Bac Baculovirus Expression System provides an efficient and safe method to generate recombinant baculoviruses, enabling the expression of proteins in the eukaryotic Sf9 insect cell line. The method is based on the site-specific transposition of a gene of interest from a pFastBac donor plasmid into a baculovirus shuttle vector (bacmid). This occurs via the Tn7 transposon, thereby producing a recombinant bacmid, which is produced and propagated in DH10Bac *E. coli* cells (Figure 4.11). There are a number of advantages of using eukaryotic Sf9 insect cells for protein expression. These cells are robust and carry out the same post-translational modifications that take place in mammalian cells. This ensures that the correct disulphide bridges are formed, producing correctly folded proteins. Insect cells also utilise the same glycosylation sites as mammalian cells, adding mannose-rich glycans, and are able to secrete expressed proteins into the culture media, therefore aiding protein recovery.

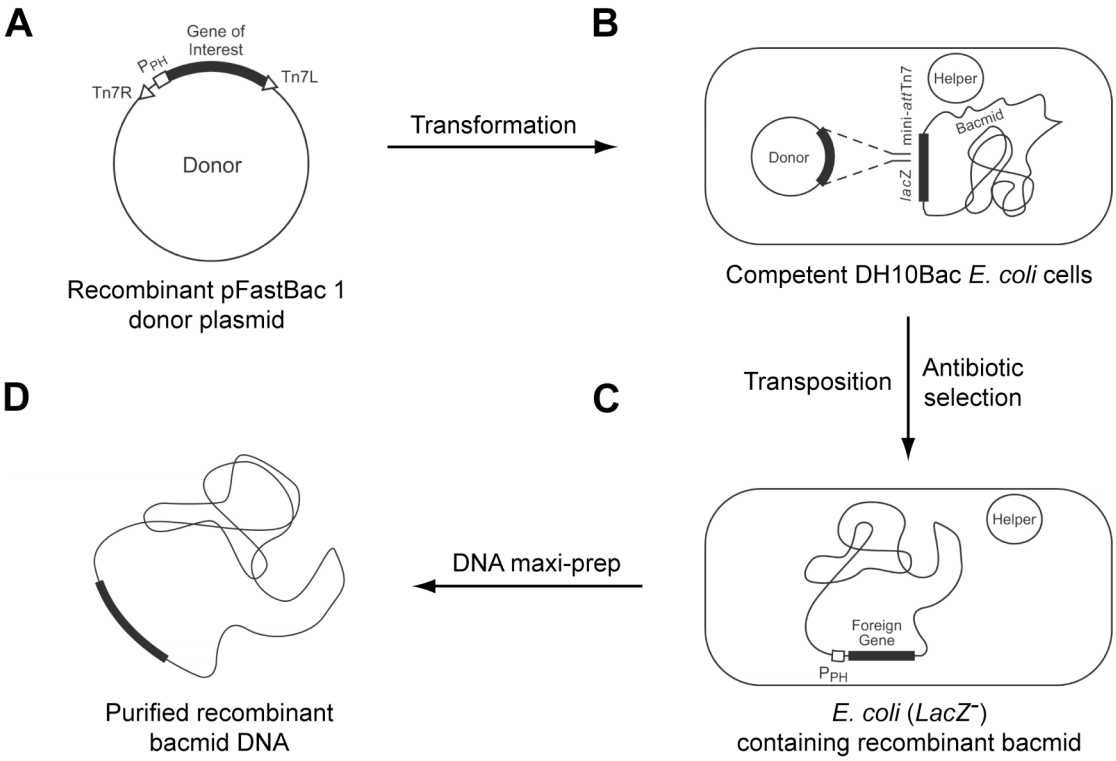

Figure 4.11 The Bac-to-Bac Baculovirus Expression System
The Bac-to-Bac Baculovirus expression system (Invitrogen) provides a convenient method for producing a recombinant baculovirus that can be used for the expression of proteins in insect cells. The gene of interest is cloned into the pFastBac 1 donor plasmid (A), and transformed into competent DH10Bac *E. coli* cells that contain the baculovirus shuttle vector, also known as the bacmid (B). Once transformed, site-specific transposition of the gene of interest from the donor plasmid to the bacmid occurs inside the DH10Bac cells, producing a recombinant bacmid (C). The high molecular weight recombinant bacmid DNA is extracted and purified by carrying out a DNA maxi-prep (D). (Image adapted from that presented in the Invitrogen Bac-to-Bac product manual).

4.2.6.1 Generation of the recombinant bacmid

For expression in Sf9 cells, the BMP-7 cDNA was cloned into the pFastBac 1 donor plasmid following the procedures described in section 4.2.3. Other pFastBac donor plasmids are also available as part of this expression system, but pFastBac 1 was selected as it allows the expression of proteins without the addition of a tag. The recombinant pFastBac 1/BMP-7 plasmid was then transformed into DH10Bac *E. coli*

cells, which contained both the baculovirus shuttle vector (bacmid) and a helper plasmid. Once transformed, directional transposition occurred between the mini-Tn7 element on the pFastBac 1 vector and the mini-*att*Tn7 target attachment site within the bacmid DNA, assisted by the pMON7124 helper plasmid that encodes the necessary transposase enzyme and confers resistance to the antibiotic tetracycline. This resulted in the production of a recombinant bacmid. Colonies of DH10Bac cells that had successfully carried out this transposition step were identified after approximately 48 hours with the aid of blue/white selection. As expression of the LacZα peptide within the bacmid was disrupted upon insertion of the mini-Tn7 element into the mini-*att*Tn7 attachment site, colonies that contained the recombinant bacmid were white, whilst colonies that contained the unaltered bacmid were blue. White colonies were picked from the agar plate and the recombinant bacmid DNA was isolated and purified by carrying out a DNA maxi-prep. The presence of the BMP-7 cDNA in the recombinant bacmid was confirmed by DNA sequencing with the primers pFastBac1-S and pFastBac1-A, located at the 5' and 3' ends respectively of the multiple cloning site within the pFastBac 1 vector.

4.2.6.2 Production of the recombinant baculovirus

To produce a recombinant baculovirus, 9 x 10^5 Sf9 insect cells were transfected with 1 μg of purified bacmid DNA, containing the transposed BMP-7 cDNA, in wells of a 6-well plate. This was carried out in duplicate alongside a positive control of a bacmid containing GDNF, and a negative control containing just the Cellfectin transfection reagent without DNA. The control transfections were carried out in separate plates to minimise the chance of cross-contamination occurring. Following transfection, the cells were incubated in a 27 ºC humidified incubator for approximately 72 hours. At this time, signs of late viral infection were observed in the cells that had been transfected with bacmid DNA containing the BMP-7 cDNA or the GDNF positive control. The cells transfected in this way had ceased growing, started to detach from the plate, and many appeared lysed upon visual inspection with a microscope. However, the cells that had been transfected with the Cellfectin reagent alone remained unaffected. This indicated that the visual changes observed in the transfected cells were a result of viral infection. The media containing

the virus, and the negative control transfected media, was collected from each well and transferred to sterile 15 ml centrifuge tubes. The media was then clarified by centrifugation at 500 x g for 5 minutes, before being stored at 4 ºC protected from light and labeled as the P1 baculoviral stock. The titre of the P1 baculoviral stock, calculated in plaque forming units (pfu)/ml, was determined by carrying out a viral plaque assay. This stock was amplified to produce a high-titre P2 baculoviral stock, of which the titre was also determined. The results from the viral plaque assays are displayed in Table 4.1, where it can be seen that the titres of both the P1 and P2 baculoviral stocks lie towards the higher end of the expected ranges suggested by Invitrogen in their product manual. It was therefore decided that these viral titres were sufficient to be used for the infection of Sf9 cells to express the BMP-7 protein.

Baculoviral stock	Baculoviral titre (pfu/ml)	Supplier's (Invitrogen) expected baculoviral titre range (pfu/ml)
P1	0.69×10^7	1×10^6 to 1×10^7
P2	0.76×10^8	1×10^7 to 1×10^8

Table 4.1 Titres of the P1 and P2 baculoviral stocks
The titres of the P1 and P2 baculoviral stocks were determined by carrying out a viral plaque assay. The results obtained showed that the titres obtained were towards the higher end of the supplier's expected range.

4.2.6.3 Infection of Sf9 insect cells with the recombinant baculovirus

On the recommendation of the Invitrogen Bac-to-Bac Baculovirus Expression System product manual, a small-scale baculoviral infection of the Sf9 cells was initially carried out in order to optimise the conditions for protein expression. 6×10^5 Sf9 cells were seeded in wells of a 24-well plate and infected at varying multiplicities of infection (MOI, pfu/cell) ranging from 1 to 5. However, at this scale of infection for all MOIs tested, the BMP-7 protein was not detectable by ELISA in the cell culture supernatants or cell lysates (data not shown). The same remained true after producing repeat batches of the bacmid and the recombinant baculovirus. However, it should be noted that the Sf9 cells did show all the expected signs of late-stage infection (cessation of cell growth, granular appearance, detachment and cell lysis),

indicating that the baculovirus was otherwise functional. Also, the GDNF positive control infection worked as it had done previously to produce the GDNF protein (later detailed in Alfano *et al.*, 2007).

To ensure that the lack of detectable BMP-7 protein was not just a result of the infections initially being carried out on a small scale, the infections were repeated on a larger scale. To prepare for baculoviral infection, 1.8 x 10^7 Sf9 cells were seeded in 100 mm diameter dishes in 12 ml of growth media, and allowed to attach for 1 hour. After this time, the media was aspirated, the cells were rinsed once with fresh growth media, and 12 ml of fresh media was added to the dishes. To express the BMP-7 protein, the seeded cells were infected with the P2 baculoviral stock at a MOI of 2, which had previously worked well for the expression of GDNF in these cells. This was again carried out alongside a positive control of an infection using a GDNF-expressing recombinant baculovirus, and a negative control infection using media collected from cells that were transfected with the Cellfectin transfection reagent alone.

When the Sf9 cell culture supernatants and lysates from the second round of baculoviral infections described above were subjected to ELISA (data not shown), the BMP-7 protein was once again undetectable despite the cells showing the expected signs of late-stage infection. This finding therefore suggested that the BMP-7 protein was not being expressed or was only being expressed at very low and undetectable levels. The same supernatants and cell lysates were also subjected to SDS-PAGE under reducing conditions and Western blotted (Figure 4.12).

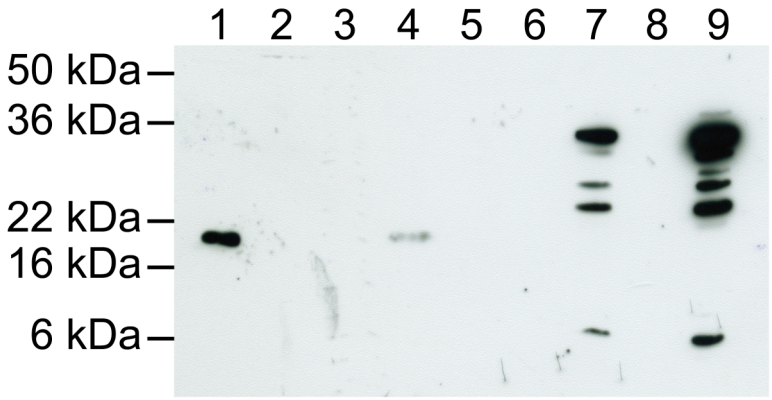

Figure 4.12 BMP-7 protein expression using Sf9 insect cells
Sf9 insect cells were infected with recombinant baculoviruses containing cDNA sequences that encoded for the BMP-7 protein. After approximately 72 hours, the supernatants were collected and whole-cell lysates were produced. The proteins were separated by SDS-PAGE under reducing conditions on a 15 % polyacrylamide gel and then Western blotted. *Lane 1:* 5 ng rhBMP-7 standard (R&D). *Lane 2:* unconditioned cell culture medium. *Lane 3:* uninfected conditioned cell culture medium. *Lane 4:* 2.5 ng rhBMP-7 standard diluted in uninfected conditioned cell culture medium. *Lane 5:* uninfected cell lysate. *Lane 6:* BMP-7 clone 1-infected supernatant. *Lane 7:* BMP-7 clone 1-infected cell lysate. *Lane 8:* frameshifted BMP-7 clone 2-infected supernatant. *Lane 9:* frameshifted BMP-7 clone 2-infected cell lysate.

A study carried out by Jones *et al.* (1994) showed that the human BMP-7 protein is initially synthesised in the form of a monomeric 50 kDa pro-protein. This pro-protein is dimerised, glycosylated and then proteolytically cleaved at its arginine-X-X-arginine maturation site, before being secreted by the cells into the culture medium. The secreted mature protein consists of 34-38 kDa disulphide-linked homodimers, which migrate upon reduction as 17-23 kDa monomers depending on the extent of glycosylation. If the BMP-7 protein was present in the infected Sf9 cell supernatants and lysates, one would have expected the pattern of bands observed on the developed Western blot to closely resemble those on the polyacrylamide gel images that were published by Jones *et al.* (1994). However, Figure 4.12 shows that this was not the case.

The developed Western blot shown in Figure 4.12 shows that the recombinant BMP-7 protein is either absent or at such low levels in secreted form in the culture supernatant that it is undetectable. This is apparent due to there being no

immunoreactivity difference between the lanes containing the supernatants collected from cultured Sf9 cells that were infected with BMP-7 cDNA-containing baculoviruses (lanes 6 and 8) and the unconditioned and conditioned medium-containing negative control lanes (lanes 2 and 3); no immunoreactivity whatsoever was observed in any of these lanes. This finding therefore appears to support the aforementioned ELISA data. To ensure that the presence of other proteins in the culture supernatants was not hindering the detection of BMP-7, 2.5 ng of rhBMP-7 was diluted in conditioned medium and electrophoresed in lane 4, where it remained detectable.

It can also be seen in Figure 4.12 that immunoreactivity was observed in lanes 7 and 9. In these lanes, the lysates of Sf9 cells that were infected with baculoviruses containing the cDNA of BMP-7 clones 1 and 2 respectively had been electrophoresed. Initially, it appeared that the presence of immunoreactivity in these lanes contradicted the ELISA data by suggesting that the BMP-7 protein was expressing at detectable levels, albeit remaining within the cells rather than being secreted. However, upon further inspection and consideration of the pattern of bands displayed within these lysate lanes, this no longer seems to be the case. The reasons for this are as follows: Firstly, if the BMP-7 protein was responsible for the bands in these lanes, one would have expected to have seen a pro-protein monomer band of approximately 50 kDa in size [based on the findings of Jones *et al.* (2004)]. A band of this size is notably absent. Secondly, although bands are present in these lysate lanes at approximately 36 kDa in size, which is the size of the mature BMP-7 protein dimer, it is unlikely that the BMP-7 protein is responsible for these bands. This is because under reducing conditions, one would instead expect to see 17-23 kDa mature monomer bands, as was the case in the control lanes 1 and 4 that contained reduced commercial recombinant human BMP-7 derived from CHO cells. Depending on the time-scale between cleavage of the pro-protein and the secretion of the mature protein, one might not even expect to observe bands corresponding to the mature protein in the cell lysates.

One explanation for the absence of the BMP-7 protein in the supernatants and the absence of a 50 kDa pro-protein monomer band in the lysates, as well as the presence of alternative unexpected bands between 36 kDa and 22 kDa in size in the lysates, is that the protein was not being correctly processed by the cells. It is possible that this may have led to the degradation of the protein within the cells prior to

secretion, which may have also been responsible for the presence of low molecular weight bands of around 6 kDa in size.

However, a later finding following further DNA sequence analysis of BMP-7 clones 1 and 2 casts further doubt over this theory and provides more evidence to suggest that the BMP-7 protein is not responsible for the presence of the immunoreactivity seen in lanes 7 and 9. The sequence analysis revealed that clone 2 contained a single nucleotide base insertion, which caused a frameshift to occur. This led to the creation of a very early stop codon only 18 bases downstream of the insertion point, and approximately one third of the way through the sequence portion that encodes the mature component of the BMP-7 protein. Although this would have resulted in clone 2 containing only a short section of the mature BMP-7 protein that would have a lower molecular weight than the full mature protein that would be produced by clone 1, it is apparent from Figure 4.12 that there are no differences between the molecular weights of the bands seen for clones 1 and 2. Therefore, the BMP-7 protein is unlikely to be responsible for producing the bands in these lanes. Instead, it appears likely that the bands were produced by a non-specific antibody-antigen interaction. Furthermore, it can be seen that these bands are clearly not present in the negative control lysate lane (lane 5), which contained a lysate prepared from cells that were mock infected with supernatants that did not contain any baculovirus. This immunoreactivity therefore cannot have been produced by a protein found natively within the Sf9 cells. Thus, it is more probable that the immunoreactivity displayed was the result of a non-specific interaction of the polyclonal anti-BMP-7 antibody with baculoviral proteins in the infected cell lysates, which one would expect to be in abundance.

In hindsight, a more appropriate negative control for the Western blot would have been a lysate produced from cells infected with the GDNF-expressing baculovirus. This may have assisted with the interpretation of the bands, perhaps shedding light on the origin of the immunoreactivity and possibly enabling firmer conclusions to be drawn about whether or not it was the result of a non-specific antibody-antigen binding interaction.

4.2.7 Optimisation of the pIRESbla/BMP-7 expression vector

After stably transfecting CHO cells with the pIRESbla/BMP-7 plasmid construct, the BMP-7 protein was undetectable in supernatants and cell lysates, as described earlier in section 4.2.5. However, the cells survived and grew in the presence of the antibiotic blasticidin, so they were stably expressing the blasticidin resistance gene and translating its protein product. Because the BMP-7 cDNA was cloned upstream of the blasticidin resistance gene, separated by an IRES element, and the expression of both genes was driven from a single CMV promoter, it is unlikely that the mRNA transcript for the blasticidin resistance gene would have been present without the mRNA for the BMP-7 gene. It was therefore a possibility that a lack of efficiency during the translation stage of protein synthesis might have been responsible for the absence of a detectable level of the BMP-7 protein. As a result of this, the decision was made to modify the original pIRESbla/BMP-7 expression cassette in order to optimise the translation of the protein.

Whilst investigating ways in which BMP-7 protein translation could be improved, it was noticed that some of the commercial cytokine companies, such as R&D Systems and Sigma Aldrich, express many of their BMP recombinant proteins in CHO cells, but as chimeras. In this situation, the mature sequence of the BMP of choice is fused onto the pre-pro sequence of BMP-2 (Figure 4.13). When contacted, the companies were unable to divulge the reason that this approach was adopted due to it being proprietary information, and have since removed the small amount of information they had previously provided from the product datasheets. However, a publication by Hammonds *et al.* (1991) may provide some insight as to why this method for protein expression was used. The authors of this paper have shown that by using the pre-pro region of BMP-2, fused to the mature region of BMP-4, the expression of the mature BMP-4 protein in mammalian cells was "dramatically improved". It is purely speculative, but quite plausible, that the commercial suppliers saw the considerable benefit that could be gained from this, and adapted this method for the production of the mature protein forms of other BMP family members.

Although Hammonds *et al.* (1991) provide no explanation of the reason why the BMP-2 pre-pro domain had such an effect on increasing the expression of the mature BMP-4 protein that was fused to it, this is a very interesting phenomenon that

might be taken advantage of, and which provoked much thought. It is quite possible that the enhanced translation of BMP-2 mRNA into protein could be a consequence of a regulatory difference, which may have developed during the evolution of the BMP family. To explore this avenue of thought at the simplest level, a brief analysis was carried out on the mRNA sequences of some of the BMP family members.

To initiate the translation of protein from mRNA in eukaryotic cells, the small ribosomal subunit scans for specific sequences on the transcribed mRNA strand. These short translation initiation sequences begin several nucleotide bases upstream of the translation start site, and incorporate the required AUG^{Start} triplet codon within them (Kozak, 2002 and references within). In mammals, the optimal context for recognition of the AUG^{Start} codon is (GCCGCC)**A/G**CCaug**G**, with the A or G at position –3, and the G at position +4 (both highlighted in bold), being the most conserved and functionally important bases (Kozak, 2002). The bases with less importance are enclosed within brackets. Sequences in this optimal context are generally referred to as Kozak consensus sequences, named after Marilyn Kozak who is the author that first described them (Kozak, 1981). A comparison of the translation initiation sequences of some of the BMP family members (Figure 4.14), shows that BMP-2 mRNA contains a complete match of the most important core component of the optimal Kozak consensus sequence. However, it can also be seen that BMPs -4, -5 and -7, which the commercial suppliers produce in mature form using the BMP-2 pre-pro sequence, show an obvious variation in this region. Therefore, the strong Kozak sequence that BMP-2 possesses may be responsible for its enhanced expression compared to other BMP family members. If this is the case, because the BMP-7 translation initiation sequence appears to be weaker than that of BMP-4, one might expect the BMP-2 pre-pro domain to have an even greater effect on the production of the mature BMP-7 protein than was seen for BMP-4.

In light of these findings and observations, an attempt was made to optimise the translation of the BMP-7 protein by the addition of an ideal Kozak consensus sequence at the 5' end of the BMP-7 cDNA. Although other elements might exist in the mRNA or protein sequences of the pre-pro domain of BMP-2, which might be responsible for its favourable expression, this approach provided a convenient starting point without the added complexity of producing a chimeric protein.

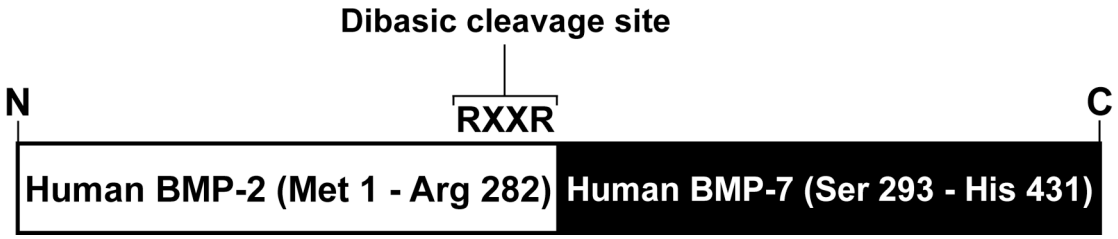

Figure 4.13 Commercial recombinant BMP-2/7 chimeric protein
It has been noted that a few of the commercial suppliers express some of their recombinant BMPs as chimeras. In this case, the mature component of the BMP-7 protein is fused to the C-terminal end of the pre-pro region of BMP-2, and is released by proteolytic cleavage at the indicated RXXR dibasic site.

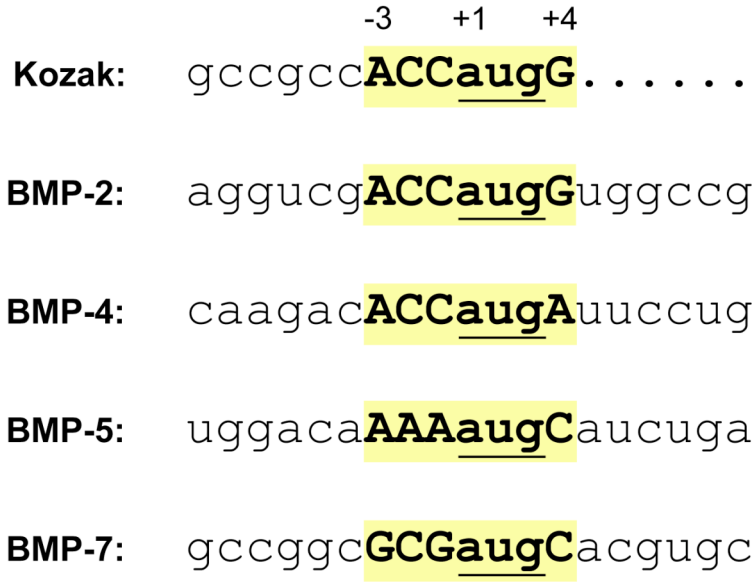

Figure 4.14 BMP translation initiation sequences
A comparison of the 5' mRNA sequences of some of the BMP family members. The core component (-3 to +4) of the translation initiation sequences is highlighted in yellow, and the AUG^{Start} codon (+1 to +3) is underlined. BMP-2 can be seen to contain a particularly strong core sequence, matching the optimal Kozak consensus of ACCaugG.

4.2.7.1 The production and cloning of a BMP-7 cDNA insert containing an optimised Kozak consensus sequence

To try to increase the efficiency of BMP-7 protein translation, a modified BMP-7 cDNA insert that contained an optimal Kozak consensus sequence at the 5' end was produced by carrying out a PCR reaction. The original pIRESbla/BMP-7 vector was used as a template, and the sequence was amplified using the BMP7WT2-S and BMP7WT-A forward and reverse primers respectively. The BMP7WT2-S forward primer incorporated the complete Kozak consensus sequence of GCCGCCACCatgG within it, as well as the same BamHI restriction site that the reverse primer contained to aid the subsequent cloning of the insert. The addition of the Kozak sequence resulted in the first base following the start codon (position +4) to be changed from a C to a G, which in turn led to the substitution of the second amino acid in the signal peptide from a histidine residue to an aspartic acid residue. In the same way as described earlier in section 4.2.3, the resulting PCR product was purified and cloned into the pIRESbla expression vector via its BamHI restriction site (Figure 4.15) to produce the pIRESbla/Kozak-BMP-7 vector.

Figure 4.15 Addition of a Kozak consensus sequence to the BMP-7 cDNA
In an effort to increase the efficiency of BMP-7 protein translation, an optimised Kozak consensus sequence (GCCGCCACCatgG) was introduced by PCR at the 5' end of the BMP-7 cDNA. This modified insert was then cloned into pIRESbla via its BamHI site to produce the pIRESbla/Kozak-BMP-7 vector. The 5' region of this vector is shown.

4.2.8 Stable transfection of CHO-K1 cells with the pIRESbla/Kozak-BMP-7 vector

CHO-K1 cells were stably transfected with the pIRESbla/Kozak-BMP-7 vector using the same procedure that was described in section 4.2.5. The same control transfections were also carried out, with the addition of another transfection using the pIRESbla/BMP-7 vector that had previously failed to produce a detectable level of BMP-7 protein for comparison. In order to determine the effect that the addition of an optimal Kozak consensus sequence had on the production of the BMP-7 protein, a time-course experiment was conducted. Supernatant samples were collected daily from the flasks containing the transfected cells over a 10-day time period, and their BMP-7 content was determined by ELISA.

As before, the BMP-7 protein was undetectable in the supernatants from the cells stably transfected with the pIRESbla/BMP-7 vector, producing absorbance readings at background levels, as did the pIRESbla vector only transfected supernatants. However, in contrast to these findings, Figure 4.16 shows that the addition of a Kozak consensus sequence to the BMP-7 cDNA had a positive impact on protein expression. It can be seen that the CHO cells that were stably transfected with the pIRESbla/Kozak-BMP-7 vector produced and secreted detectable levels of the BMP-7 protein. Under normal growth conditions, in 10 % foetal bovine serum (FBS), the amount of BMP-7 protein in the culture supernatant peaked after 2 days at a concentration of 22.4 ng/ml. After 4 days, the concentration of secreted protein decreased to 15.8 ng/ml before stabilising in the region of 13-14 ng/ml, with the exception of a temporary drop to 12 ng/ml after 7 days.

Although this was the first time that detectable levels of protein had been achieved, the levels were relatively low in comparison to the quantities that were required to carry out heparin-binding studies. The supernatants also contained a lot of extraneous protein due to the presence of the 10 % FBS, which may have interfered with such studies. It was therefore apparent that the supernatants would need to be both concentrated and at least partially purified before further use. To assist with the removal of the serum proteins, the CHO cells were adapted to growth in media containing 2 % FBS. Samples were collected again over a 10-day time period to determine the effect that the five-fold reduction in FBS had on BMP-7 protein

expression. It can be seen in Figure 4.16 that under these conditions the concentration of BMP-7 in the media was considerably lower, at a maximum of 9.5 ng/ml on day 1 and minimum of 1.03 ng/ml on day 8. A similar experiment was also carried out in serum-free conditions using CHO-S-SFM II medium (Invitrogen), but the concentration of BMP-7 in the supernatant was even lower than that found in the presence of 2 % FBS, not exceeding 2 ng/ml (data not shown). The decrease in BMP-7 production that was observed as the concentration of FBS in the media was reduced was most likely a result of the growth conditions no longer being optimal for the cells, even after adaptation. It is also possible that the secreted protein became more susceptible to being degraded when the concentration of extraneous serum proteins in the media was reduced.

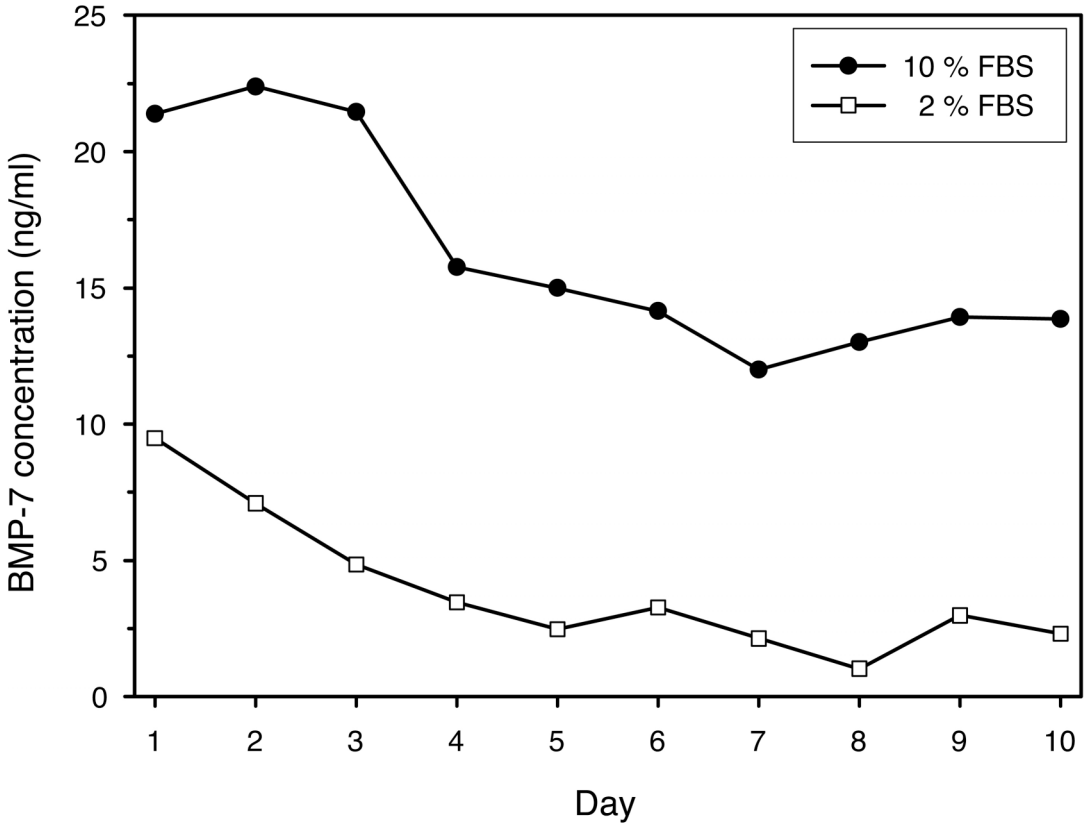

Figure 4.16 Expression of BMP-7 in stably transfected CHO-K1 cells
CHO-K1 cells were stably transfected with the pIRESbla/Kozak-BMP-7 vector, and grown in media containing 10 % or 2 % FBS. Supernatant samples were collected daily over a 10-day period and their BMP-7 content was determined by ELISA.

4.2.9 Site-directed mutagenesis

4.2.9.1 C-terminal point mutations

Having successfully expressed detectable levels of the wildtype recombinant human BMP-7 protein, attention was turned to producing mutant DNA constructs to be used for the expression of mutant BMP-7 protein variants. The molecular docking simulations described in Chapter 3 predicted the C-terminal basic amino acids lysine 419, arginine 421 and arginine 426 to be the key contact residues in the binding interaction between BMP-7 and heparin/HS. Depending on whether the BMP-7 protein dimer possesses two independent heparin/HS-binding sites - one on each monomer - or a single bridged cooperative binding site, either 3 or 6 basic residues in total may take part in the binding interaction based on the results of these simulations.

To maximise the chance of reducing the heparin/HS-binding affinity of BMP-7, whilst hopefully maintaining the structural integrity of the protein, the decision was made to carry out point substitutions of these predicted key residues for alanine in pairs (section 3.2.3.5). Based on either of the two binding scenarios described above, this would result in a reduction of the number of predicted basic contact residues in the C-terminal region by two-thirds. Only one of the predicted key basic residues would remain on each monomer, which would be insufficient to form a heparin/HS-binding site, even if the protein monomers were to bind cooperatively to a single GAG chain.

As explained in Chapter 3 (section 3.2.3.5), the first pair of amino acids selected for substitution to alanine were lysine 419 and arginine 421. To produce these two amino acid changes (K419A and R421A) in the translated BMP-7 protein, it was necessary to make a total of four nucleotide base substitutions in the corresponding cDNA sequence. As shown in Figure 4.17A, these point mutations and their positions were as follows: a1255g, a1256c, a1261g and g1262c. The resulting amino acid changes in the C-terminal region are shown in Figure 4.17B. To introduce these point substitutions into the BMP-7 cDNA sequence, the Stratagene QuikChange II Site-Directed Mutagenesis Kit was used. The QuikChange II kit provides a fast and convenient three-step method for making site-specific mutations in DNA inserts

within double-stranded plasmids, therefore eliminating the need for sub-cloning (Figure 4.18).

During the first step of the procedure, in which thermal cycling was carried out, 20 ng of the double-stranded pIRESbla/Kozak-BMP-7 vector template was denatured at 95 ºC for 30 seconds. This vector was selected as the template so that the K419A/R421A mutant would also contain the optimal Kozak consensus sequence, which was shown in section 4.2.8 to increase the production of recombinant human BMP-7 in CHO-K1 cells. After denaturing the template, the mutagenic sense and antisense primers were annealed to the template at 55 ºC for 1 minute. These primers, named BMP7K419A/R421A-S and BMP7K419A/R421A-A respectively, both contained the desired mutations and were complementary to opposite strands of the same BMP-7 cDNA region. The annealed primers were then extended without displacement at 68 ºC for 6 minutes (1 minute/kb of plasmid length) using *PfuUltra* high-fidelity DNA polymerase, generating a mutated plasmid containing staggered nicks. The temperature cycle was repeated 18 times.

Although the first thermal cycling step was very similar to a typical PCR reaction, it differed due to the template amplification taking place in a linear manner rather than logarithmically. This occurred as a direct result of the location of the staggered nicks, positioned immediately upstream of the 5'-termini of both primers. These were the points where the *PfuUltra* DNA polymerase had completed synthesising the mutated circular plasmid strands, and detached once it returned to the 5' end of the primer that it started extending from. Because of the nicks, the primers could only be extended when annealed to the parental DNA template strands, and not when annealed to the newly synthesised mutant strands as would normally be permitted during a typical PCR reaction. Along with using a lower number of thermal cycles, this has the benefit of reducing the chance of any unwanted second-site errors from occurring.

After producing the mutant plasmids, the wildtype parental template DNA was removed from the reaction mixture. The parental DNA was differentiated from the newly synthesised mutant DNA due to it being isolated from DH5α *E. coli* cells, and therefore Dam (DNA adenine methylase) methylated. Unlike the mutant DNA, this made it susceptible to digestion by the DpnI endonuclease. The DpnI treatment was carried out in a water bath at 37 ºC for 2 hours, after which time 1 µl of the mixture

was transformed into XL-1 Blue supercompetent *E. coli* cells. Single colonies were picked from transformation plates, and the mutated plasmid DNA was isolated by carrying out DNA mini-preps. In preparation for transfection, this DNA was scaled-up by carrying out an endotoxin-free DNA maxi-prep. Finally, the purified plasmid DNA was sent for sequencing, confirming the presence of the desired mutations, and that the mutant BMP-7 cDNA insert was free of any unwanted errors. This mutant vector construct was given the name pIRESbla/BMP-7-K419A/R421A.

Figure 4.17 The BMP-7 K419A and R421A C-terminal point substitutions
In an attempt to reduce the heparin-binding affinity of BMP-7, efforts were made to produce a mutant protein containing a pair of C-terminal point substitutions, termed K419A/R421A (B). To introduce these mutations, it was necessary to make at total of 4 nucleotide base changes in the cDNA sequence (A).

Figure 4.18 An overview of the Stratagene QuikChange II site-directed mutagenesis method
The three-step QuikChange method allows point-specific mutations to be made directly in DNA inserts located within double-stranded plasmids. After generating the mutant strands using suitable primers, the methylated parental template DNA is eliminated by digestion with the DpnI enzyme. The remaining mutated plasmid DNA is then transformed into XL-1 Blue supercompetent cells, to repair nicks and produce sufficient quantities of the plasmid for transfection. (Image adapted from that presented in the Stratagene QuikChange II Site-Directed Mutagenesis Kit product manual).

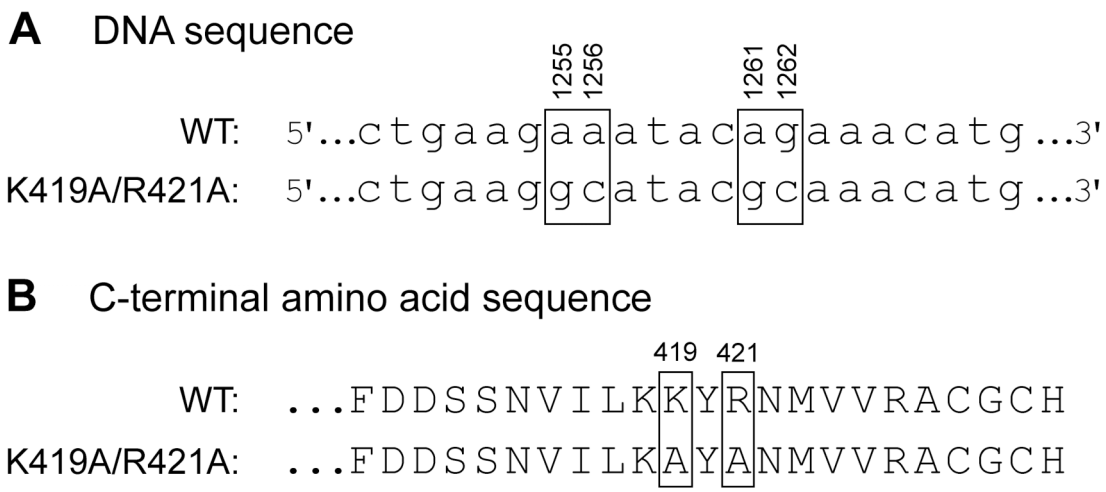

Figure 4.17 The BMP-7 K419A and R421A C-terminal point substitutions
Please refer to the figure legend on the opposite page.

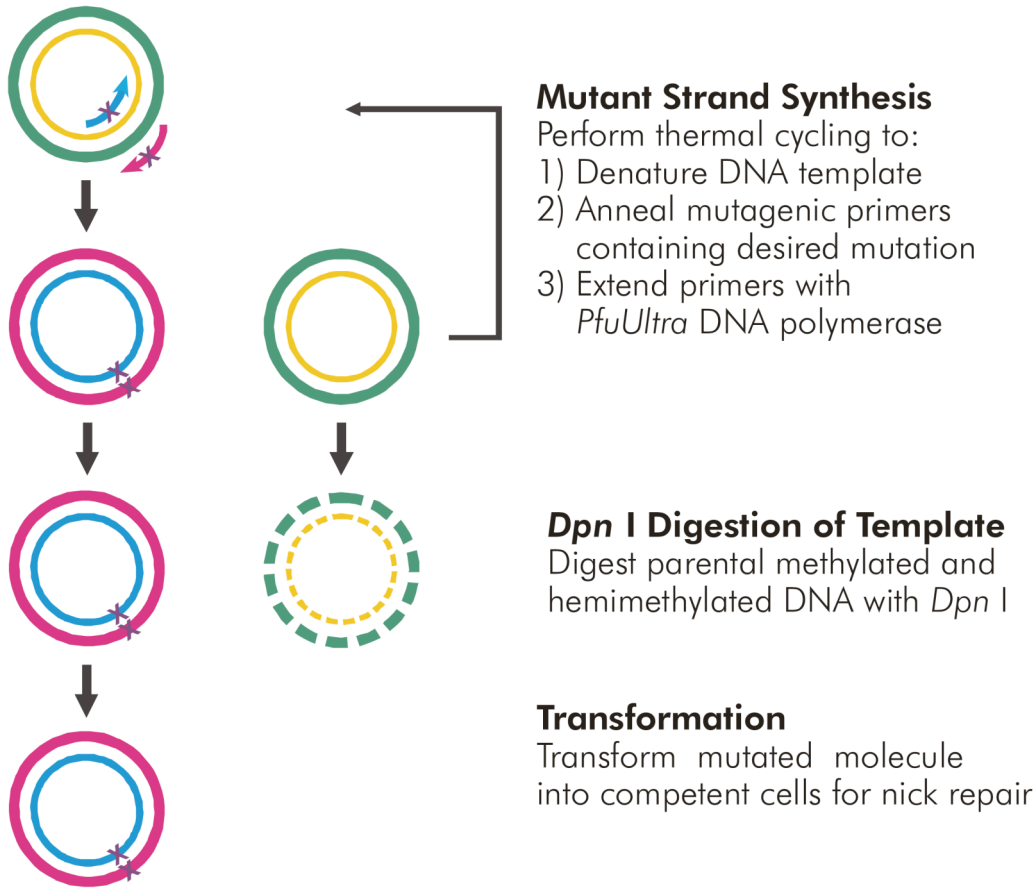

Figure 4.18 An overview of the Stratagene QuikChange II site-directed mutagenesis method
Please refer to the figure legend on the opposite page.

4.2.9.2 N-terminal deletion

As discussed above (section 4.2.9.1), the molecular docking simulations carried out in Chapter 3 predicted the C-terminal basic amino acids lysine 419, arginine 421 and arginine 426 to be the key contact residues in the binding interaction between BMP-7 and heparin/HS. However, a limitation of the published BMP-7 crystal structures used to carry out these simulations was that they were missing 27 to 35 of the 37 amino acids in their N-terminal regions, upstream of the first cysteine residue. This missing portion of the structure remains unresolved as a result of it being disordered (Griffith *et al.*, 1996; Greenwald *et al.*, 2003), but contains either 6 or 7 (depending on the structure) of the 15 basic residues in total found within the mature BMP-7 protein. Therefore, when considering elements of the BMP-7 protein that may have the potential to act as heparin/HS-binding sites, this region cannot be disregarded.

To determine the importance of the unresolved N-terminal region for heparin/HS-binding, the decision was made to produce a truncated BMP-7 mutant that was absent of this region, directly mimicking the available crystal structures. In doing so, all 7 of the basic lysine and arginine residues located within this structural component would be removed. A diagrammatic representation of the proposed N-terminal deletion can be seen in Figure 4.19. In case the initial amino acids at the N-terminus of the mature BMP-7 protein were important for cellular recognition of the RXXR dibasic cleavage site, situated at the C-terminal end of the pre-pro-protein, the first three residues (STG) were left in place. As a result of the deletion, these residues were shifted towards the first cysteine of the TGF-β domain. It was thought that this would also provide some distance between the cleavage site and the cystine-knot motif, therefore reducing the chance of any cleavage problems due to steric hindrance.

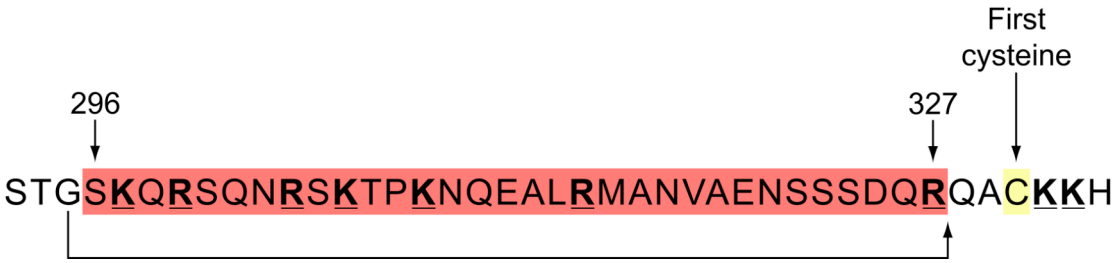

Figure 4.19 The BMP-7 N-terminal deletion
To help determine the importance of the unresolved N-terminal region for heparin/HS-binding, a truncated BMP-7 mutant was prepared. 32 amino acids were removed upstream of the first cysteine residue of the mature protein (ΔS296-R327, shown in red), consequently eliminating 7 basic arginine and lysine residues (highlighted in bold text and underlined).

To produce the N-terminal deletion (ΔS296-R327) shown in Figure 4.19, it was necessary to delete 96 nucleotide bases from the BMP-7 cDNA (Δ886-981) (Figure 4.20A). This was achieved using a PCR-based technique known as overlap extension PCR (OE-PCR), requiring a total of three independent PCR reactions to be carried out. The first of these reactions utilised the primer pair pIRESbla-S and BMP7ΔS296-R327-A, as shown in Figure 4.20B, producing a 999 bp product (Figure 4.21 lane 2). In the second reaction, the primer pair BMP7ΔS296-R327-S and pIRESbla-A were used, producing a 457 bp amplicon (Figure 4.21 lane 1). For both of these reactions, the pIRESbla/Kozak-BMP-7 vector was used as a template to once again include the optimal Kozak consensus in the cDNA of the truncated mutant. The BMP7ΔS296-R327-S and BMP7ΔS296-R327-A sense and antisense primers annealed to the BMP-7 cDNA sequence at opposite sides of the deleted region. However, to produce an overlap that was used to fuse the two PCR products shown in Figure 4.20C together, both of these primers incorporated non-annealing sequence overhangs. These overhanging sequences were complimentary to the flanking regions on opposite sides of the deleted section of cDNA.

To reconnect the two cDNA fragments generated by the previous PCR amplifications, a third and final PCR reaction was performed. In this reaction, equal amounts (20 ng each) of the purified 999 bp and 457 bp amplicons were used as a

template. An initial denaturation step was carried out, which separated the double-stranded fragments into their composite strands. The two previous products were then able to anneal to one another, combining via their complementary flanking sequences that were introduced in the primer overhangs (Figure 4.20D). Once annealed, the proofreading Platinum *Pfx* DNA polymerase (Invitrogen) was able to fill-in the missing parts of each strand in the 5' to 3' direction. The result of this was a 1408 bp product, which contained the complete 1221 bp truncated BMP-7 mutant cDNA insert (Figure 4.20E). As the overlap formed by the template fragments shown in Figure 4.20D also acted as a primer for the polymerase in both directions, no additional primers were required to initially fill-in the missing nucleotides. However, after the first five thermal cycles of the reaction, the pIRESbla-S and pIRESbla-A primers were added to amplify the 1408 bp product (Figure 4.21 lane 3).

The final stage in producing the truncated BMP-7 ΔS296-R327 mutant expression construct was to clone the newly generated cDNA sequence into the pIRESbla vector. To remove the extraneous vector DNA and prepare the 1221 bp insert for ligation, the 1408 bp PCR product was digested with the BamHI restriction enzyme (Figure 4.20E). Due to the presence of the excess vector DNA either side of the BamHI cut-site, the PCR product could be cut efficiently without first requiring it to be sub-cloned into the pGEM-T vector. The digested DNA was then separated on a 1 % agarose gel. After gel extracting and purifying the required 1221 bp band, the ΔS296-R327 mutant cDNA insert was ligated into the BamHI site of the pIRESbla vector, and sequence verified. The resulting mutant BMP-7 expression construct was given the name pIRESbla/BMP-7-ΔS296-R327.

Figure 4.20 Production of the BMP-7 ΔS296-R327 mutant cDNA sequence
The truncated BMP-7 ΔS296-R327 cDNA sequence was generated using a PCR-based method known as overlap extension PCR (OE-PCR). Three PCR reactions were required in total. (A) The pIRESbla/Kozak-BMP-7 template, with the 96 bp region to be deleted highlighted in red and its flanking regions coloured yellow and green. (B) The first two PCR reactions were carried out to produce the overlapping 999 bp and 457 bp fragments shown in (C). These overlaps were introduced by including non-annealing sequences in the BMP7ΔS296-R327-S and BMP7ΔS296-R327-A primers. These overhangs were complementary to the flanking sequences on opposite sides of the deleted region. (D) The overlapping fragments shown in (C) were utilised in a final PCR reaction to fill-in the missing nucleotides. The product of this reaction was the complete truncated product shown in (E). The additional vector DNA was removed by digesting the 1408 bp PCR product with the BamHI restriction enzyme. The 1221 bp BMP-7 ΔS296-R327 cDNA insert was then purified and cloned into pIRESbla.

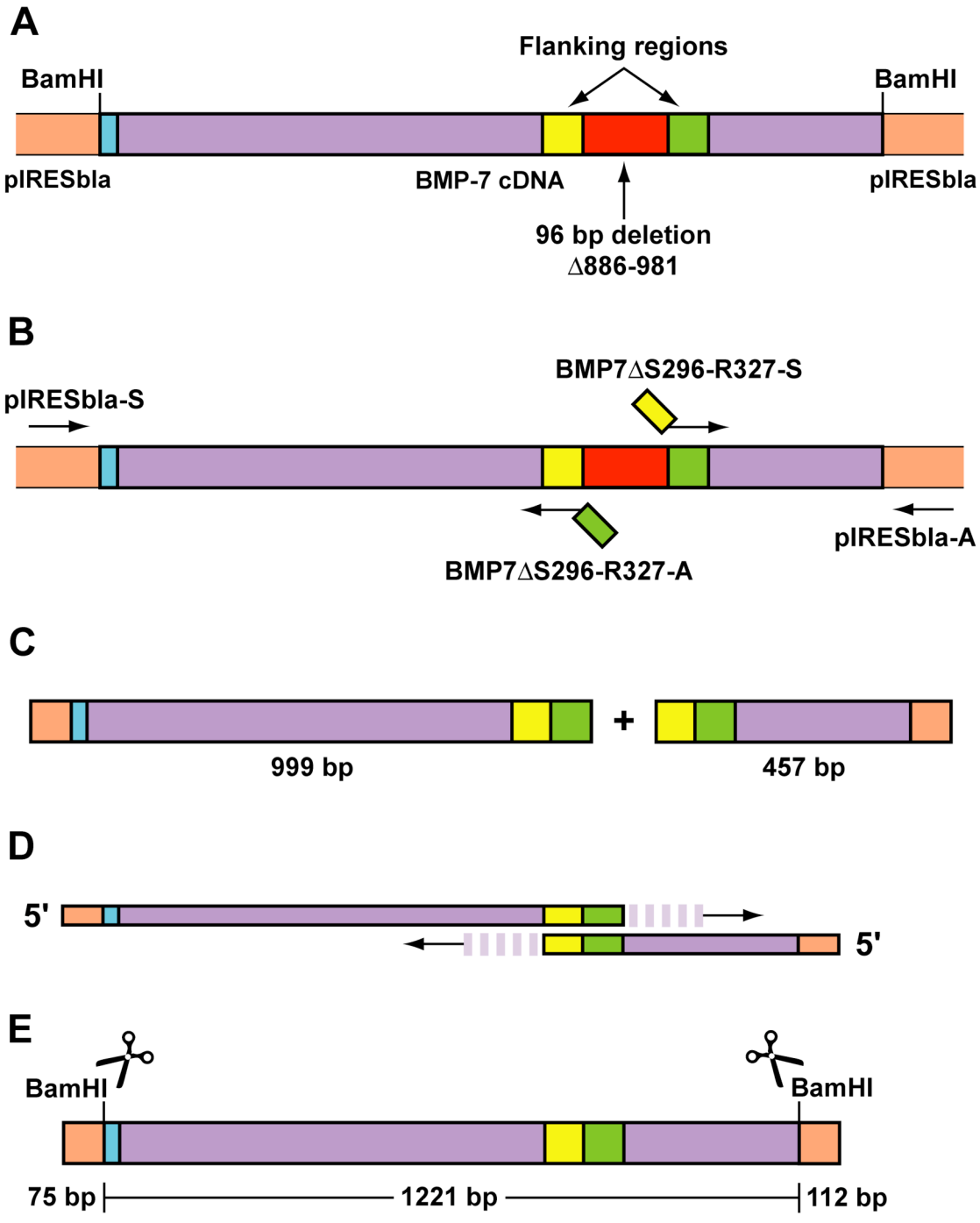

Figure 4.20 Production of the BMP-7 ΔS296-R327 mutant cDNA sequence
Please refer to the figure legend on the opposite page.

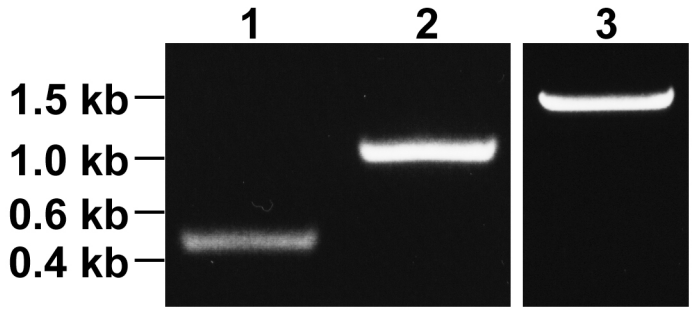

Figure 4.21 Overlap extension PCR (OE-PCR)
The DNA fragments produced when creating the BMP-7 ΔS296-R327 mutant cDNA sequence were analysed on 1 % agarose gels. *Lane 1:* The 457 bp amplicon generated by the reaction using the primer pair BMP7ΔS296-R327-S and pIRESbla-A. *Lane 2:* The 999 bp amplicon generated by the reaction using the primer pair pIRESbla-S and BMP7ΔS296-R327-A. *Lane 3:* The complete 1408 bp amplicon generated by the overlap extension PCR reaction. This reaction utilised both the 457 bp and 999 bp DNA fragments, and amplification was achieved using the primer pair pIRESbla-S and pIRESbla-A.

4.2.10 Stable transfection of CHO-K1 cells with the mutant BMP-7 expression constructs

To express the mutant BMP-7 proteins, the pIRESbla/BMP-7-K419A/R421A and pIRESbla/BMP-7-ΔS296-R327 vector constructs were individually stably transfected into CHO-K1 cells. This was carried out following the same procedures described in section 4.2.5, using blasticidin as the selective antibiotic. These transfections were performed alongside a positive control using the pIRESbla/Kozak-BMP-7 vector, an empty pIRESbla vector negative control and a sham transfection using the transfection reagent alone in the absence of any DNA. As before, a time-course experiment was then conducted to monitor the production of the BMP-7 mutant proteins over a 10-day period. Supernatant samples were collected daily and their BMP-7 content was determined by ELISA. A summary of the ELISA data can be found in Figure 4.22.

The results obtained from all three of the control transfections were as expected, and as seen previously. This indicated that the transfections were successful. Briefly, the CHO-K1 cells that were sham-transfected died within 48 hours after the addition of the selective antibiotic, due to them being absent of the blasticidin

resistance gene. Also, the cells that were stably transfected with the empty pIRESbla vector - as a negative control - survived but did not produce any BMP-7 protein due to the absence of the required BMP-7 cDNA sequence. Finally, the positive control - in which the cells were stably transfected with the pIRESbla/Kozak-BMP-7 vector - produced similar levels of the BMP-7 protein to those observed before, at 21.1 ng/ml compared with the 22.4 ng/ml obtained previously.

Following transfection with the BMP-7 mutant cDNA constructs, the CHO-K1 cells survived in the presence of blasticidin and grew stably. However, despite this and the success of the control transfections, neither of the mutant BMP-7 proteins were detectable in the culture supernatants at any time during the 10-day period. This was also true when the scale of expression experiments was increased by growing the CHO cells in larger 150 cm^2 flasks. Therefore, cell lysates were produced to check if the proteins were accumulating within the cell rather than being secreted. The BMP-7 content of these lysates was also determined by ELISA. Whilst the pIRESbla/Kozak-BMP-7 vector control-transfected cell lysate contained 2.25 ng/ml of recombinant BMP-7 protein/1 x 10^6 cells, the mutant variants were again undetectable. This suggested that no protein was being synthesised. The same results were observed when the stable transfections were repeated. In case the mutant proteins were present but only at very low levels, the proteins in the supernatants were concentrated twenty-fold using Vivaspin sample concentrators. However, when the concentrated supernatants were analysed by ELISA, the mutant proteins still remained undetectable (data not shown). This again suggested that there was a lack of mutant protein production taking place. The same result was also obtained after attempting to partially purify and concentrate the supernatants by carrying out both cation- and anion-exchange chromatography (data not shown).

Figure 4.22 Expression of the mutant BMP-7 DNA constructs using CHO-K1 cells

Adherent CHO-K1 cells were stably transfected with either the mutant BMP-7 pIRESbla/BMP-7-K419A/R421A or pIRESbla/BMP-7-ΔS296-R327 vector constructs. At the same time, positive and negative control stable transfections were also carried out using the wildtype BMP-7 pIRESbla/Kozak-BMP-7 DNA construct and empty pIRESbla vector respectively. (A) Supernatant samples were collected over a period of 10 days and the BMP-7 content of these samples was determined by ELISA. The maximum concentration of BMP-7 that was detected in the samples during this time period is shown. (B) Cell lysates were also produced from 1 x 10^6 CHO-K1 cells and their BMP-7 content was also determined by ELISA. It can be seen in (A) and (B) that the mutant BMP-7 proteins were undetectable in both the supernatants and lysates.

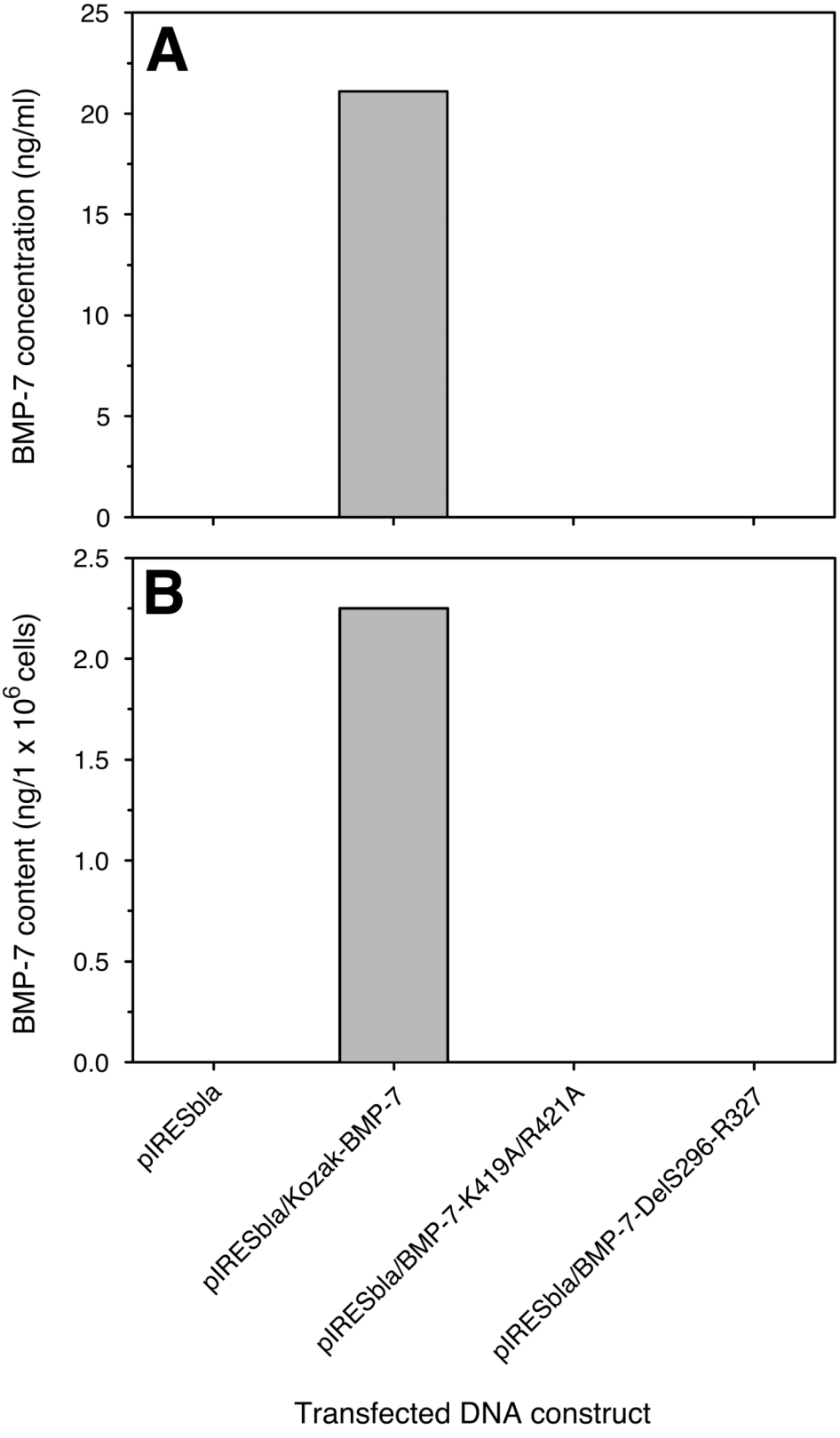

Figure 4.22 Expression of the mutant BMP-7 DNA constructs using CHO-K1 cells

Please refer to the figure legend on the opposite page.

4.2.11 Reverse transcription polymerase chain reaction (RT-PCR)

The experiments described in section 4.2.10 above showed that the stably transfected CHO-K1 cells were not generating detectable levels of the BMP-7 mutant proteins, but the reason for this was unclear. One possibility was that the mutations that were introduced might have caused complications during either the production or post-translational modification of the muteins. This may have resulted in the cells degrading any protein that they had produced, rendering it undetectable. Another key process from which the expression problems may potentially have arisen was the transcription of the mutant mRNA sequences, an essential prerequisite of protein translation. However, the stably transfected cells clearly demonstrated resistance to blasticidin. As an IRES element was utilized in the expression cassette, the BMP-7 mutant and blasticidin sequences would have been expressed from the same promoter and been present on the same mRNA transcript. Therefore, the occurrence of any transcriptional irregularities was unlikely, but needed to be ruled out before any conclusions could be drawn.

To confirm the presence of the mutant mRNA transcripts, a reverse transcription polymerase chain reaction (RT-PCR) experiment was performed. The RNA was extracted from 7.5 x 10^6 stably transfected cells using a Qiagen RNeasy kit, and any residual DNA was eliminated by digestion with DNase I. The reverse transcription step was then completed using random primers to synthesise cDNA from the purified RNA. To detect the presence of the BMP-7 mutant mRNA transcripts, a PCR reaction was carried out using the BMP7WT2-S and BMP7WT-A sense and antisense primers. These primers annealed to regions at the termini of the reverse transcribed cDNA sequences, outside of the mutation sites. They were therefore suitable for use in the PCR amplification of both the wildtype and mutant BMP-7 sequences. A number of control RNA extractions and RT-PCRs were also conducted.

As a positive control for the extraction, reverse transcription and PCR steps, RNA was also extracted from the CHO-K1 cells that were producing detectable levels of the wildtype BMP-7 protein, and RT-PCR was again performed using the same primers. To ensure that the BMP-7 PCR amplification was working correctly, a further PCR control was included in which the pIRESbla/Kozak-BMP-7 vector was used as the template. The same procedure was also followed for the negative control,

using RNA that was purified from the CHO-K1 cells that were stably transfected with the empty pIRESbla vector. Finally, actin control amplifications were incorporated using the Actin-S and Actin-A primers, to ensure that the whole procedure remained consistent throughout. A CHO cell cDNA library, previously produced and kindly provided by Chris Ball at NIBSC, was used as an actin positive control template.

The results from the RT-PCR experiment described above can be seen in Figure 4.23. The pIRESbla/Kozak-BMP-7 vector control PCR reaction in lane 1 shows that the BMP-7 cDNA amplification was successful, producing a band of the expected 1.3 kb size. No product was generated when the actin primers were used with this template, as an actin negative control, due to the absence of any actin cDNA. The opposite result was seen in lane 6, when BMP-7 or actin primers were paired with the actin positive control template. The actin primers produced a correctly sized 208 bp product, whilst no amplification product was obtained when using the BMP-7 primers. The pattern of results from the reactions in lanes 1 and 6 confirmed that the PCR reactions were specific, only producing an amplicon when the appropriate template and primer combination were present. Lane 2 shows the result obtained when the cDNA produced from the cells stably transfected with the empty pIRESbla vector was used as a template. As one would expect, no BMP-7 product was obtained due to the absence of the BMP-7 cDNA insert. However, the actin cDNA did amplify, confirming that the reverse transcription step was successful.

Most importantly, Figure 4.23 clearly showed that the CHO-K1 cells that were stably transfected with either the pIRESbla/BMP-7-K419A/R421A (lane 4) or pIRESbla/BMP-7-ΔS296-R327 (lane 5) mutant vector constructs, were expressing the respective mRNA transcripts. The cDNA template from the cells that were stably transfected with the pIRESbla/Kozak-BMP-7 vector (lane 3) - which were also secreting detectable levels of the wildtype BMP-7 protein - produced a 1.3 kb PCR amplification product. The same size product was obtained from the cDNA template that was derived from the cells transfected with the pIRESbla/BMP-7-K419A/R421A vector (lane 4). It can be seen that the ΔS296-R327 amplification product in lane 5 was shorter at 1.2 kb because of the truncation. Overall, this experiment confirmed that the lack of mutant protein production was not a result of any transcriptional defect, suggesting that the problems lied at the protein level.

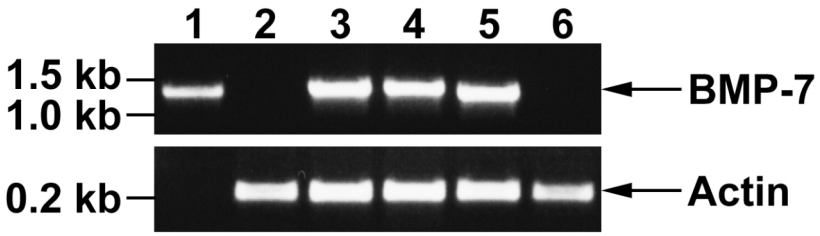

Figure 4.23 Detection of the mutant BMP-7 mRNA in CHO-K1 cells by RT-PCR
The mRNA was isolated from CHO-K1 cells that were stably transfected with the wildtype and mutant BMP-7 expression constructs, and reverse transcribed. To detect the presence of the reverse transcribed BMP-7 cDNA, PCR reactions were carried out using the BMP7WT2-S and BMP7WT-A sense and antisense primers. Actin control amplifications were also carried out using the same samples with the Actin-S and Actin-A primers. The cDNA template samples were as follows: *Lane 1:* pIRESbla/Kozak-BMP-7 vector positive control. *Lane 2:* cDNA from cells transfected with the empty pIRESbla vector. *Lane 3:* cDNA from cells transfected with the wildtype pIRESbla/Kozak-BMP-7 vector. *Lane 4:* cDNA from cells transfected with the mutant pIRESbla/BMP-7-K419A/R421A vector. *Lane 5:* cDNA from cells transfected with the mutant pIRESbla/BMP-7-ΔS296-R327 vector. *Lane 6:* CHO cell cDNA actin positive control.

4.2.12 Expression of the BMP-7 protein variants using suspension cultures of Freestyle CHO-S cells

It remained unclear whether the lack of detectable mutant BMP-7 protein production resulted from an underlying protein processing difficulty (caused by the mutations themselves), or was a side-effect of generally low levels of protein expression overall. As efforts had been made to concentrate cell culture supernatants twenty-fold, and the mutant proteins were also undetectable in cell lysates, the later was unlikely but not implausible. Therefore, a final attempt was made to express the BMP-7 mutant variants using Invitrogen's FreeStyle MAX CHO Expression System. This system utilises high density CHO-S cell suspension cultures to allow large-scale transient transfection and recombinant protein expression. It was thought that if the overall level of protein production could be increased, there would be a greater chance of detecting the mutant proteins if present at all, and their quantity was also consequently increased. Unfortunately, there was no published data to suggest that this expression method would enhance the production of the BMP-7 protein compared

to those used previously. However, communications with Chris Ball at NIBSC indicated that favourable increases had been obtained when expressing other proteins using this system.

To express the wildtype and mutant BMP-7 variants, 3 x 10^7 CHO-S cells were transfected in suspension with 37.5 µg of either the pIRESbla/Kozak-BMP-7, pIRESbla/BMP-7-K419A/R421A or pIRESbla/BMP-7-ΔS296-R327 vector constructs. The transfected cell cultures were then incubated at 37 ºC with 8 % CO_2 on an orbital shaker platform rotating at 135 rpm. Approximately 72 hours post-transfection, the medium from the cultures was collected and clarified by centrifugation. The BMP-7 content of the supernatants was determined by ELISA.

In comparison to the results obtained from the stable transfections (section 4.2.8), Figure 4.24 shows that a 4.7 fold increase in the production of the wildtype BMP-7 protein was achieved when using the FreeStyle MAX CHO Expression System. Despite this wildtype protein expression increase, from 22.4 ng/ml to 104.94 ng/ml, the mutant BMP-7 proteins remained undetectable. It was therefore concluded that the mutations themselves were having a negative impact on the production of the proteins, most likely causing folding or processing complications.

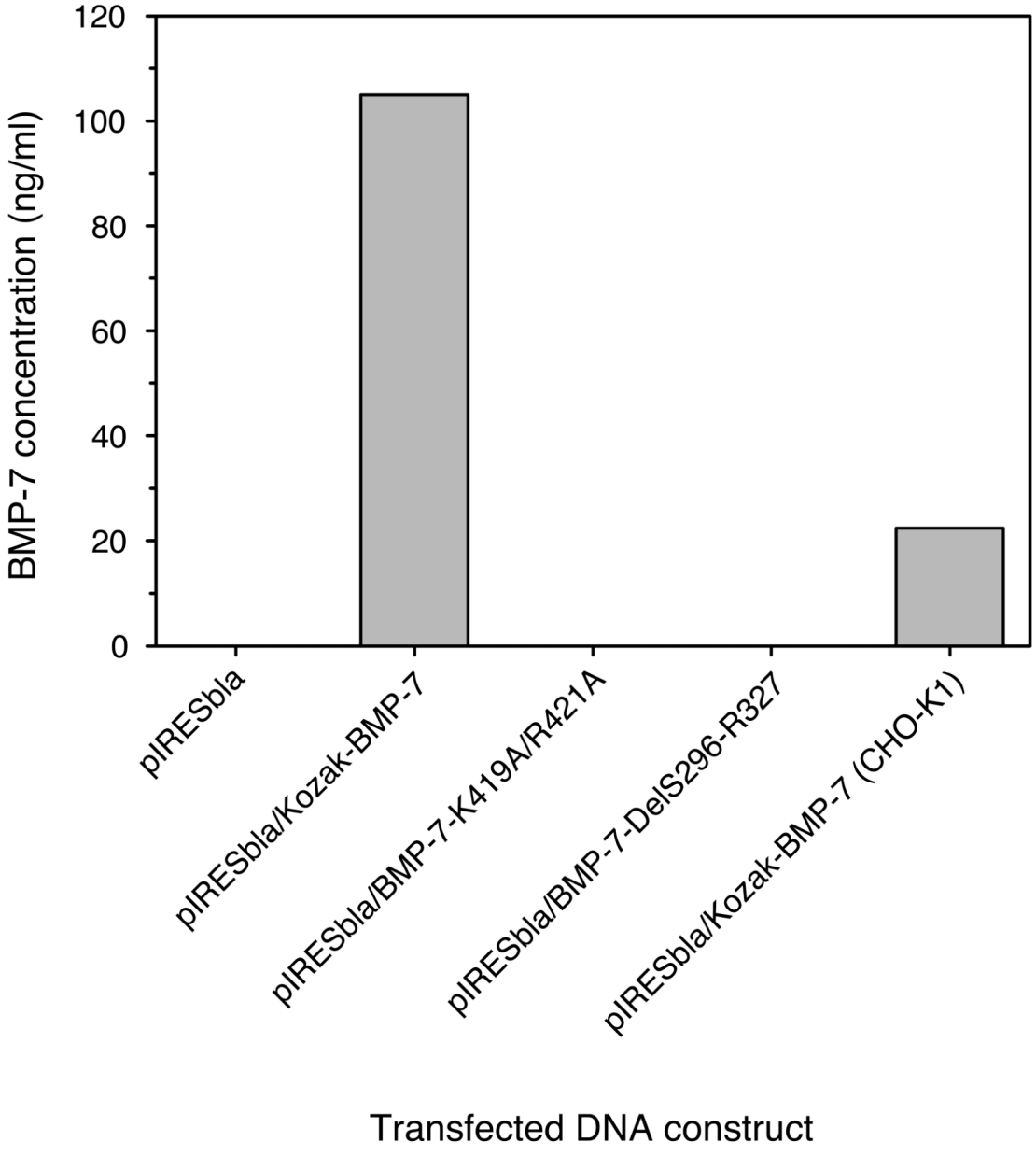

Figure 4.24 Expression of the mutant BMP-7 DNA constructs using FreeStyle CHO-S cells

Suspension Freestyle CHO-S cells were transiently transfected with either the mutant BMP-7 pIRESbla/BMP-7-K419A/R421A or pIRESbla/BMP-7-ΔS296-R327 vector constructs. At the same time, positive and negative control transfections were also carried out using the wildtype BMP-7 pIRESbla/Kozak-BMP-7 DNA construct and empty pIRESbla vector respectively. Supernatants were collected approximately 72 hours post-transfection and their BMP-7 content was determined by ELISA. Whilst it can be seen that the mutant BMP-7 proteins were undetectable, the level of the wildtype BMP-7 protein that was obtained (104.94 ng/ml) was 4.7-fold higher than the level previously obtained when the same pIRESbla/Kozak-BMP-7 DNA construct was expressed using stably transfected adherent CHO-K1 cells (22.4 ng/ml – shown for comparison).

4.2.13 Transient transfection of CHO-K1 cells with mutant BMP-7 expression constructs produced by Centocor Inc

During the later stages of the mutagenesis work described previously, a recombinant BMP-7 expression study was published by a group from Centocor Inc, PA, USA (Swencki-Underwood *et al.*, 2008). This group had also recognised that the production of recombinant BMP-7 in mammalian cells presented a number of challenges:

> *"Specifically, the expression level of recombinant mature BMP-7 protein in mammalian cells is very low, the molecule has poor solubility at neutral pH, and intracellular proteolytic processing events result in a secreted BMP-7 having multiple amino-termini, creating a heterogeneous mixture of proteins."*

The authors of this publication suggested that these difficulties were caused by a few main factors. They explain that electrostatics calculations show that the mature BMP-7 protein has a strongly bi-polar charge distribution, which may be unfavourable for its folding, stability and solubility. In comparison, the mature BMP-2 protein has a more even charge distribution. By N-terminal sequencing, the authors also identified that the BMP-7 precursor protein contains multiple sites at which it is proteolytically cleaved during the prodomain removal step. This differential processing results in the production of a mixture of incorrectly processed truncated BMP-7 isoforms.

Using the available BMP-7 structural information, Swencki-Underwood *et al.* (2008) counteracted these difficulties by designing and generating a number of mutant BMP-7 variants, containing point substitutions in the N- and C-terminal regions of the mature protein. These substitutions increased the expression level of the recombinant BMP-7 protein in CHO cells by approximately eight- to ten-fold when compared to the levels obtained for the wildtype protein. This was accomplished by reducing the overall charge of the mature protein and removing the alternative cleavage sites.

These findings were in contrast to those described in this study, where the introduction of mutations in the same regions resulted in either a lack of, or substantial decrease in protein production. Either way, the mutant proteins were undetectable.

However, the mutations that were made by Swencki-Underwood *et al.* (2008) were either of a different type (i.e. substitutions in the N-terminus rather than a deletion), or were in different positional combinations. The substitutions that they made in the C-terminal region were also of a different chemical nature to those in this study, with basic amino acids being replaced with negatively charged acidic residues rather than alanine, which is neutral and has a much smaller side chain. Despite these differences, the mutations described were located in the same C- and N-terminal target regions of the mature BMP-7 protein as those in the K419A/R421A and ΔS296-R327 mutants, which were produced in section 4.2.9 of this study. Therefore, the Centocor mutants were of particular interest, and were requested for use in heparin-binding experiments as part of this project. Centocor kindly provided these mutants (Table 4.2) in the forms of both DNA expression constructs and clarified conditioned cell culture supernatants.

Construct identifier	Description of point substitutions
3255	C-terminal: R421E/N422D/R426E
3267	N- and C-terminal: R299S/R314S, R421E/N422D/R426E
3281	N-terminal: R299S/R314S

Table 4.2 Centocor mutant BMP-7 expression constructs
The identifications of the mutant BMP-7 constructs produced by Centocor (Swencki-Underwood *et al*, 2008), and a description of the substitutions that each contained.

The mutant constructs and proteins provided by Centocor were identified by the unique numbers that they had been given (Table 4.2). Mutant 3255 contained the C-terminal substitutions R421E/N422D/R426E, and mutant 3281 contained the N-terminal substitutions R299S/R314S. All of these point substitutions were combined to produce the mutant identified as 3267 (R299S/R314S, R421E/N422D/R426E). Notably, the amino acids R421 and R426 were two of the residues - along with K419 - that were predicted by the molecular docking simulations in Chapter 3 to be important for heparin-binding. To express these mutants, which also contained optimised Kozak consensus sequences, 1 x 10^7 CHO-K1 cells were transiently transfected with the supplied constructs using the procedure described in Swencki-Underwood *et al.* (2008). A transfection was also carried out using the pIRESbla/Kozak-BMP-7

wildtype construct in this expression system for comparison. Four days post-transfection, the supernatants were collected from the cell cultures and clarified by centrifugation. The BMP-7 content of both these supernatants and those provided by Centocor was determined by ELISA (Figure 4.25).

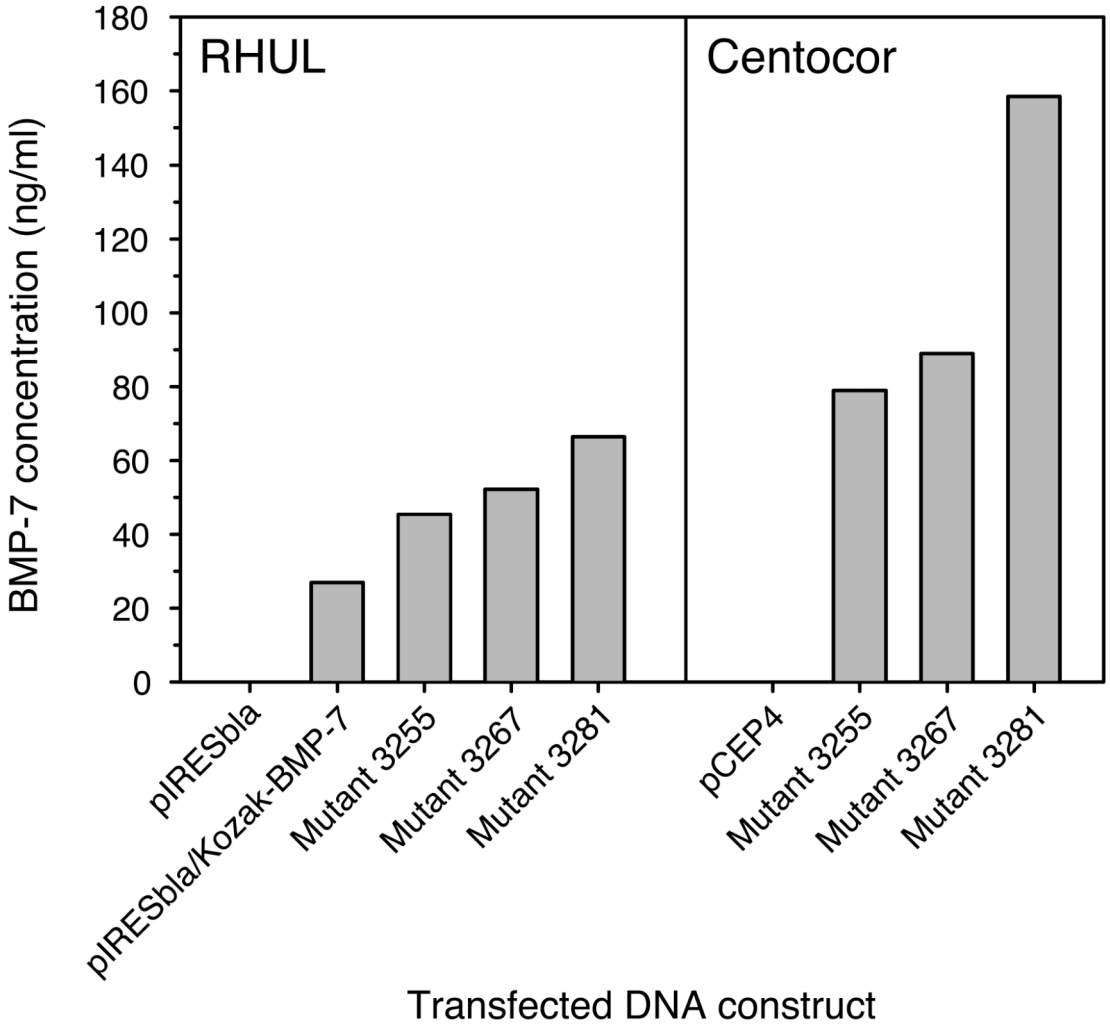

Figure 4.25 Expression of the Centocor mutant BMP-7 proteins
Adherent CHO-K1 cells were transiently transfected with the Centocor 3255 (R421E/N422D/R426E), 3267 (R299S/R314S, R421E/N422D/R426E) and 3281 (R299S/R314S) mutant BMP-7 DNA constructs in our own laboratory (panel labeled RHUL) and in the laboratory of Swencki-Underwood *et al.* (2008) at Centocor (panel labeled Centocor). Transfections that were carried out in our own laboratory were conducted alongside positive and negative control transfections using the wildtype BMP-7 pIRESbla/Kozak-BMP-7 DNA construct and empty pIRESbla vector respectively. Transfections that were carried out by the Centocor group were conducted alongside a negative control using an empty pCEP4 vector (Invitrogen). Approximately 72 hours post-transfection, supernatants were collected from the transfected cell cultures and their BMP-7 content was determined by ELISA.

It can be seen in Figure 4.25 that the supernatants that were provided by the Centocor group (labeled Centocor) contained 79.0 ng/ml, 89.0 ng/ml and 158.5 ng/ml of the 3255, 3267 and 3281 BMP-7 mutant proteins respectively. In comparison, the supernatants that were collected from CHO cells that had been transfected with the same mutant BMP-7 expression constructs in our own laboratory (labeled RHUL) contained lower concentrations of the respective mutant BMP-7 proteins, at 45.5 ng/ml (3255), 52.2 ng/ml (3267) and 66.4 ng/ml (3281). It is clear from these results that the levels of the mutant BMP-7 proteins that were produced by the CHO cells following all of these transfections were greater than the 27.0 ng/ml of wildtype BMP-7 protein that was produced under the same conditions. However, these concentrations were still somewhat lower than the concentrations that were previously published by Centocor (Swencki-Underwood *et al.*, 2008), which were in the range of approximately 230-260 ng/ml. It is therefore apparent that the expression level of the BMP-7 protein remains variable from one transfection to another despite the considerable effort that has been put into optimising its biochemical characteristics. This once again serves to highlight the challenge that expressing consistent levels of the BMP-7 protein presents. It is also noteworthy that in almost all instances, the levels of the optimised BMP-7 mutant proteins that were produced by both Centocor and ourselves using this expression approach were lower than the level of the wildtype BMP-7 protein that was produced by the suspension-cultured CHO-S cells when using the Invitrogen FreeStyle MAX CHO Expression System in our own laboratory (104.94 ng/ml, as discussed in section 4.2.12). This shows that for the purpose of increasing the yield of the BMP-7 protein alone, such optimisation of its biochemical characteristics is not necessary when similar gains in production can be obtained by simply adopting an alternative expression method. Even so, this work provided us with sufficient quantities of mutant proteins that could be used to determine whether or not certain basic residues in the N- and C-terminal ends of the BMP-7 protein play a key part in BMP-7-HS/heparin interactions. This was assessed by subjecting these muteins to heparin-affinitiy chromatography, as discussed in Chapter 5.

Chapter 5: Heparin-binding studies

5.1 Introduction

As described in Chapter 4, the efforts made to express the BMP-7 K419A/R421A and ΔS296-R327 mutants did not result in the production of detectable levels of protein. However, the Centocor mutants discussed in section 4.2.13 (Swencki-Underwood *et al*, 2008) were both expressed and supplied in sufficient quantities that their heparin-binding properties could be investigated. As explained previously, these proteins contained similar mutations to those attempted in this study, which were located in the same regions of interest. To study the heparin-binding properties of the wildtype and mutant BMP-7 proteins, heparin affinity chromatography was employed in this chapter, just as it was previously to uncover the heparin-binding site of GDNF (Alfano *et al.*, 2007). The BMP-7 protein variants were applied to heparin columns at physiological ionic strength and pH, and the relative affinities of the protein-heparin interactions were determined by the concentration of NaCl required to elute the proteins from the columns.

5.2 Results and discussion

5.2.1 Heparin affinity chromatography

5.2.1.1 Heparin affinity chromatography of wildtype recombinant human BMP-7

The CHO-K1 cells that were transfected to express the Centocor mutants secreted the recombinant proteins into CD CHO medium (Invitrogen). CD CHO medium is a chemically defined serum-free and protein-free medium, which also contains no peptide components of animal, plant or synthetic origin. The clarified supernatants containing the mutant proteins (section 4.2.13) were therefore deemed to be of a sufficient quality to be used directly in initial heparin affinity chromatography experiments after dialysis, without prior purification. Any mutant that demonstrated a

favourable reduction in its ability to bind heparin after the initial screen could then be purified and investigated further.

Before being able to determine the affect, if any, that the mutations made by Centocor had on the heparin-binding ability of BMP-7, it was first necessary to determine the NaCl concentration at which the wildtype protein eluted from heparin affinity columns. For consistency, the commercially produced wildtype recombinant human BMP-7 protein (R&D Systems) was diluted in conditioned CD CHO medium taken from cells that were transfected with the empty pCEP4 vector alone. This BMP-7-containing supernatant was then dialysed against PBS to ensure that the protein was applied to the heparin affinity column at physiological pH and ionic strength. After equilibrating a 1 ml Heparin HiTrap HP column (GE Healthcare UK Ltd) with PBS, 500 ng of the wildtype BMP-7 protein was applied to the column in a 5 ml volume, at a flow rate of 0.5 ml/min. The column was washed with 5 ml of PBS, and the protein was eluted by applying a linear gradient of NaCl in PBS (0.14 to 1.2 M). The whole procedure was conducted at 4 ºC and 1 ml fractions were collected throughout. The BMP-7 content of the fractions was determined by ELISA, and their NaCl concentration was determined by carrying out conductivity measurements and standardising against a series of solutions of known concentration.

With the exception of a minor pass-through peak, it can be seen in Figure 5.1 that the wildtype recombinant human BMP-7 bound to the heparin column at physiological pH and ionic strength. To elute the protein from the column, approximately 0.5 M NaCl was required. This represented a modest affinity ionic interaction with heparin when compared with the higher affinity interactions observed for the GDNF-family ligands, which required at least 0.8 M NaCl for elution from the column (Alfano *et al.*, 2007).

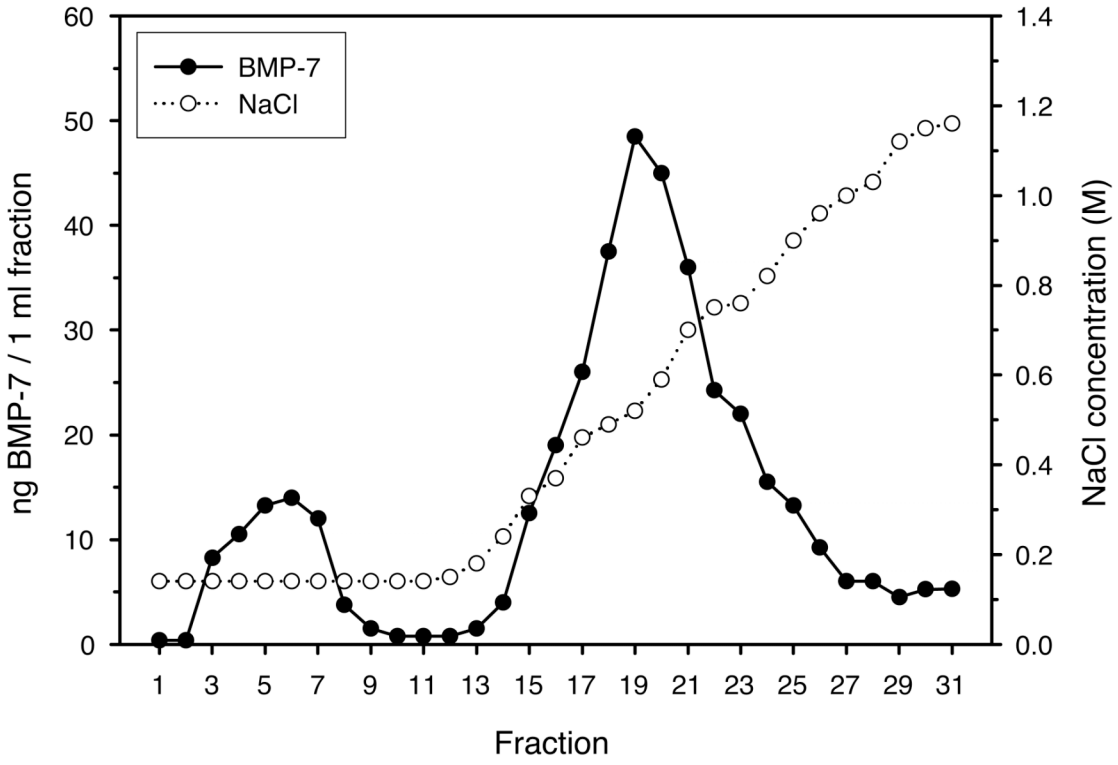

Figure 5.1 Heparin-affinity chromatography of the wildtype BMP-7 protein
500 ng of wildtype recombinant human BMP-7 (R&D Systems) was applied to a Heparin HiTrap HP column (GE Healthcare UK Ltd) in 5 ml of conditioned CD CHO medium at physiological pH and ionic strength. The column was washed with 5 ml of PBS and the bound protein was eluted by applying a linear gradient of NaCl in PBS. 1 ml fractions were collected throughout. The BMP-7 content of the fractions was determined by ELISA and their NaCl concentration was determined by carrying out conductivity measurements and standardising against a series of solutions of known concentration. It can be seen that approximately 0.5 M NaCl was required to elute the wildtype BMP-7 protein from the column.

5.2.1.2 Heparin affinity chromatography of the Centocor 3255 BMP-7 mutant

Having established the relative affinity of the wildtype BMP-7 protein for heparin, attention was diverted to investigating the heparin-binding properties of the Centocor mutants. The first of these mutants to be studied was that denoted 3255, containing the C-terminal substitutions R421E/N422D/R426E. From the molecular docking simulations carried out in Chapter 3, the amino acids R421 and R426 were two of the three C-terminal residues that were predicted to be important for heparin-binding. If the predicted models of the interaction between BMP-7 and HS/heparin

presented in Chapter 3 were correct, it would be expected that a pronounced decrease would be observed in the heparin-binding affinity of the BMP-7 3255 mutant, compared to that of the wildtype protein. To test this hypothesis, heparin affinity chromatography was again utilised in the same way as described in section 5.2.1.1 above.

The clarified supernatant containing the 3255 mutant protein was dialysed against PBS, and a volume containing 500 ng of the mutant protein was applied to a 1 ml Heparin HiTrap HP column. As shown in Figure 5.2, the result obtained was not as hypothesised. Like the wildtype BMP-7 protein, the 3255 mutant also required approximately 0.5 M NaCl for elution from the column, indicating that its heparin-binding affinity was unaltered. As the 3255 mutant was missing half of the basic residues in the C-terminal region of the BMP-7 protein - and two-thirds of those predicted to be key for binding to heparin - this data suggests that the heparin-binding site of BMP-7 is not located in the C-terminal region. This meant that the prediction made by the molecular docking simulations was incorrect, most probably resulting from the limitation of the missing N-terminus in the available BMP-7 crystal structures. Based on the uneven distribution of basic residues in the mature BMP-7 protein sequence, and the lack of any alternative clusters of positive charge in the folded three-dimensional structure, it is likely that the heparin-binding site of BMP-7 lies within its N-terminal region. As mentioned previously, this region contains approximately half of the basic residues found within the mature BMP-7 protein.

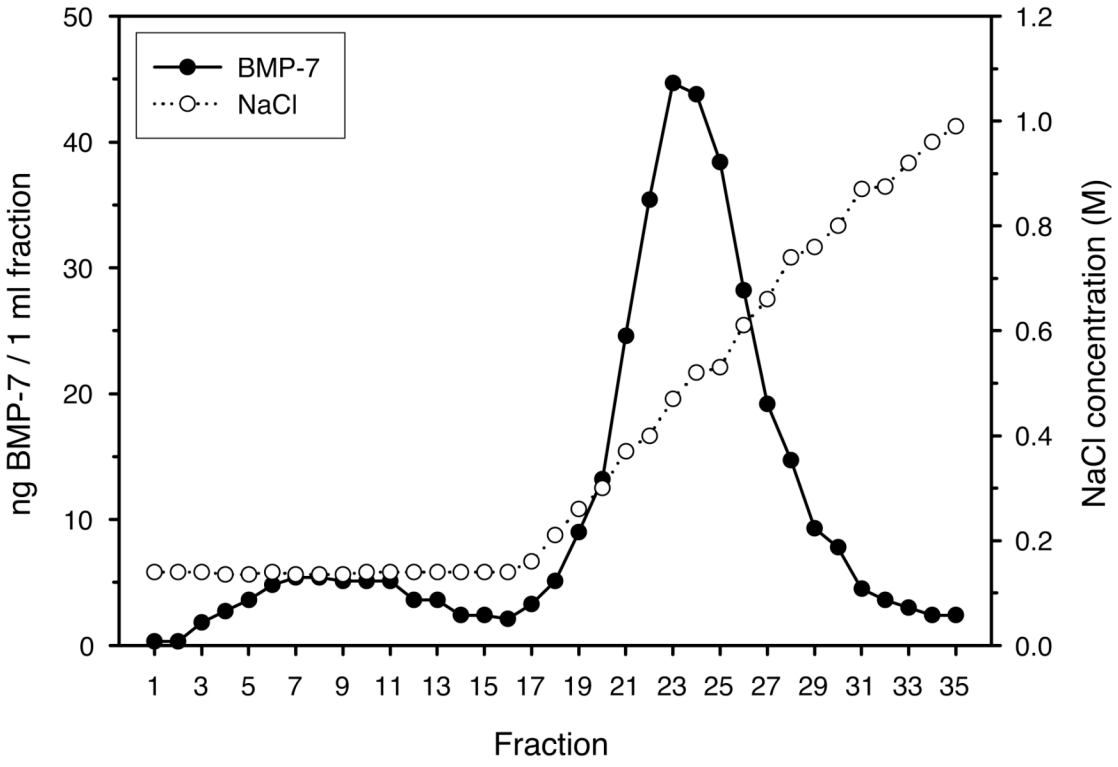

Figure 5.2 Heparin-affinity chromatography of the Centocor 3255 mutant BMP-7 protein
500 ng of the Centocor 3255 mutant BMP-7 protein was applied to a Heparin HiTrap HP column (GE Healthcare UK Ltd) in 5 ml of conditioned CD CHO medium. The column was washed with 5 ml of PBS and the bound protein was eluted by applying a linear gradient of NaCl in PBS. 1 ml fractions were collected throughout. It can be seen that approximately 0.5 M NaCl was required to elute the 3255 mutant BMP-7 protein from the column.

5.2.1.3 Heparin affinity chromatography of the Centocor 3281 BMP-7 mutant

As explained in section 5.2.1.2, it appears likely that the heparin-binding site of BMP-7 is situated in its unstructured N-terminal sequence. However, as detectable levels of the BMP-7 ΔS296-R327 mutant could not be produced, it was not possible to study the heparin-binding ability of the whole N-terminal region of BMP-7 experimentally. Even still, the BMP-7 3281 mutant provided by Centocor contained two N-terminal mutations of interest; the basic arginine residues at positions 299 and 314 had been substituted with serine residues (R299S/R314S). Either one, or both, of these residues may potentially play a part in the heparin-binding site of BMP-7.

Heparin affinity chromatography was carried out to determine if these two point mutations had any affect on the heparin-binding affinity of the BMP-7 protein. The supernatant containing the 3281 mutant was dialysed against PBS, and 500 ng of the mutant protein was applied to a 1 ml heparin column. It can be seen in Figure 5.3 that the R299S/R314S double substitution failed to alter the heparin-binding affinity of BMP-7. Again, approximately 0.5 M NaCl was required for its elution from the column. Despite this finding, it remains possible that the heparin-binding site of BMP-7 is situated in its N-terminal region. This is because there are a number of alternative basic residues located within this region, which also have the potential to form a suitable binding site.

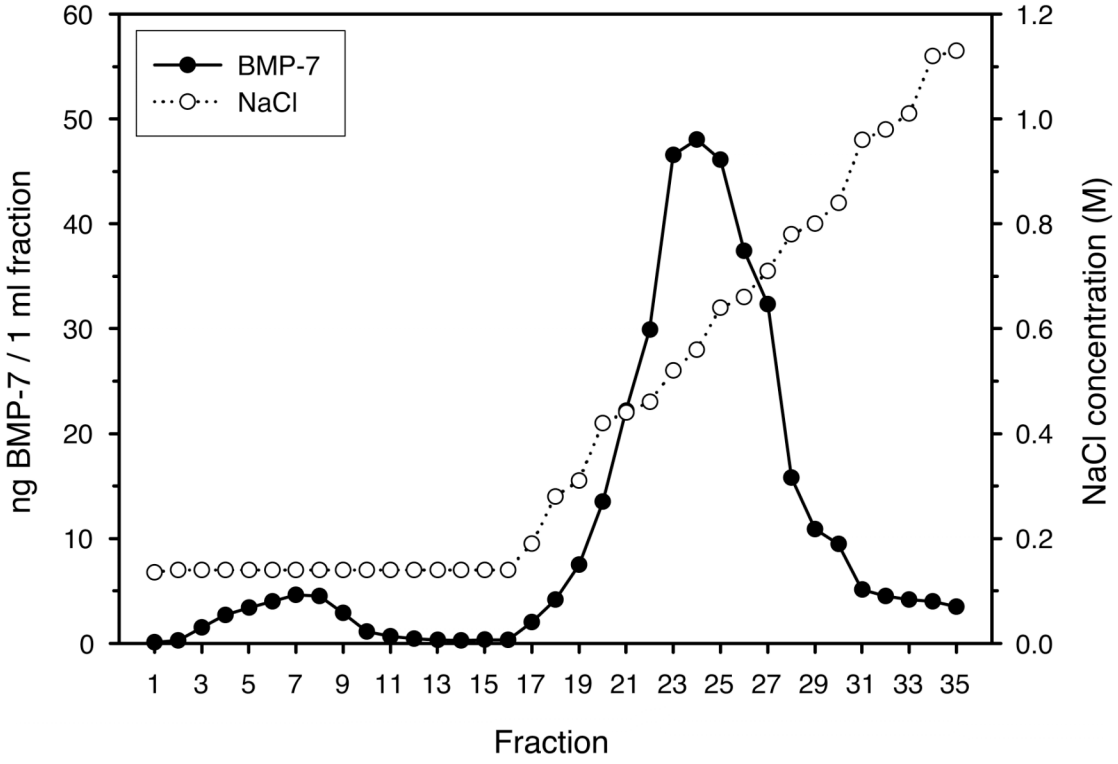

Figure 5.3 Heparin-affinity chromatography of the Centocor 3281 mutant BMP-7 protein
500 ng of the Centocor 3281 mutant BMP-7 protein was applied to a Heparin HiTrap HP column (GE Healthcare UK Ltd) in 5 ml of conditioned CD CHO medium. The column was washed with 5 ml of PBS and the bound protein was eluted by applying a linear gradient of NaCl in PBS. 1 ml fractions were collected throughout. It can be seen that approximately 0.5 M NaCl was required to elute the 3281 mutant BMP-7 protein from the column.

5.2.1.4 Heparin affinity chromatography of the Centocor 3267 BMP-7 mutant

Although neither the Centocor 3255 mutant nor the 3281 mutant individually demonstrated a reduction in their affinities for heparin compared to the wildtype protein, it remained to be seen if combining the mutations would have any affect. Therefore, the heparin-binding ability of the Centocor 3267 BMP-7 mutant (R299S/R314S, R421E/N422D/R426E) was studied using heparin affinity chromatography.

Figure 5.4 shows that combining the N-and C-terminal mutations also had no affect on the heparin-binding affinity of BMP-7. The 3267 mutant eluted from the column with a NaCl concentration of approximately 0.5 M, just as the wildtype protein and other mutants had previously. However, as the N-terminal mutations in the 3267 mutant were by no means comprehensive, the possibility of a N-terminal or cooperative N- and C-terminal heparin-binding site cannot be ruled out completely.

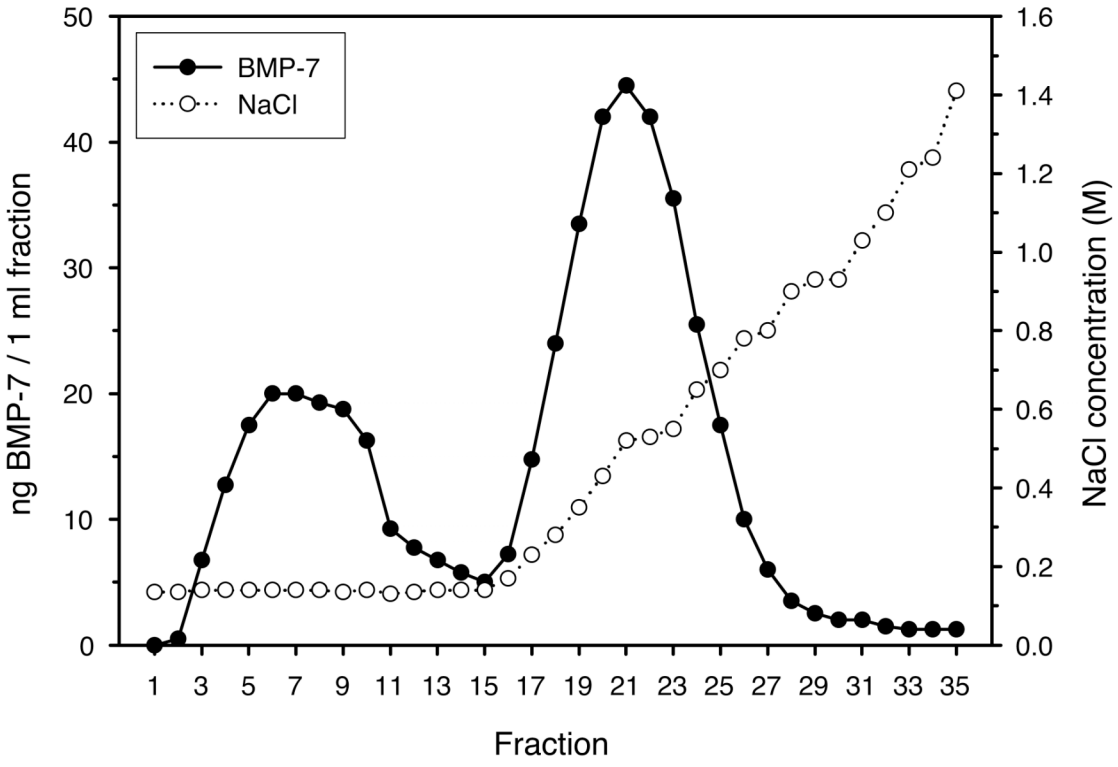

Figure 5.4 Heparin-affinity chromatography of the Centocor 3267 mutant BMP-7 protein
500 ng of the Centocor 3267 mutant BMP-7 protein was applied to a Heparin HiTrap HP column (GE Healthcare UK Ltd) in 5 ml of conditioned CD CHO medium. The column was washed with 5 ml of PBS and the bound protein was eluted by applying a linear gradient of NaCl in PBS. 1 ml fractions were collected throughout. It can be seen that approximately 0.5 M NaCl was required to elute the 3267 mutant BMP-7 protein from the column.

5.2.1.5 Further investigation of the heparin column elution profiles of the BMP-7 protein variants

Although the Centocor mutants failed to demonstrate any change in their heparin-binding affinities compared to the wildtype BMP-7 protein, some small differences were observed between the column elution profiles that were obtained whilst carrying out this investigation. In particular, it can be seen that in the cases of the wildtype and Centocor 3267 mutant proteins (Figures 5.1 and 5.4 respectively), the minor pass-through peaks were more pronounced in relation to the major peak when compared to the profiles of the other BMP-7 variants. Also, following the minor peak in the profile of the 3267 mutant, the levels of BMP-7 in the fractions preceding

the major peak remained higher than those in the other profiles. These findings were consistently true and were observed irrespective of the protein loading (data not shown). It was thought that the pronounced peaks consistently obtained for the unbound BMP-7 protein might suggest that two forms of the protein were in existence. If this was the case, the increased level of protein between the two peaks in the chromatographic profile of the 3267 mutant might represent an intermediate state.

To test this theory, some further investigation was conducted. The component fractions from both the minor and major peak in the profile of the BMP-7 3267 mutant were pooled separately and dialysed against PBS. This ensured that the eluates were returned to physiological ionic strength and pH. The two fraction pools were then applied to separate heparin columns, and eluted by applying a linear gradient of NaCl in PBS as before. The same procedure was also followed using the component fractions from both peaks of the profile of the wildtype BMP-7 protein. The eluted fractions were then assayed for BMP-7 content by ELISA.

When the pooled fractions that formed the major peak of the 3267 mutant were re-subjected to heparin affinity chromatography, the same pattern of results was seen as previously described in section 5.2.1.4 above. It can be seen in Figure 5.5 that two peaks were produced once again, with the minor peak representing the unbound protein. The BMP-7 protein in the major peak eluted as before at a NaCl concentration of approximately 0.5 M. Furthermore, when the fraction pool that formed the previously observed minor peak of the 3267 mutant was applied to another heparin column, only a single peak was obtained (Figure 5.6). This peak solely contained material that had passed through the column without binding, as did the minor peak in Figure 5.4 that the pooled sample was obtained from. However, these findings were not unique to the 3267 mutant, as exactly the same results were obtained when the pooled fractions from the previous wildtype BMP-7 profile were re-subjected to heparin affinity chromatography (data not shown).

Together, these data show that at some point during the dialysis or heparin chromatography procedures, a portion of the BMP-7 protein underwent a transformation. The nature of this transformation was not clear but it was unidirectional and resulted in the protein being unable to bind to heparin. As the resulting BMP-7 protein could still be detected using two independent monoclonal antibodies in the sandwich ELISA assay, it is unlikely that it had been proteolytically

fragmented. Instead, one possibility is that the protein had become structurally denatured during the process, with the degree of denaturation varying from one BMP-7 variant to another. Another possibility, although it is purely speculative at this stage, is that a small component of the protein encompassing the heparin-binding site had been clipped off by a protease, leaving the rest of the protein intact. As the heparin affinity chromatography experiments suggest that the heparin-binding site of BMP-7 probably lies within its unstructured N-terminal extension, this explanation is quite feasible but would require further investigation before any firm conclusions could be made.

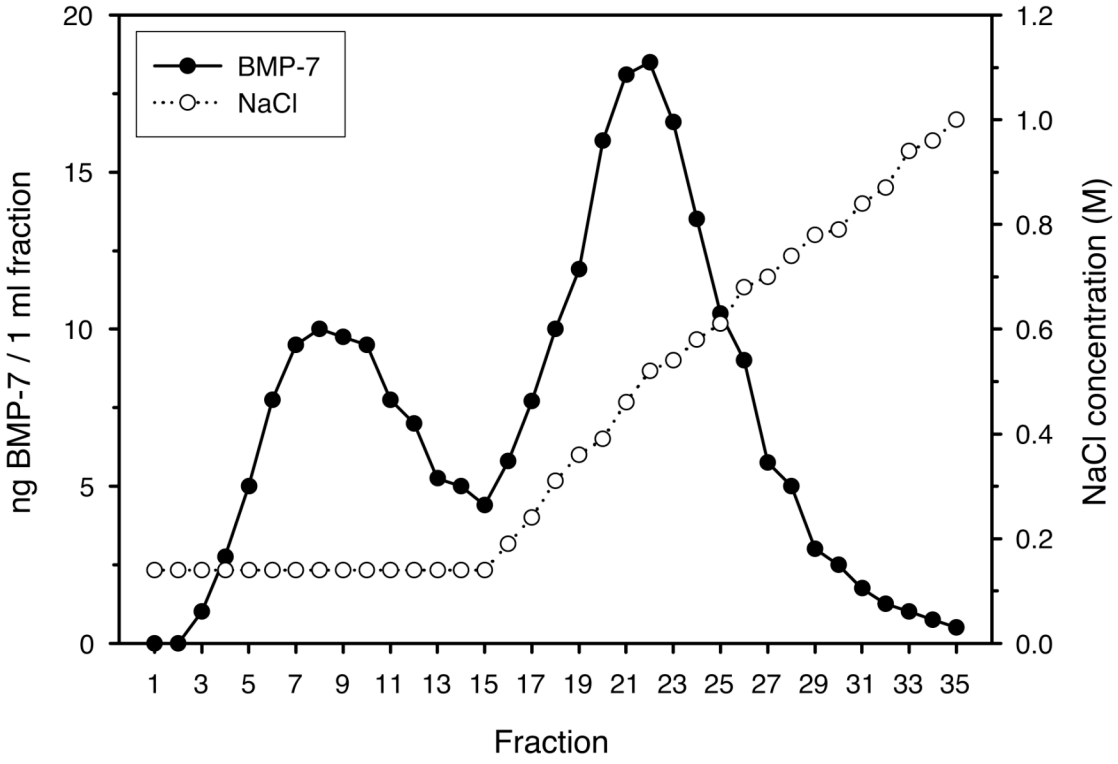

Figure 5.5 Heparin-affinity chromatography of the BMP-7 3267 mutant pooled major peak

The component fractions of the major peak in the elution profile of the BMP-7 3267 mutant were pooled and dialysed against PBS. The pooled fractions were then applied to a Heparin HiTrap HP column (GE Healthcare UK Ltd). The column was washed with 5 ml of PBS and the bound protein was eluted by applying a linear gradient of NaCl in PBS. 1 ml fractions were collected throughout. It can be seen that the 3267 mutant BMP-7 protein that was present in the previous major peak once again eluted from the column with approximately 0.5 M NaCl.

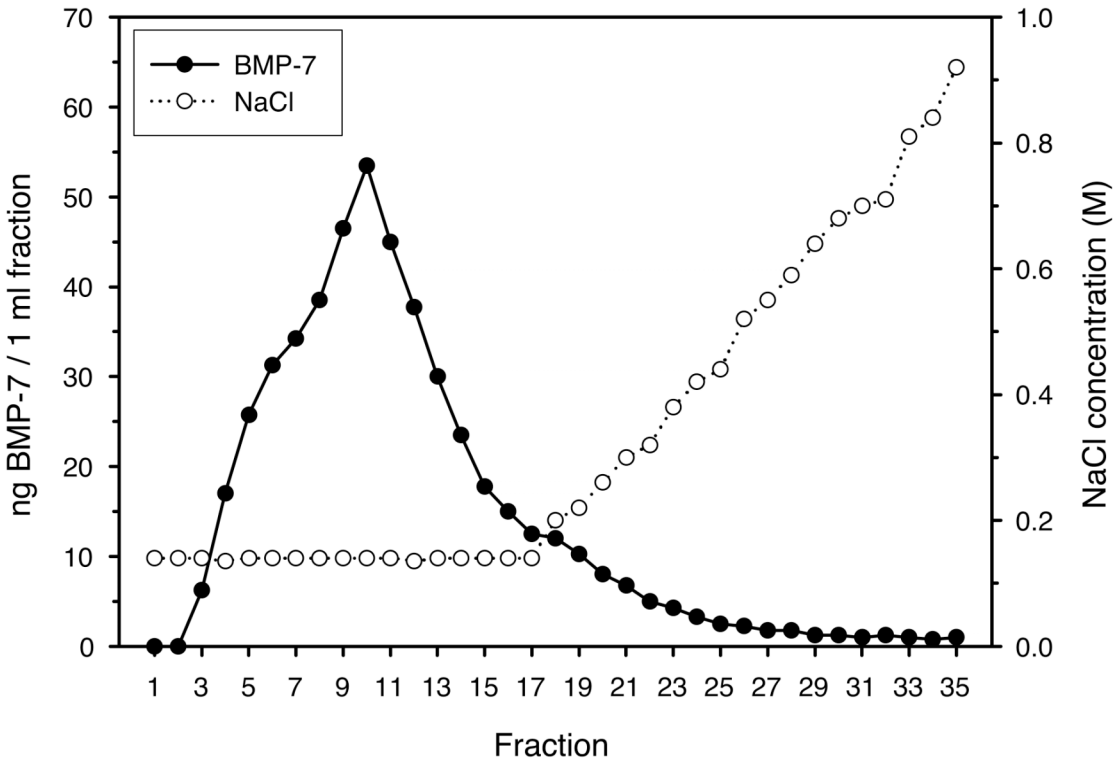

Figure 5.6 Heparin-affinity chromatography of the BMP-7 3267 mutant pooled minor peak
The component fractions of the minor peak in the elution profile of the BMP-7 3267 mutant were pooled and dialysed against PBS. The pooled fractions were then applied to a Heparin HiTrap HP column (GE Healthcare UK Ltd). The column was washed with 5 ml of PBS and the bound protein was eluted by applying a linear gradient of NaCl in PBS. 1 ml fractions were collected throughout. It can be seen that the 3267 mutant BMP-7 protein that was present in the previous minor peak once again passed through the heparin column without binding.

5.2.2 Protection of recombinant human BMP-7 from proteolysis by Endoproteinase Lys-C

It has been previously found that binding to heparin can serve to protect a protein from proteolysis (Lortat-Jacob *et al.*, 1996). This can be demonstrated using Endoproteinase Lys-C (Mummery and Rider, 2000; Mummery *et al.*, 2007; Rickard *et al.*, 2003). Lys-C is a serine endopeptidase isolated from *Lysobacter enzymogenes*, which hydrolyses peptide bonds specifically at the carboxyl side of lysine residues. Proteins generally bind to heparin via the basic side chains of lysine and arginine residues. When lysine residues are involved in the interaction, they become masked

by the heparin and inaccessible to Lys-C, therefore preventing proteolysis occurring. An experiment was carried out to determine if this was also true for the BMP-7 protein, and to demonstrate the binding of BMP-7 to heparin by yet another method independent of the aforementioned heparin affinity chromatography and previous heparin-binding ELISA (C. Rider *et al*, unpublished data).

25 µl reaction mixtures were assembled containing 50 ng recombinant human BMP-7 (R & D Systems) in the presence and absence of 5 µg/ml heparin (Sigma). The mixtures were incubated for 30 minutes at room temperature before 1 ng Endoproteinase Lys-C (Sigma) was added to each tube. The digestion mixtures were then incubated in a 37 ºC water bath for the specified time, after which Laemmli sample buffer was added and they were boiled immediately. Following digestion, the samples were analysed by carrying out SDS-PAGE and Western blotting.

Figure 5.7 shows that under these conditions, the recombinant human BMP-7 protein was almost completely degraded in the absence of heparin. This was demonstrated by an almost complete loss of BMP-7 immunoreactivity after a 120 minute digestion with Lys-C, with a decrease being apparent after only 30 minutes. BMP-7 peptide fragments were not detectable, suggesting that the epitopes necessary for detection were removed upon cleavage. In the presence of heparin, very little proteolysis of the BMP-7 protein occurred, if any, over the same time interval. This indicated that by binding to heparin, the BMP-7 protein was protected from digestion by Lys-C. It is quite possible that by interacting with heparin-related glycosaminoglycans, the BMP-7 protein might be similarly protected from proteolytic degradation *in vivo*.

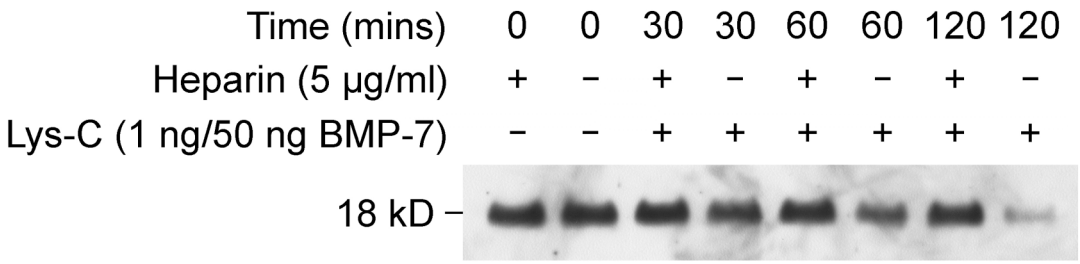

Figure 5.7 Digestion of human BMP-7 with endoproteinase Lys-C
In the presence and absence of 5 µg/ml heparin (Sigma), 50 ng quantities of the recombinant human BMP-7 protein (R&D Systems) were subjected to proteolytic digestion with endoproteinase Lys-C for the indicated time intervals. Following digestion, the samples were analysed by carrying out SDS-PAGE and Western blotting. It can be seen that in the absence of heparin, the BMP-7 protein was almost completely degraded after 120 minutes. In the presence of heparin, the BMP-7 was protected from proteolysis by endoproteinase Lys-C.

Chapter 6: General discussion

Prior to commencing this investigation, it was clear that BMPs -2 and -4 bind to HS and heparin GAGs via a small cluster of basic amino acids in their short N-terminal extensions (Ruppert *et al.*, 1996; Ohkawara *et al.*, 2002). It had also been demonstrated that BMP-7 has the ability to bind to HS/heparin (Irie *et al.*, 2003; Rider *et al.*, unpublished data). However, BMP-7 belongs to a different BMP sub-group from BMPs -2 and -4 and it differs from them considerably in its N-terminal region. Consequently, it remained unclear as to where its HS/heparin-binding site is situated. The aim of this study was therefore to determine the location of the HS/heparin-binding site of human BMP-7. This goal was approached using a combination of predictive computational molecular docking calculations, site-directed mutagenesis techniques and heparin-affinity chromatography.

The findings from a series of predictive docking calculations that were carried out using published BMP-7 and heparin structures suggested that BMP-7 binds to HS/heparin through three basic residues close to the C-terminal ends of each of its constituent monomers (K419, R421 and R426). Although difficulties were encountered in expressing both wildtype and mutant BMP-7 protein variants (discussed later on in this chapter), a mutein that was suitable for testing the validity of the above prediction experimentally was kindly provided by Centocor Inc (PA, USA). In this mutein, two of the three C-terminal basic residues that had been predicted to play a key part in BMP-7-HS/heparin interactions (R421 and R426) had been removed from each monomer by substituting them for glutamic acid residues, leaving only K419 unchanged. In addition, N422 had been substituted for an aspartic acid residue. Based on the aforementioned prediction, it was expected that when this particular BMP-7 mutant was subjected to heparin-affinity chromatography it would either not bind to the heparin column or its heparin-binding affinity would be markedly reduced. This is because the two remaining K419 residues (one on each monomer) would not be sufficient to bind a HS/heparin chain either independently or in cooperation with each other. Also, it was thought likely that the introduction of acidic residues in place of the basic arginine residues (and N422) would alter the overall charge of this particular stretch of C-terminal sequence and perhaps even serve

to repel like-charged acidic HS/heparin chains. One would expect either of these occurrences to have a negative effect on HS/heparin-binding affinity. However, the result obtained from this experiment was not as expected. Instead, the removal of R421 and R426 from each BMP-7 monomer was demonstrated to have no affect on the heparin-binding affinity of BMP-7.

The fact that the removal of R421 and R426 failed to decrease the heparin-binding affinity of BMP-7 whatsoever indicates that these residues do not play a critical part in BMP-7-HS/heparin interactions. This finding (and the demonstration that the introduction of acidic residues was without effect) also suggests that the prediction that was made by the docking calculations was incorrect and casts considerable doubt on the hypothesis that the key HS/heparin-binding regions of the BMP-7 protein are situated close to the C-terminal ends of its two constituent monomers. Even so, at this point in time, no firm conclusions can be made regarding this matter. This is because the interpretation of the findings described above is complicated by the fact that two C-terminal K418 basic residues also remain in the R421E/N422D/R426E mutant. It was explained in Chapter 3 that the results from the molecular docking calculations suggested that the basic side chain of K418 is not oriented in a way that would be conducive to it cooperating with K419, R421 and R426 to bind a HS/heparin chain. However, there are two reasons why one cannot rule out the possibility that K418 may play a part in BMP-7-HS/heparin interactions based on these predictions. Firstly, experimental data now appears to show that the predictions made by the docking calculations are incorrect and cannot be relied upon. Secondly, during the docking process, the BMP-7 protein entity was treated as a rigid body with no flexibility in the structure being allowed for. This was due to a limitation of the Autodock 2.4 software that was used to carry out the calculations and was a reason why it was always the case that the predictions made by the docking predictions would need to be treated with caution. It therefore remains a possibility that there may be enough flexibility in the BMP-7 protein structure for the side chains of the two K418/K419 residue pairs (one pair on each monomer) to cooperate in binding a HS/heparin chain between them. Consequently, before any firm conclusions can be made about the role that the C-termini of BMP-7 may or may not play in BMP-7-HS/heparin interactions, it needs to be determined whether or not BMP-7 will still bind to HS/heparin with the same relative affinity after the two K418/K419 residue

pairs that remain in the R421E/R426E mutant are also removed. This will require further site-directed mutagenesis studies to be carried out.

Because the results obtained during this investigation appear to show that the HS/heparin-binding ability of BMP-7 is unlikely to be solely dependent on the predicted C-terminal basic residues, one may hypothesise that the key HS/heparin-binding residues are located within either or both of the two alternative basic residue clusters that BMP-7 possesses. As explained previously in Chapter 1, these clusters are situated in the N-terminal extension of BMP-7 and the sequence stretch that lies immediately downstream of it. Because other closely related BMP family and TGF-β superfamily members, such as BMPs -2 and -4 (Ruppert *et al.*, 1996; Ohkawara *et al.*, 2002) and GDNF (Alfano *et al.*, 2007) have already been shown to bind to HS/heparin via basic residues in their N-terminal extensions, it would not be completely unexpected for BMP-7 to do the same, albeit through basic residues in different positions within these sequences. There is also still a possibility that residues from these N-terminal clusters could cooperate with some of the C-terminal basic residues to bind HS/heparin chains. Unfortunately, due to the protein expression problems that were encountered during this investigation, suitable mutants were not available to test these hypotheses comprehensively. As a result, further investigation is required in order to fulfill the aim of this project.

The inconsistency between the results obtained from the computational docking predictions and the experimental data seems to have been caused by a limitation of all of the BMP-7 structures that have been published to date and which were used in these docking calculations. These structures are missing the majority of their N-terminal extensions. It is likely that this component of the structure remained unresolved as a result of it being disordered (Griffith *et al.*, 1996; Greenwald *et al.*, 2003). Because this missing region contains almost half of the fifteen basic residues that can be found within the mature BMP-7 protein, a number of potentially important N-terminal basic residues could not be taken into consideration during the molecular docking calculations. It was therefore not possible to predict the extent to which the missing residues are (or are not) involved in BMP-7-HS/heparin interactions. As a result, it appears that the Autodock 2.4 software incorrectly predicted that the C-terminal basic residues of BMP-7 would form the most suitable site for a HS/heparin chain to bind to.

As mentioned above and outlined in detail in Chapter 4, a number of problems were encountered during this investigation when attempting to express both the wildtype and mutant recombinant human BMP-7 proteins. Firstly, difficulties were experienced when trying to produce the wildtype recombinant human BMP-7 using a CHO cell expression system. These problems appeared to be caused not only by complexities in the BMP-7 protein structure (Swencki-Underwood *et al.*, 2008) but also by the presence of a weak translation initiation sequence in the BMP-7 mRNA transcript. These difficulties were overcome by replacing the native BMP-7 translation initiation sequence with an optimised Kozak consensus sequence, and by switching to another CHO cell-based expression system in which transfections were carried out on a larger-scale.

Secondly, problems were encountered when attempting to express BMP-7 proteins in Sf9 insect cells using the Invitrogen Bac-to-Bac Baculovirus Expression System. This was surprising as another close TGF-β superfamily member, GDNF, had previously expressed well using this system in our own laboratory. Without carrying out a full investigation into this matter, it is not possible to draw any firm conclusions on the reasons why detectable levels of the BMP-7 protein were not produced by the Sf9 cells. However, a key difference between GDNF and BMP-7 is that while GDNF contains a short signal peptide upstream of its mature protein domain, BMP-7 contains both a signal peptide and a large pro-protein sequence. It is possible that the additional bulk (compared to GDNF) and the extra processing step that is required to liberate the mature domain of BMP-7 from its pro-protein region caused complications that prevented it from expressing properly and perhaps promoted its breakdown instead. It is also plausible to suggest that the structural complexities highlighted by Centocor Inc. (Swencki-Underwood *et al.*, 2008) may have been at least partly to blame for these difficulties, as they were when using mammalian cells.

Thirdly, great difficulty was experienced when trying to express two different mutant BMP-7 proteins. One of these mutants contained a double substitution close to its C-terminus (K419A/R421A), and the other had a large section of sequence removed from its N-terminal extension (ΔS296-R327). The reason that detectable levels of these mutant proteins could not be expressed is still unclear. Even so, reverse transcription PCR experiments have provided us with some insight into this matter. These experiments showed that the mRNA transcripts that encoded for these mutant

proteins were present in the cells. It therefore appears that any problems arose during their translation or post-translational processing/modification. Further insight into some potential causes of the problems encountered with both of the aforementioned mutants can be gained from the BMP-7 expression study that was carried out by Swencki-Underwood *et al.* (2008).

In contrast to the findings from this study, Swencki-Underwood *et al.* (2008) demonstrated that the expression level of BMP-7 increased when substitution mutations were introduced into the regions of the protein that lie close to the C-terminal ends of each of its constituent monomers. However, Swencki-Underwood and colleagues substituted different combinations of residues compared to the residues that were substituted in our own laboratory (R421, N422 and R426 rather than K419 and R421). Also, the replacement amino acids that Swencki-Underwood and colleagues inserted in place of those that were removed were either aspartic acid or glutamic acid residues rather than alanine, which has a smaller, neutral side chain. Based on this comparison of the findings from these two studies alone, it appears that the problems that were encountered when trying to express detectable levels of the K419A/R421A mutant in our laboratory may have been caused by one or more of the following factors: the positions/combinations of the substituted residues, the chemical nature of the replacement residues, and the size of the side chains of the replacement residues. Swencki-Underwood *et al.* (2008) have also shed some light on the potential reasons why detectable levels of the ΔS296-R327 N-terminal deletion mutant could not be expressed by demonstrating that mutants containing shorter N-terminal deletions (7-23 residues) were poorly expressed due to both processing and secretion problems. Based on this finding, it is apparent that deletion mutations should be avoided when carrying out any future mutagenesis studies that necessitate the expression of BMP-7 protein variants.

Despite the difficulties that have been experienced during this investigation, the use of site-directed mutagenesis techniques may still prove to be important during the ongoing study of BMP-7-HS/heparin interactions. Not only will a site-directed mutagenesis approach enable the location of the HS/heparin-binding site of BMP-7 to be resolved, but it will also yield non-HS/heparin-binding mutant proteins that can be used in functional studies that may help to determine the biological significance of these interactions. However, using such an approach to test the effect that all the

possible combinations of basic residue substitutions have on the HS/heparin-binding ability of the BMP-7 protein is likely to be a laborious task. Therefore, alternative approaches must also be considered.

One idea for an alternative approach that could be employed to identify the key HS/heparin-binding residues of the BMP-7 protein arises from the results that were obtained from studies conducted by Ruppert *et al.* (1996) and Choi *et al.* (2010). As mentioned previously, Ruppert and colleagues demonstrated that the HS/heparin-binding site of BMP-2 is situated close to its N-terminus, residing within its flexible N-terminal extension. In addition, their data suggests that a peptide containing the first 17 residues of the BMP-2 protein, which includes its complete N-terminal extension and key HS/heparin-binding residues, is able to bind to heparin independently of the rest of the mature protein. Similarly, Choi *et al.* (2010) have recently shown that a peptide containing ten amino acids from the N-terminal region of BMP-4, which included its key basic HS/heparin-binding residues (Ohkawara *et al.*, 2002), is able to bind to HS/heparin. As it now appears that the HS/heparin-binding site of BMP-7 is also likely to be situated within or immediately downstream of its flexible N-terminal extension, there is a possibility that a peptide-based approach could be employed in the future to identify its key HS/heparin-binding residues.

Before commencing a full peptide-based investigation, it would first be necessary to determine if a peptide containing the N-terminal sequence of BMP-7 will bind to HS/heparin. This could be achieved by synthesising this peptide and subjecting it to heparin-affinity column chromatography (as described in Chapters 2 and 5). To aid the detection of the peptide in fractions following its elution from heparin columns, a fluorescent label could be added during its synthesis. If it were to be found that this wildtype peptide does indeed bind to heparin, a number of mutant peptides that contain different deletions or basic residue substitutions could then be produced, and their heparin-binding abilities could be determined in a similar manner. One would expect any mutant peptides that were missing key HS/heparin-binding basic residues to exhibit a reduction in their heparin-binding affinity compared to that of the wildtype peptide.

However, this approach is by no means guaranteed to be successful and has a number of potential limitations. Firstly, if the BMP-7 protein has a combined N- and C-terminal HS/heparin-binding site, attempts to identify its key HS/heparin-binding

residues using N-terminal peptides alone will either be unsuccessful or only partially informative. Secondly, it is possible that the binding of BMP-7 to HS/heparin chains may require the participation of both its N-terminal extensions (one from each monomer). If this is the case, the two N-terminal extensions may need to be held in close proximity and/or in an appropriate orientation by the rest of the mature protein structure. Under such circumstances, this approach of investigating the binding of free peptides to immobilised heparin chains will be unsuitable. Thirdly, this approach could potentially be very expensive. This is because peptides can be costly and there are a wide variety of possible deletions and combinations of basic residue substitutions that can be made in this N-terminal region.

During the time in which this investigation has been underway, a limited number of alternative studies relating to BMP-HS/heparin interactions have been conducted. These studies have been confined to the Dpp-type BMPs, and the findings from them have generally been in agreement with those reported by Ruppert *et al.* (1996) and Takada *et al.* (2003). As explained previously (Chapter 1, section 1.4), Ruppert, Takada and colleagues demonstrated that the addition of exogenous heparin potentiated the activity of BMPs -2 and -4 in two different *in vitro* cell-based assays. Takada *et al.* (2003) also showed that the addition of exogenous heparin reduced the amount of BMP-2 that accumulated in the cell layer and prolonged both its half-life and activity in the culture media. Since then, similar findings have been published by Fisher *et al.* (2006), Zhao *et al.* (2006) and Jiao *et al.* (2007). Furthermore, Jiao *et al.* (2007) reported that an increase in BMP-2 activity was observed when the extracellular surfaces of C2C12 cells were depleted of HS by heparinase III treatment, or when the sulphation of cell surface HS chains was inhibited by chlorate treatment. In another study, Hu *et al.* (2009) have shown that in the lungs of knockout mice lacking NDST1 - one of the *N*-acetylglucosamine *N*-deacetylase/*N*-sulfotransferase enzymes that participates in synthesising HS chains - the binding of BMPs -2 and -4 to endogenous cell surface HS was decreased. As a consequence, the internalisation of these proteins was impaired and their signaling activity was enhanced. This caused abnormalities during lung development due to defective cell differentiation and an increase in cell proliferation. More recently, Johnson *et al.* (2011) have demonstrated that when delivered precomplexed with heparin, the ability of BMP-2 to promote the

repair of challenging bone defects and restore long bone mechanical function *in vivo* was increased.

Based on the collection of findings described above, it would appear that endogenous cell surface HS GAGs modulate the signaling activities of BMPs -2 and -4 by limiting their effective extracellular concentration, and that they do this by sequestering them close to the cell surface and mediating their internalisation. If this is the case, it is likely that exogenous heparin potentiates the activity of BMPs -2 and -4 by competitively inhibiting their binding to endogenous HS, therefore preventing them from being internalised, and instead, maintaining them in the extracellular environment. However, at the present time, it is not possible to draw any firm conclusions as to the role that HS/heparin GAGs play in the cellular processes that take place under the control of BMPs -2 and -4. This is because there have been some inconsistencies in the published findings, which may or may not have occurred as a result of the different experimental approaches and conditions that have been employed. For example, in contrast to the results described above, Khan *et al.* (2008) reported that the addition of exogenous heparin had a negative effect on BMP-4 signaling in human osteosarcoma SaOS-2 cells. Also, Kuo *et al.* (2010) demonstrated that the treatment of C2C12 and PC12 cells with heparitinase or chlorate markedly reduced their response to BMP-2 or BMP-4 stimulation. In addition, Kuo *et al.* (2010) have provided evidence to suggest that cell surface HS may serve to promote the signaling activities of BMPs -2 and -4 by acting as a co-receptor and catalysing the formation of their signaling complexes. Specifically, the experimental data that has been published by Kuo and colleagues indicates that HS might fulfill this role by enhancing the recruitment of type II receptor subunits to the tetrameric BMP-type I receptor assemblies that form initially.

Unlike the interactions that take place between the Dpp-type BMPs and HS/heparin, BMP-7-HS/heparin interactions have remained little studied and there have been no additional publications relating to them and their biological significance since this investigation commenced. Even so, it was explained previously in section 1.4 that the findings from *in vitro* studies that were performed in both our own laboratory (unpublished data) and that of Irie *et al.* (2003) have shown that the response of C2C12 and ROS 17/2.8 cells to BMP-7 stimulation was greatly reduced in the absence of cell surface HS or in the presence of exogenous heparin. Irie *et al.*

(2003) also showed that the binding of BMP-7 to the surfaces of ROS 17/2.8 cells was markedly decreased when the cells were treated with heparitinase or chlorate. Based on these findings, it appears that cell surface HS plays a part in BMP-7-mediated processes, although the exact function of HS in these processes remains unclear. It is possible that HS GAGs may facilitate BMP-7 signaling by sequestering the BMP-7 protein close to the cell surface where its transmembrane receptors are situated, therefore increasing the chance of ligand-receptor interactions taking place. Irie and colleagues have also suggested that HS may catalyse or stabilise BMP-7-receptor interactions by directly binding to both BMP-7 and its receptor(s). In order for BMP-7 to simultaneously interact with its receptor(s) and HS without any steric obstruction occurring, the HS/heparin-binding site(s) of BMP-7 would need to be independent of, and perhaps distant from, its receptor binding site(s), which are located in the wrist and knuckle regions of the cystine-knot domains of each BMP-7 monomer (Chapter 1, section 1.1.6). It is not yet clear whether this is the case or not, but as the results from this study now suggest that BMP-7 is likely to interact with HS/heparin via basic residues in its long, flexible N-terminal sequences, which could extend away from the cystine-knot domains of the structure, this is a feasible possibility and the formation of such complexes may be permitted. However, further investigation is required before any firm conclusions can be drawn on this matter.

Overall, it can be said that the findings from this study and those described herein have furthered our understanding of BMP-HS/heparin interactions. It is now known that BMPs -2, -4 and -7 have the ability to interact with HS/heparin, and there is evidence to suggest that such interactions influence the activity of these BMPs. In addition, it has been demonstrated that BMPs -2 and -4 bind to HS/heparin via a small cluster of basic amino acids in their N-terminal regions. Furthermore, the results obtained from this investigation suggest that BMP-7 is also likely to bind to HS/heparin through basic residues in its N-terminal region. However, despite this progress, much work is still to be conducted and a great deal more to be learned before our understanding of these interactions is anything like the level of understanding that we already have of FGF-HS/heparin interactions and their biological significance. With this level of understanding, it should become apparent whether or not heparin mimetics have a part to play in therapeutic interventions that involve the application of recombinant BMPs.

Acknowledgements

I would like to take this opportunity to express my gratitude to a number of people for a variety of reasons:

My supervisors, Dr Chris Rider and Professor Barbara Mulloy, for giving me the opportunity to work on this interesting project, and for their advice and guidance.

Professor Philip Beesley, Vice-Principal, for the useful feedback he has given me during review meetings in his position as my advisor. Also, for giving me the opportunity to study biochemistry as an undergraduate at Royal Holloway, University of London when working in his previous role as Director of Teaching in the School of Biological Sciences.

Chris Ball at The National Institute for Biological Standards and Control (NIBSC) for her advice, for kindly providing me with a number of useful reagents, and for the use of her laboratory and facilities to carry out components of the protein expression work that are detailed in this thesis.

Dr Bethany Swencki-Underwood, Dr Ben Amegadzie, Dr Michael Naso and colleagues at Centocor Inc. for kindly providing me with mutant BMP-7 expression constructs and proteins.

The Biotechnology and Biological Sciences Research Council (BBSRC) and NIBSC for the financial support they provided.

My friends and colleagues in the School of Biological Sciences, especially those in laboratories 302A and 302B, who have made the time I have spent working in the department enjoyable.

Last but certainly not least, my parents and Sue for always having belief in me, for showing a great deal of interest in my work, and for their continued support and encouragement.

References

Aikawa J, Grobe K, Tsujimoto M, Esko JD (2001) Multiple isozymes of heparan sulfate/heparin GlcNAc N-deacetylase/GlcN N-sulfotransferase. Structure and activity of the fourth member, NDST4. J Biol Chem. Feb 23;276(8):5876-82

Akiyama T, Kamimura K, Firkus C, Takeo S, Shimmi O, Nakato H (2008) Dally regulates Dpp morphogen gradient formation by stabilizing Dpp on the cell surface. Dev Biol. Jan 1;313(1):408-19

Alfano I, Vora P, Mummery RS, Mulloy B, Rider CC (2007) The major determinant of the heparin binding of glial cell-line-derived neurotrophic factor is near the N-terminus and is dispensable for receptor binding. Biochem J. May 15;404(1):131-40

Almeida R, Levery SB, Mandel U, Kresse H, Schwientek T, Bennett EP, Clausen H (1999) Cloning and expression of a proteoglycan UDP-galactose:beta-xylose beta1,4-galactosyltransferase I. A seventh member of the human beta4-galactosyltransferase gene family. J Biol Chem. Sep 10;274(37):26165-71

Attisano L, Wrana JL (2002) Signal transduction by the TGF-beta superfamily. Science. May 31;296(5573):1646-7

Attisano L, Wrana JL, Montalvo E, Massagué J (1996) Activation of signalling by the activin receptor complex. Mol Cell Biol. Mar;16(3):1066-73

Avsian-Kretchmer O, Hsueh AJ (2004) Comparative genomic analysis of the eight-membered ring cystine knot-containing bone morphogenetic protein antagonists. Mol Endocrinol. Jan;18(1):1-12

Bai X, Esko JD (1996) An animal cell mutant defective in heparan sulfate hexuronic acid 2-O-sulfation. J Biol Chem. Jul 26;271(30):17711-7

Bai X, Zhou D, Brown JR, Crawford BE, Hennet T, Esko JD (2001) Biosynthesis of the linkage region of glycosaminoglycans: cloning and activity of galactosyltransferase II, the sixth member of the beta 1,3-galactosyltransferase family (beta 3GalT6). J Biol Chem. Dec 21;276(51):48189-95

Balemans W, Ebeling M, Patel N, Van Hul E, Olson P, Dioszegi M, Lacza C, Wuyts W, Van Den Ende J, Willems P, Paes-Alves AF, Hill S, Bueno M, Ramos FJ, Tacconi P, Dikkers FG, Stratakis C, Lindpaintner K, Vickery B, Foernzler D, Van Hul W (2001) Increased bone density in sclerosteosis is due to the deficiency of a novel secreted protein (SOST). Hum Mol Genet. Mar 1;10(5):537-43

Belenkaya TY, Han C, Yan D, Opoka RJ, Khodoun M, Liu H, Lin X (2004) Drosophila Dpp morphogen movement is independent of dynamin-mediated endocytosis but regulated by the glypican members of heparan sulfate proteoglycans. Cell. Oct 15;119(2):231-44

Bernfield M, Kokenyesi R, Kato M, Hinkes MT, Spring J, Gallo RL, Lose EJ (1992) Biology of the syndecans: a family of transmembrane heparan sulfate proteoglycans. Annu Rev Cell Biol. Nov;8:365-93

Bienkowski MJ, Conrad HE (1985) Structural characterization of the oligosaccharides formed by depolymerization of heparin with nitrous acid. J Biol Chem. Jan 10;260(1):356-65

Bitomsky W, Wade RC (1999) Docking of glycosaminoglycans to heparin-binding proteins: validation for aFGF, bFGF, and antithrombin and application to IL-8. J Am Chem Soc. Mar 19;121(13):3004-3013

Border WA, Noble NA (1994) Transforming growth factor beta in tissue fibrosis. N Engl J Med. Nov 10;331(19):1286-92

Bourin MC, Lindahl U (1993) Glycosaminoglycans and the regulation of blood coagulation. Biochem J. Jan 15;289(Pt 2):313-30

Brandan E, Hirschberg CB (1988) Purification of rat liver N-heparan-sulfate sulfotransferase. J Biol Chem. Feb 15;263(5):2417-22

Brown MA, Zhao Q, Baker KA, Naik C, Chen C, Pukac L, Singh M, Tsareva T, Parice Y, Mahoney A, Roschke V, Sanyal I, Choe S (2005) Crystal structure of BMP-9 and functional interactions with pro-region and receptors. J Biol Chem. Jul 1;280(26):25111-8

Campbell P, Hannesson HH, Sandbäck D, Rodén L, Lindahl U, Li JP (1994) Biosynthesis of heparin/heparan sulfate. Purification of the D-glucuronyl C-5 epimerase from bovine liver. J Biol Chem. Oct 28;269(43):26953-8

Capdevila J, Guerrero I (1994) Targeted expression of the signaling molecule decapentaplegic induces pattern duplications and growth alterations in Drosophila wings. EMBO J. Oct 3;13(19):4459-68

Carlsson P, Presto J, Spillmann D, Lindahl U, Kjellén L (2008) Heparin/heparan sulfate biosynthesis: processive formation of N-sulfated domains. J Biol Chem. Jul 18;283(29):20008-14

Celeste AJ, Iannazzi JA, Taylor RC, Hewick RM, Rosen V, Wang EA, Wozney JM (1990) Identification of transforming growth factor beta family members present in bone-inductive protein purified from bovine bone. Proc Natl Acad Sci U S A. Dec;87(24):9843-7

Chang H, Brown CW, Matzuk MM (2002) Genetic analysis of the mammalian transforming growth factor-beta superfamily. Endocr Rev. Dec;23(6):787-823

Chen C, Grzegorzewski KJ, Barash S, Zhao Q, Schneider H, Wang Q, Singh M, Pukac L, Bell AC, Duan R, Coleman T, Duttaroy A, Cheng S, Hirsch J, Zhang

L, Lazard Y, Fischer C, Barber MC, Ma ZD, Zhang YQ, Reavey P, Zhong L, Teng B, Sanyal I, Ruben SM, Blondel O, Birse CE (2003) An integrated functional genomics screening program reveals a role for BMP-9 in glucose homeostasis. Nat Biotechnol. Mar;21(3):294-301

Chen H, Shi S, Acosta L, Li W, Lu J, Bao S, Chen Z, Yang Z, Schneider MD, Chien KR, Conway SJ, Yoder MC, Haneline LS, Franco D, Shou W (2004) BMP10 is essential for maintaining cardiac growth during murine cardiogenesis. Development. May;131(9):2219-31

Chen X, Rubock MJ, Whitman M (1996) A transcriptional partner for MAD proteins in TGF-beta signalling. Nature. Oct 24;383(6602):691-6

Choay J, Petitou M, Lormeau JC, Sinaÿ P, Casu B, Gatti G (1983) Structure-activity relationship in heparin: a synthetic pentasaccharide with high affinity for antithrombin III and eliciting high anti-factor Xa activity. Biochem Biophys Res Commun. Oct 31;116(2):492-9

Choi YJ, Lee JY, Park JH, Park JB, Suh JS, Choi YS, Lee SJ, Chung CP, Park YJ (2010) The identification of a heparin binding domain peptide from bone morphogenetic protein-4 and its role on osteogenesis. Biomaterials. Oct;31(28):7226-38

Chuang YJ, Swanson R, Raja SM, Olson ST (2001) Heparin enhances the specificity of antithrombin for thrombin and factor Xa independent of the reactive center loop sequence. Evidence for an exosite determinant of factor Xa specificity in heparin-activated antithrombin. J Biol Chem. May 4;276(18):14961-71

Cole GJ, Halfter W (1996) Agrin: an extracellular matrix heparan sulfate proteoglycan involved in cell interactions and synaptogenesis. Perspect Dev Neurobiol. 3(4):359-71

Constam DB, Robertson EJ (1999) Regulation of bone morphogenetic protein activity by pro domains and proprotein convertases. J Cell Biol. Jan 11;144(1):139-49

Cui Y, Jean F, Thomas G, Christian JL (1998) BMP-4 is proteolytically activated by furin and/or PC6 during vertebrate embryonic development. EMBO J. Aug 17;17(16):4735-43

Danielsson A, Raub E, Lindahl U, Björk I (1986) Role of ternary complexes, in which heparin binds both antithrombin and proteinase, in the acceleration of the reactions between antithrombin and thrombin or factor Xa. J Biol Chem. Nov 25;261(33):15467-73

Daopin S, Piez KA, Ogawa Y, Davies DR (1992) Crystal structure of transforming growth factor-beta 2: an unusual fold for the superfamily. Science. Jul 17;257(5068):369-73

Dietrich CP, Silva ME, Michelacci YM (1973) Sequential degradation of heparin in Flavobacterium heparinum. Purification and properties of five enzymes involved in heparin degradation. J Biol Chem. Sep 25;248(18):6408-15

Dionne MS, Skarnes WC, Harland RM (2001) Mutation and analysis of Dan, the founding member of the Dan family of transforming growth factor beta antagonists. Mol Cell Biol. Jan;21(2):636-43

Ducy P, Karsenty G (2000) The family of bone morphogenetic proteins. Kidney Int. Jun;57(6):2207-14

Dudley AT, Lyons KM, Robertson EJ (1995) A requirement for bone morphogenetic protein-7 during development of the mammalian kidney and eye. Genes Dev. Nov 15;9(22):2795-807

Ebendal T, Bengtsson H, Söderström S (1998) Bone morphogenetic proteins and their receptors: potential functions in the brain. J Neurosci Res. Jan 15;51(2):139-46

Esko JD, Lindahl U (2001) Molecular diversity of heparan sulfate. J Clin Invest. Jul;108(2):169-73

Esko JD, Selleck SB (2002) Order out of chaos: assembly of ligand binding sites in heparan sulfate. Annu Rev Biochem. 71:435-71

Esko JD, Zhang L (1996) Influence of core protein sequence on glycosaminoglycan assembly. Curr Opin Struct Biol. Oct;6(5):663-70

Fedarko NS, Conrad HE (1986) A unique heparan sulfate in the nuclei of hepatocytes: structural changes with the growth state of the cells. J Cell Biol. Feb;102(2):587-99

Ferro DR, Provasoli A, Ragazzi M, Casu B, Torri G, Bossennec V, Perly B, Sinaÿ P, Petitou M, Choay J (1990) Conformer populations of L-iduronic acid residues in glycosaminoglycan sequences. Carbohydr Res. Jan 15;195(2):157-67

Filmus J, Selleck SB (2001) Glypicans: proteoglycans with a surprise. J Clin Invest. Aug;108(4):497-501

Fisher MC, Li Y, Seghatoleslami MR, Dealy CN, Kosher RA (2006) Heparan sulfate proteoglycans including syndecan-3 modulate BMP activity during limb cartilage differentiation. Matrix Biol. Jan;25(1):27-39

Forster M, Mulloy B (2006) Computational approaches to the identification of heparin-binding sites on the surfaces of proteins. Biochem Soc Trans. Jun;34(Pt 3):431-4

Fritz TA, Gabb MM, Wei G, Esko JD (1994) Two N-acetylglucosaminyltransferases catalyze the biosynthesis of heparan sulfate. J Biol Chem. Nov 18;269(46):28809-14

Gallagher JT (2001) Heparan sulfate: growth control with a restricted sequence menu. J Clin Invest. Aug;108(3):357-61

Gallagher JT (2006) Multiprotein signaling complexes: regional assembly on heparan sulphate. Biochem Soc Trans. Jun;34(Pt 3):438-41

Gallagher JT, Lyon M, Steward WP (1986) Structure and function of heparan sulphate proteoglycans. Biochem J. Jun 1;236(2):313-25

Gallagher JT, Walker A (1985) Molecular distinctions between heparan sulphate and heparin. Analysis of sulphation patterns indicates that heparan sulphate and heparin are separate families of N-sulphated polysaccharides. Biochem J. Sep 15;230(3):665-74

Ge G, Hopkins DR, Ho WB, Greenspan DS (2005) GDF11 forms a bone morphogenetic protein 1-activated latent complex that can modulate nerve growth factor-induced differentiation of PC12 cells. Mol Cell Biol. Jul;25(14):5846-58

Gettins PG, Fan B, Crews BC, Turko IV, Olson ST, Streusand VJ (1993) Transmission of conformational change from the heparin binding site to the reactive center of antithrombin. Biochemistry. Aug 24;32(33):8385-9

Götting C, Kuhn J, Zahn R, Brinkmann T, Kleesiek K (2000) Molecular cloning and expression of human UDP-d-Xylose:proteoglycan core protein beta-d-xylosyltransferase and its first isoform XT-II. J Mol Biol. Dec 8;304(4):517-28

Granjeiro JM, Oliveira RC, Bustos-Valenzuela JC, Sogayar MC, Taga R (2005) Bone morphogenetic proteins: from structure to clinical use. Braz J Med Biol Res. Oct;38(10):1463-73

Greenwald J, Groppe J, Gray P, Wiater E, Kwiatkowski W, Vale W, Choe S (2003) The BMP7/ActRII extracellular domain complex provides new insights into the cooperative nature of receptor assembly. Mol Cell. Mar;11(3):605-17

Gregory KE, Ono RN, Charbonneau NL, Kuo CL, Keene DR, Bächinger HP, Sakai LY (2005) The prodomain of BMP-7 targets the BMP-7 complex to the extracellular matrix. J Biol Chem. Jul 29;280(30):27970-80

Griffith DL, Keck PC, Sampath TK, Rueger DC, Carlson WD (1996) Three-dimensional structure of recombinant human osteogenic protein 1: structural paradigm for the transforming growth factor beta superfamily. Proc Natl Acad Sci U S A. Jan 23;93(2):878-83

Grimsrud CD, Romano PR, D'Souza M, Puzas JE, Reynolds PR, Rosier RN, O'Keefe RJ (1999) BMP-6 is an autocrine stimulator of chondrocyte differentiation. J Bone Miner Res. Apr;14(4):475-82

Groppe J, Greenwald J, Wiater E, Rodriguez-Leon J, Economides AN, Kwiatkowski W, Affolter M, Vale WW, Belmonte JC, Choe S (2002) Structural basis of BMP signaling inhibition by the cystine knot protein Noggin. Nature. Dec 12;420(6916):636-42

Habuchi H, Habuchi O, Kimata K (1995) Purification and characterization of heparan sulfate 6-sulfotransferase from the culture medium of Chinese hamster ovary cells. J Biol Chem. Feb 24;270(8):4172-9

Habuchi H, Kobayashi M, Kimata K (1998) Molecular characterization and expression of heparan-sulfate 6-sulfotransferase. Complete cDNA cloning in human and partial cloning in Chinese hamster ovary cells. J Biol Chem. Apr 10;273(15):9208-13

Habuchi H, Tanaka M, Habuchi O, Yoshida K, Suzuki H, Ban K, Kimata K (2000) The occurrence of three isoforms of heparan sulfate 6-O-sulfotransferase having

different specificities for hexuronic acid adjacent to the targeted N-sulfoglucosamine. J Biol Chem. Jan 28;275(4):2859-68

Hammonds RG Jr, Schwall R, Dudley A, Berkemeier L, Lai C, Lee J, Cunningham N, Reddi AH, Wood WI, Mason AJ (1991) Bone-inducing activity of mature BMP-2b produced from a hybrid BMP-2a/2b precursor. Mol Endocrinol. Jan;5(1):149-55

Hashimoto Y, Orellana A, Gil G, Hirschberg CB (1992) Molecular cloning and expression of rat liver N-heparan sulfate sulfotransferase. J Biol Chem. Aug 5;267(22):15744-50

Hazama M, Aono A, Ueno N, Fujisawa Y (1995) Efficient expression of a heterodimer of bone morphogenetic protein subunits using a baculovirus expression system. Biochem Biophys Res Commun. Apr 26;209(3):859-66

Herpin A, Lelong C, Favrel P (2004) Transforming growth factor-beta-related proteins: an ancestral and widespread superfamily of cytokines in metazoans. Dev Comp Immunol. May 3;28(5):461-85

Hileman RE, Fromm JR, Weiler JM, Linhardt RJ (1998) Glycosaminoglycan-protein interactions: definition of consensus sites in glycosaminoglycan binding proteins. Bioessays. Feb;20(2):156-67

Hinck AP, Archer SJ, Qian SW, Roberts AB, Sporn MB, Weatherbee JA, Tsang ML, Lucas R, Zhang BL, Wenker J, Torchia DA (1996) Transforming growth factor beta 1: three-dimensional structure in solution and comparison with the X-ray structure of transforming growth factor beta 2. Biochemistry. Jul 2;35(26):8517-34

Hogan BL (1996a) Bone morphogenetic proteins: multifunctional regulators of vertebrate development. Genes Dev. Jul 1;10(13):1580-94

Hogan BL (1996b) Bone morphogenetic proteins in development. Curr Opin Genet Dev. Aug;6(4):432-8

Hoodless PA, Haerry T, Abdollah S, Stapleton M, O'Connor MB, Attisano L, Wrana JL (1996) MADR1, a MAD-related protein that functions in BMP2 signaling pathways. Cell. May 17;85(4):489-500

Höök M, Lindahl U, Iverius PH (1974) Distribution of sulphate and iduronic acid residues in heparin and heparan sulphate. Biochem J. Jan;137(1):33-43

Hu Z, Wang C, Xiao Y, Sheng N, Chen Y, Xu Y, Zhang L, Mo W, Jing N, Hu G (2009) NDST1-dependent heparan sulfate regulates BMP signaling and internalization in lung development. J Cell Sci. Apr 15;122(Pt 8):1145-54

Iozzo RV, Cohen IR, Grässel S, Murdoch AD (1994). The biology of perlecan: the multifaceted heparan sulphate proteoglycan of basement membranes and pericellular matrices. Biochem J. Sep 15;302(Pt 3):625-39

Irie A, Habuchi H, Kimata K, Sanai Y (2003) Heparan sulfate is required for bone morphogenetic protein-7 signaling. Biochem Biophys Res Commun. Sep 5;308(4):858-65

Israel DI, Nove J, Kerns KM, Moutsatsos IK, Kaufman RJ (1992) Expression and characterization of bone morphogenetic protein-2 in Chinese hamster ovary cells. Growth Factors. 7(2):139-50

Iwano M, Plieth D, Danoff TM, Xue C, Okada H, Neilson EG (2002) Evidence that fibroblasts derive from epithelium during tissue fibrosis. J Clin Invest. Aug;110(3):341-50

Jacobsson I, Lindahl U, Jensen JW, Rodén L, Prihar H, Feingold DS (1984) Biosynthesis of heparin. Substrate specificity of heparosan N-sulfate D-glucuronosyl 5-epimerase. J Biol Chem. Jan 25;259(2):1056-63

Jiao X, Billings PC, O'Connell MP, Kaplan FS, Shore EM, Glaser DL (2007) Heparan sulfate proteoglycans (HSPGs) modulate BMP2 osteogenic bioactivity in C2C12 cells. J Biol Chem. Jan 12;282(2):1080-6

Johnson MR, Boerckel JD, Dupont KM, Guldberg RE (2011) Functional restoration of critically sized segmental defects with bone morphogenetic protein-2 and heparin treatment. Clin Orthop Relat Res. Nov;469(11):3111-7

Jones WK, Richmond EA, White K, Sasak H, Kusmik W, Smart J, Oppermann H, Rueger DC, Tucker RF (1994) Osteogenic protein-1 (OP-1) expression and processing in Chinese hamster ovary cells: isolation of a soluble complex containing the mature and pro-domains of OP-1. Growth Factors. 11(3):215-25

Kalluri R, Zeisberg M (2003) Exploring the connection between chronic renal fibrosis and bone morphogenic protein-7. Histol Histopathol. Jan;18(1):217-24

Katagiri T, Yamaguchi A, Komaki M, Abe E, Takahashi N, Ikeda T, Rosen V, Wozney JM, Fujisawa-Sehara A, Suda T (1994) Bone morphogenetic protein-2 converts the differentiation pathway of C2C12 myoblasts into the osteoblast lineage. J Cell Biol. Dec;127(6 Pt 1):1755-66

Khan SA, Nelson MS, Pan C, Gaffney PM, Gupta P (2008) Endogenous heparan sulfate and heparin modulate bone morphogenetic protein-4 signaling and activity. Am J Physiol Cell Physiol. Jun;294(6):C1387-97

Kim BT, Kitagawa H, Tamura J, Saito T, Kusche-Gullberg M, Lindahl U, Sugahara K (2001) Human tumor suppressor EXT gene family members EXTL1 and EXTL3 encode alpha 1,4- N-acetylglucosaminyltransferases that likely are involved in heparan sulfate/ heparin biosynthesis. Proc Natl Acad Sci U S A. Jun 19;98(13):7176-81

Kim AS, Pleasure SJ (2003) Expression of the BMP antagonist Dan during murine forebrain development. Brain Res Dev Brain Res. Oct 10;145(1):159-62

Kingsley DM (1994) The TGF-beta superfamily: new members, new receptors, and new genetic tests of function in different organisms. Genes Dev. Jan;8(2):133-46

Kingsley DM, Bland AE, Grubber JM, Marker PC, Russell LB, Copeland NG, Jenkins NA (1992) The mouse short ear skeletal morphogenesis locus is associated with defects in a bone morphogenetic member of the TGF beta superfamily. Cell. Oct 30;71(3):399-410

Kirsch T, Sebald W, Dreyer MK (2000) Crystal structure of the BMP-2-BRIA ectodomain complex. Nat Struct Biol. Jun;7(6):492-6

Kitagawa H, Tone Y, Tamura J, Neumann KW, Ogawa T, Oka S, Kawasaki T, Sugahara K (1998) Molecular cloning and expression of glucuronyltransferase I involved in the biosynthesis of the glycosaminoglycan-protein linkage region of proteoglycans. J Biol Chem. Mar 20;273(12):6615-8

Kitchen DB, Decornez H, Furr JR, Bajorath J (2004) Docking and scoring in virtual screening for drug discovery: methods and applications. Nat Rev Drug Discov. Nov;3(11):935-49

Kobayashi M, Habuchi H, Habuchi O, Saito M, Kimata K (1996) Purification and characterization of heparan sulfate 2-sulfotransferase from cultured Chinese hamster ovary cells. J Biol Chem. Mar 29;271(13):7645-53

Kobayashi M, Habuchi H, Yoneda M, Habuchi O, Kimata K (1997) Molecular cloning and expression of Chinese hamster ovary cell heparan-sulfate 2-sulfotransferase. J Biol Chem. May 23;272(21):13980-5

Kopp JB (2002) BMP-7 and the proximal tubule. Kidney Int. Jan;61(1):351-2

Kounnas MZ, Church FC, Argraves WS, Strickland DK (1996) Cellular internalization and degradation of antithrombin III-thrombin, heparin cofactor II-thrombin, and alpha 1-antitrypsin-trypsin complexes is mediated by the low density lipoprotein receptor-related protein. J Biol Chem. Mar 15;271(11):6523-9

Kozak M (1981) Possible role of flanking nucleotides in recognition of the AUG initiator codon by eukaryotic ribosomes. Nucleic Acids Res. Oct 24;9(20):5233-52

Kozak M (2002) Pushing the limits of the scanning mechanism for initiation of translation. Gene. Oct 16;299(1-2):1-34

Kretzschmar M, Liu F, Hata A, Doody J, Massagué J (1997) The TGF-beta family mediator Smad1 is phosphorylated directly and activated functionally by the BMP receptor kinase. Genes Dev. Apr 15;11(8):984-95

Kreuger J, Salmivirta M, Sturiale L, Giménez-Gallego G, Lindahl U (2001) Sequence analysis of heparan sulfate epitopes with graded affinities for fibroblast growth factors 1 and 2. J Biol Chem. Aug 17;276(33):30744-52

Kreuger J, Spillmann D, Li JP, Lindahl U (2006) Interactions between heparan sulfate and proteins: the concept of specificity. J Cell Biol. Jul 31;174(3):323-7

Kuo WJ, Digman MA, Lander AD (2010) Heparan sulfate acts as a bone morphogenetic protein coreceptor by facilitating ligand-induced receptor hetero-oligomerization. Mol Biol Cell. Nov 15;21(22):4028-41

Kusche M, Lindahl U (1990) Biosynthesis of heparin. O-sulfation of D-glucuronic acid units. J Biol Chem. Sep 15;265(26):15403-9

Kusu N, Laurikkala J, Imanishi M, Usui H, Konishi M, Miyake A, Thesleff I, Itoh N (2003) Sclerostin is a novel secreted osteoclast-derived bone morphogenetic protein antagonist with unique ligand specificity. J Biol Chem. Jun 27;278(26):24113-7

Laemmli UK (1970) Cleavage of structural proteins during the assembly of the head of bacteriophage T4. Nature. Aug 15;227(5259):680-5

Lagna G, Hata A, Hemmati-Brivanlou A, Massagué J (1996) Partnership between DPC4 and SMAD proteins in TGF-beta signalling pathways. Nature. Oct 31;383(6603):832-6

Li W, Johnson DJ, Esmon CT, Huntington JA (2004) Structure of the antithrombin-thrombin-heparin ternary complex reveals the antithrombotic mechanism of heparin. Nat Struct Mol Biol. Sep;11(9):857-62

Liao WX, Moore RK, Otsuka F, Shimasaki S (2003) Effect of intracellular interactions on the processing and secretion of bone morphogenetic protein-15 (BMP-15) and growth and differentiation factor-9. Implication of the aberrant ovarian phenotype of BMP-15 mutant sheep. J Biol Chem. Feb 7;278(6):3713-9

Lin SJ, Lerch TF, Cook RW, Jardetzky TS, Woodruff TK (2006) The structural basis of TGF-beta, bone morphogenetic protein, and activin ligand binding. Reproduction. Aug;132(2):179-90

Lindahl U, Höök M (1978) Glycosaminoglycans and their binding to biological macromolecules. Annu Rev Biochem. 47:385-417

Lindahl U, Kusche-Gullberg M, Kjellén L (1998) Regulated diversity of heparan sulfate. J Biol Chem. Sep 25;273(39):24979-82

Lindahl U, Thunberg L, Bäckström G, Riesenfeld J, Nordling K, Björk I (1984) Extension and structural variability of the antithrombin-binding sequence in heparin. J Biol Chem. Oct 25;259(20):12368-76

Liu F, Hata A, Baker JC, Doody J, Cárcamo J, Harland RM, Massagué J (1996) A human Mad protein acting as a BMP-regulated transcriptional activator. Nature. Jun 13;381(6583):620-3

Liu J, Shworak NW, Fritze LM, Edelberg JM, Rosenberg RD (1996) Purification of heparan sulfate D-glucosaminyl 3-O-sulfotransferase. J Biol Chem. Oct 25;271(43):27072-82

Lortat-Jacob H, Baltzer F, Grimaud JA (1996) Heparin decreases the blood clearance of interferon-gamma and increases its activity by limiting the processing of its carboxyl-terminal sequence. J Biol Chem. Jul 5;271(27):16139-43

Lortat-Jacob H, Grimaud JA (1992) Binding of interferon gamma to heparan sulfate is restricted to the heparin-like domains and involves carboxylic--but not N-sulfated--groups. Biochim Biophys Acta. Sep 15;1117(2):126-30

Lortat-Jacob H, Kleinman HK, Grimaud JA (1991) High affinity binding of interferon-gamma to a basement membrane complex (matrigel). J Clin Invest. Mar;87(3):878-83

Lortat-Jacob H, Turnbull JE, Grimaud JA (1995) Molecular organization of the interferon gamma-binding domain in heparan sulphate. Biochem J. Sep 1;310(Pt 2):497-505

Luo G, Hofmann C, Bronckers AL, Sohocki M, Bradley A, Karsenty G (1995) BMP-7 is an inducer of nephrogenesis, and is also required for eye development and skeletal patterning. Genes Dev. Nov 15;9(22):2808-20

Luyten FP, Cunningham NS, Ma S, Muthukumaran N, Hammonds RG, Nevins WB, Woods WI, Reddi AH (1989) Purification and partial amino acid sequence of osteogenin, a protein initiating bone differentiation. J Biol Chem. Aug 15;264(23):13377-80

Lyon M, Deakin JA, Gallagher JT (1994) Liver heparan sulfate structure. A novel molecular design. J Biol Chem. Apr 15;269(15):11208-15

Lyon M, Gallagher JT (1998) Bio-specific sequences and domains in heparan sulphate and the regulation of cell growth and adhesion. Matrix Biol. Nov;17(7):485-93

Lyon M, Rushton G, Gallagher JT (1997) The interaction of the transforming growth factor-betas with heparin/heparan sulfate is isoform-specific. J Biol Chem. Jul 18;272(29):18000-6

Maccarana M, Sakura Y, Tawada A, Yoshida K, Lindahl U (1996) Domain structure of heparan sulfates from bovine organs. J Biol Chem. Jul 26;271(30):17804-10

Mac Sweeney A, Gil-Parrado S, Vinzenz D, Bernardi A, Hein A, Bodendorf U, Erbel P, Logel C, Gerhartz B (2008) Structural basis for the substrate specificity of bone morphogenetic protein 1/tolloid-like metalloproteases. J Mol Biol. Dec 5;384(1):228-39

Malmström A, Rodén L, Feingold DS, Jacobsson I, Bäckström G, Lindahl U (1980) Biosynthesis of heparin. Partial purification of the uronosyl C-5 epimerase. J Biol Chem. May 10;255(9):3878-83

Massagué J (2000) How cells read TGF-beta signals. Nat Rev Mol Cell Biol. Dec;1(3):169-78

Massagué J, Wotton D (2000) Transcriptional control by the TGF-beta/Smad signaling system. EMBO J. Apr 17;19(8):1745-54

Mathews LS, Vale WW (1991) Expression cloning of an activin receptor, a predicted transmembrane serine kinase. Cell. Jun 14;65(6):973-82

Mazerbourg S, Hsueh AJ (2006) Genomic analyses facilitate identification of receptors and signalling pathways for growth differentiation factor 9 and related orphan bone morphogenetic protein/growth differentiation factor ligands. Hum Reprod Update. Jul-Aug;12(4):373-83

Mazumder B, Seshadri V, Fox PL (2003) Translational control by the 3'-UTR: the ends specify the means. Trends Biochem Sci. Feb;28(2):91-8

McCormick C, Duncan G, Goutsos KT, Tufaro F (2000) The putative tumor suppressors EXT1 and EXT2 form a stable complex that accumulates in the Golgi apparatus and catalyzes the synthesis of heparan sulfate. Proc Natl Acad Sci U S A. Jan 18;97(2):668-73

McDonald NQ, Hendrickson WA (1993) A structural superfamily of growth factors containing a cystine knot motif. Cell. May 7;73(3):421-4

McGrath SA, Esquela AF, Lee SJ (1995) Oocyte-specific expression of growth/differentiation factor-9. Mol Endocrinol. Jan;9(1):131-6

Mehler MF, Mabie PC, Zhang D, Kessler JA (1997) Bone morphogenetic proteins in the nervous system. Trends Neurosci. Jul;20(7):309-17

Miller AF, Harvey SA, Thies RS, Olson MS (2000) Bone morphogenetic protein-9. An autocrine/paracrine cytokine in the liver. J Biol Chem. Jun 16;275(24):17937-45

Mittl PR, Priestle JP, Cox DA, McMaster G, Cerletti N, Grütter MG (1996) The crystal structure of TGF-beta 3 and comparison to TGF-beta 2: implications for receptor binding. Protein Sci. Jul;5(7):1261-71

Mobli M, Nilsson M, Almond A (2008) The structural plasticity of heparan sulfate NA-domains and hence their role in mediating multivalent interactions is confirmed by high-accuracy (15)N-NMR relaxation studies. Glycoconj J. Jul;25(5):401-14

Morris GM, Goodsell DS, Huey R, Olson AJ (1996) Distributed automated docking of flexible ligands to proteins: parallel applications of AutoDock 2.4. J Comput Aided Mol Des. Aug;10(4):293-304

Morrissey J, Hruska K, Guo G, Wang S, Chen Q, Klahr S (2002) Bone morphogenetic protein-7 improves renal fibrosis and accelerates the return of renal function. J Am Soc Nephrol. Jan;13 Suppl 1:S14-21

Mulloy B, Forster M (2008) Application of drug discovery software to the identification of heparin-binding sites on protein surfaces: a computational survey of the 4-helix cytokines. Mol Simulat. Apr;34(4):481-489

Mulloy B, Forster MJ, Jones C, Davies DB (1993) N.m.r. and molecular-modelling studies of the solution conformation of heparin. Biochem J. Aug 1;293(Pt 3):849-58

Mulloy B, Forster MJ, Jones C, Drake AF, Johnson EA, Davies DB (1994) The effect of variation of substitution on the solution conformation of heparin: a spectroscopic and molecular modelling study. Carbohydr Res. Mar 4;255:1-26

Mulloy B, Rider CC (2006). Cytokines and proteoglycans: an introductory overview. Biochem Soc Trans. Jun;34(Pt 3):409-13

Mummery RS, Mulloy B, Rider CC (2007) The binding of human betacellulin to heparin, heparan sulfate and related polysaccharides. Glycobiology. Oct;17(10):1094-103

Mummery RS, Rider CC (2000) Characterization of the heparin-binding properties of IL-6. J Immunol. Nov 15;165(10):5671-9

Murphy KJ, Merry CL, Lyon M, Thompson JE, Roberts IS, Gallagher JT (2004) A new model for the domain structure of heparan sulfate based on the novel specificity of K5 lyase. J Biol Chem. Jun 25;279(26):27239-45

Nicholls PK, Harrison CA, Gilchrist RB, Farnworth PG, Stanton PG (2009) Growth differentiation factor 9 is a germ cell regulator of Sertoli cell function. Endocrinology. May;150(5):2481-90

Ohkawara B, Iemura S, ten Dijke P, Ueno N (2002) Action range of BMP is defined by its N-terminal basic amino acid core. Curr Biol. Feb 5;12(3):205-9

Okajima T, Yoshida K, Kondo T, Furukawa K (1999) Human homolog of Caenorhabditis elegans sqv-3 gene is galactosyltransferase I involved in the biosynthesis of the glycosaminoglycan-protein linkage region of proteoglycans. J Biol Chem. Aug 13;274(33):22915-8

Olson ST, Srinivasan KR, Björk I, Shore JD (1981) Binding of high affinity heparin to antithrombin III. Stopped flow kinetic studies of the binding interaction. J Biol Chem. Nov 10;256(21):11073-9

Ozkaynak E, Rueger DC, Drier EA, Corbett C, Ridge RJ, Sampath TK, Oppermann H (1990) OP-1 cDNA encodes an osteogenic protein in the TGF-beta family. EMBO J. Jul;9(7):2085-93

Ozkaynak E, Schnegelsberg PN, Jin DF, Clifford GM, Warren FD, Drier EA, Oppermann H (1992) Osteogenic protein-2. A new member of the transforming growth factor-beta superfamily expressed early in embryogenesis. J Biol Chem. Dec 15;267(35):25220-7

Pappano WN, Steiglitz BM, Scott IC, Keene DR, Greenspan DS (2003) Use of Bmp1/Tll1 doubly homozygous null mice and proteomics to identify and validate in vivo substrates of bone morphogenetic protein 1/tolloid-like metalloproteinases. Mol Cell Biol. Jul;23(13):4428-38

Pellegrini L, Burke DF, von Delft F, Mulloy B, Blundell TL (2000) Crystal structure of fibroblast growth factor receptor ectodomain bound to ligand and heparin. Nature.Oct 26;407(6807):1029-34

Pinhal MA, Smith B, Olson S, Aikawa J, Kimata K, Esko JD (2001) Enzyme interactions in heparan sulfate biosynthesis: uronosyl 5-epimerase and 2-O-sulfotransferase interact in vivo. Proc Natl Acad Sci U S A. Nov 6;98(23):12984-9

Piscione TD, Yager TD, Gupta IR, Grinfeld B, Pei Y, Attisano L, Wrana JL, Rosenblum ND (1997) BMP-2 and OP-1 exert direct and opposite effects on renal branching morphogenesis. Am J Physiol. Dec;273(6 Pt 2):F961-75

Posakony LG, Raftery LA, Gelbart WM (1990) Wing formation in Drosophila melanogaster requires decapentaplegic gene function along the anterior-posterior compartment boundary. Mech Dev. Dec;33(1):69-82

Reddi AH (1981) Cell biology and biochemistry of endochondral bone development. Coll Relat Res. Feb;1(2):209-26

Reddi AH (1997) Bone morphogenetic proteins: an unconventional approach to isolation of first mammalian morphogens. Cytokine Growth Factor Rev. Mar;8(1):11-20

Reddi AH, Huggins C (1972) Biochemical sequences in the transformation of normal fibroblasts in adolescent rats. Proc Natl Acad Sci U S A. Jun;69(6):1601-5

Ricard-Blum S, Féraud O, Lortat-Jacob H, Rencurosi A, Fukai N, Dkhissi F, Vittet D, Imberty A, Olsen BR, van der Rest M (2004) Characterization of endostatin binding to heparin and heparan sulfate by surface plasmon resonance and molecular modeling: role of divalent cations. J Biol Chem. Jan 23;279(4):2927-36

Rickard SM, Mummery RS, Mulloy B, Rider CC (2003) The binding of human glial cell line-derived neurotrophic factor to heparin and heparan sulfate: importance of 2-O-sulfate groups and effect on its interaction with its receptor, GFRalpha1. Glycobiology. Jun;13(6):419-26

Robinson CJ, Harmer NJ, Goodger SJ, Blundell TL, Gallagher JT (2005) Cooperative dimerization of fibroblast growth factor 1 (FGF1) upon a single heparin saccharide may drive the formation of 2:2:1 FGF1.FGFR2c.heparin ternary complexes. J Biol Chem. Dec 23;280(51):42274-82

Rosenberg RD, Armand G, Lam L (1978) Structure-function relationships of heparin species. Proc Natl Acad Sci U S A. Jul;75(7):3065-9

Ruppert R, Hoffmann E, Sebald W (1996) Human bone morphogenetic protein 2 contains a heparin-binding site which modifies its biological activity. Eur J Biochem. Apr 1;237(1):295-302

Salmivirta M, Lidholt K, Lindahl U (1996) Heparan sulfate: a piece of information. FASEB J. Sep;10(11):1270-9

Sampath TK, Maliakal JC, Hauschka PV, Jones WK, Sasak H, Tucker RF, White KH, Coughlin JE, Tucker MM, Pang RH, Corbett C, Ozkaynak E, Oppermann H, Rueger D (1992) Recombinant human osteogenic protein-1 (hOP-1) induces new bone formation in vivo with a specific activity comparable with natural bovine osteogenic protein and stimulates osteoblast proliferation and differentiation in vitro. J Biol Chem. Oct 5;267(28):20352-62

Sampath P, Mazumder B, Seshadri V, Fox PL (2003) Transcript-selective translational silencing by gamma interferon is directed by a novel structural element in the ceruloplasmin mRNA 3' untranslated region. Mol Cell Biol. Mar;23(5):1509-19

Sampath TK, Muthukumaran N, Reddi AH (1987) Isolation of osteogenin, an extracellular matrix-associated, bone-inductive protein, by heparin affinity chromatography. Proc Natl Acad Sci U S A. Oct;84(20):7109-13

Schlessinger J, Plotnikov AN, Ibrahimi OA, Eliseenkova AV, Yeh BK, Yayon A, Linhardt RJ, Mohammadi M (2000) Crystal structure of a ternary FGF-FGFR-heparin complex reveals a dual role for heparin in FGFR binding and dimerization. Mol Cell. Sep;6(3):743-50

Schlunegger MP, Grütter MG (1992) An unusual feature revealed by the crystal structure at 2.2 A resolution of human transforming growth factor-beta 2. Nature. Jul 30;358(6385):430-4

Senay C, Lind T, Muguruma K, Tone Y, Kitagawa H, Sugahara K, Lidholt K, Lindahl U, Kusche-Gullberg M (2000) The EXT1/EXT2 tumor suppressors: catalytic activities and role in heparan sulfate biosynthesis. EMBO Rep. Sep;1(3):282-6

Sharma R, Khanna A, Sharma M, Savin VJ (2000) Transforming growth factor-beta1 increases albumin permeability of isolated rat glomeruli via hydroxyl radicals. Kidney Int. Jul;58(1):131-6

Shi Y, Massagué J (2003) Mechanisms of TGF-beta signaling from cell membrane to the nucleus. Cell. Jun 13;113(6):685-700

Shworak NW, Liu J, Fritze LM, Schwartz JJ, Zhang L, Logeart D, Rosenberg RD (1997) Molecular cloning and expression of mouse and human cDNAs encoding heparan sulfate D-glucosaminyl 3-O-sulfotransferase. J Biol Chem. Oct 31;272(44):28008-19

Shworak NW, Liu J, Petros LM, Zhang L, Kobayashi M, Copeland NG, Jenkins NA, Rosenberg RD (1999) Multiple isoforms of heparan sulfate D-glucosaminyl 3-O-sulfotransferase. Isolation, characterization, and expression of human cdnas and identification of distinct genomic loci. J Biol Chem. Feb 19;274(8):5170-84

Silbert JE (1982) Structure and metabolism of proteoglycans and glycosaminoglycans. J Invest Dermatol. Jul;79 Suppl 1:31s-37s

Silva ME, Dietrich CP (1975) Structure of heparin. Characterization of the products formed from heparin by the action of a heparinase and a heparitinase from Flavobacterium heparinum. J Biol Chem. Sep 10;250(17):6841-6

Simon M, Maresh JG, Harris SE, Hernandez JD, Arar M, Olson MS, Abboud HE (1999) Expression of bone morphogenetic protein-7 mRNA in normal and ischemic adult rat kidney. Am J Physiol. Mar;276(3 Pt 2):F382-9

Smith WC, Harland RM (1992) Expression cloning of noggin, a new dorsalizing factor localized to the Spemann organizer in Xenopus embryos. Cell. Sep 4;70(5):829-40

Spillmann D, Witt D, Lindahl U (1998) Defining the interleukin-8-binding domain of heparan sulfate. J Biol Chem. Jun 19;273(25):15487-93

Stow JL, Kjéllen L, Unger E, Höök M, Farquhar MG (1985) Heparan sulfate proteoglycans are concentrated on the sinusoidal plasmalemmal domain and in intracellular organelles of hepatocytes. J Cell Biol. Mar;100(3):975-80

Stringer SE, Gallagher JT (1997) Specific binding of the chemokine platelet factor 4 to heparan sulfate. J Biol Chem. Aug 15;272(33):20508-14

Sudo M, Sato K, Chaidedgumjorn A, Toyoda H, Toida T, Imanari T (2001) (1)H nuclear magnetic resonance spectroscopic analysis for determination of

glucuronic and iduronic acids in dermatan sulfate, heparin, and heparan sulfate. Anal Biochem. Oct 1;297(1):42-51

Sugahara K, Kitagawa H (2000) Recent advances in the study of the biosynthesis and functions of sulfated glycosaminoglycans. Curr Opin Struct Biol. Oct;10(5):518-27

Swencki-Underwood B, Mills JK, Vennarini J, Boakye K, Luo J, Pomerantz S, Cunningham MR, Farrell FX, Naso MF, Amegadzie B (2008) Expression and characterization of a human BMP-7 variant with improved biochemical properties. Protein Expr Purif. Feb;57(2):312-9

Takada T, Katagiri T, Ifuku M, Morimura N, Kobayashi M, Hasegawa K, Ogamo A, Kamijo R (2003) Sulfated polysaccharides enhance the biological activities of bone morphogenetic proteins. J Biol Chem. Oct 31;278(44):43229-35

Thies RS, Chen T, Davies MV, Tomkinson KN, Pearson AA, Shakey QA, Wolfman NM (2001) GDF-8 propeptide binds to GDF-8 and antagonizes biological activity by inhibiting GDF-8 receptor binding. Growth Factors. 18(4):251-9

Thompson LD, Pantoliano MW, Springer BA (1994) Energetic characterization of the basic fibroblast growth factor-heparin interaction: identification of the heparin binding domain. Biochemistry. Apr 5;33(13):3831-40

Thorpe SJ, Ball C, Fox B, Thompson KM, Thorpe R, Bristow A (2008) Anti-D and anti-i activities are inseparable in V4-34-encoded monoclonal anti-D: the same framework 1 residues are required for both reactivities. Transfusion. May;48(5):930-40

Towbin H, Staehelin T, Gordon J (1979) Electrophoretic transfer of proteins from polyacrylamide gels to nitrocellulose sheets: procedure and some applications. Proc Natl Acad Sci U S A. Sep;76(9):4350-4

Turnbull JE, Gallagher JT (1991) Distribution of iduronate 2-sulphate residues in heparan sulphate. Evidence for an ordered polymeric structure. Biochem J. Feb 1;273(Pt 3):553-9

Urist MR (1965) Bone: formation by autoinduction. Science. Nov 12;150(698):893-9

Vukicevic S, Basic V, Rogic D, Basic N, Shih MS, Shepard A, Jin D, Dattatreyamurty B, Jones W, Dorai H, Ryan S, Griffiths D, Maliakal J, Jelic M, Pastorcic M, Stavljenic A, Sampath TK (1998) Osteogenic protein-1 (bone morphogenetic protein-7) reduces severity of injury after ischemic acute renal failure in rat. J Clin Invest. Jul 1;102(1):202-14

Vukicevic S, Kopp JB, Luyten FP, Sampath TK (1996) Induction of nephrogenic mesenchyme by osteogenic protein 1 (bone morphogenetic protein 7). Proc Natl Acad Sci U S A. Aug 20;93(17):9021-6

Wang EA, Rosen V, D'Alessandro JS, Bauduy M, Cordes P, Harada T, Israel DI, Hewick RM, Kerns KM, LaPan P, Luxenberg DP, McQuaid D, Moutsatsos IK, Nove J, Wozney JM (1990) Recombinant human bone morphogenetic protein induces bone formation. Proc Natl Acad Sci U S A. Mar;87(6):2220-4

Wang S, Chen Q, Simon TC, Strebeck F, Chaudhary L, Morrissey J, Liapis H, Klahr S, Hruska KA (2003) Bone morphogenic protein-7 (BMP-7), a novel therapy for diabetic nephropathy. Kidney Int. Jun;63(6):2037-49

Wang SN, Lapage J, Hirschberg R (2001) Loss of tubular bone morphogenetic protein-7 in diabetic nephropathy. J Am Soc Nephrol. Nov;12(11):2392-9

Warnke PH, Springer IN, Wiltfang J, Acil Y, Eufinger H, Wehmöller M, Russo PA, Bolte H, Sherry E, Behrens E, Terheyden H (2004) Growth and transplantation of a custom vascularised bone graft in a man. Lancet. Aug 28-Sep 3;364(9436):766-70

Wei G, Bai X, Sarkar AK, Esko JD (1999) Formation of HNK-1 determinants and the glycosaminoglycan tetrasaccharide linkage region by UDP-GlcUA:Galactose beta1, 3-glucuronosyltransferases. J Biol Chem. Mar 19;274(12):7857-64

Wei Z, Swiedler SJ, Ishihara M, Orellana A, Hirschberg CB (1993) A single protein catalyzes both N-deacetylation and N-sulfation during the biosynthesis of heparan sulfate. Proc Natl Acad Sci U S A. May 1;90(9):3885-8

Weiner SJ, Kollman PA, Case DA, Singh UC, Alagona G, Profeta J, Weiner P, Ghio C (1984) A new force field for molecular mechanical simulation of nucleic acids and proteins. J Am Chem Soc. Feb;106(3):765-784

Wetzel P, Haag J, Câmpean V, Goldschmeding R, Atalla A, Amann K, Aigner T (2006) Bone morphogenetic protein-7 expression and activity in the human adult normal kidney is predominantly localized to the distal nephron. Kidney Int. Aug;70(4):717-23

White AP, Vaccaro AR, Hall JA, Whang PG, Friel BC, McKee MD (2007) Clinical applications of BMP-7/OP-1 in fractures, nonunions and spinal fusion. Int Orthop. Dec;31(6):735-41

Winkler DG, Yu C, Geoghegan JC, Ojala EW, Skonier JE, Shpektor D, Sutherland MK, Latham JA (2004) Noggin and sclerostin bone morphogenetic protein antagonists form a mutually inhibitory complex. J Biol Chem. Aug 27;279(35):36293-8

Wolfman NM, McPherron AC, Pappano WN, Davies MV, Song K, Tomkinson KN, Wright JF, Zhao L, Sebald SM, Greenspan DS, Lee SJ (2003) Activation of latent myostatin by the BMP-1/tolloid family of metalloproteinases. Proc Natl Acad Sci U S A. Dec 23;100(26):15842-6

Wozney JM, Rosen V, Celeste AJ, Mitsock LM, Whitters MJ, Kriz RW, Hewick RM, Wang EA (1988) Novel regulators of bone formation: molecular clones and activities. Science. Dec 16;242(4885):1528-34

Wrana JL, Attisano L, Wieser R, Ventura F, Massagué J (1994) Mechanism of activation of the TGF-beta receptor. Nature. Aug 4;370(6488):341-7

Yamashita H, Ten Dijke P, Heldin CH, Miyazono K (1996) Bone morphogenetic protein receptors. Bone. Dec;19(6):569-74

Zeisberg M, Bottiglio C, Kumar N, Maeshima Y, Strutz F, Müller GA, Kalluri R (2003) Bone morphogenic protein-7 inhibits progression of chronic renal fibrosis associated with two genetic mouse models. Am J Physiol Renal Physiol. Dec;285(6):F1060-7

Zeisberg M, Hanai J, Sugimoto H, Mammoto T, Charytan D, Strutz F, Kalluri R (2003) BMP-7 counteracts TGF-beta1-induced epithelial-to-mesenchymal transition and reverses chronic renal injury. Nat Med. Jul;9(7):964-8

Zeisberg M, Kalluri R (2004) The role of epithelial-to-mesenchymal transition in renal fibrosis. J Mol Med. Mar;82(3):175-81

Zeisberg M, Shah AA, Kalluri R (2005) Bone morphogenic protein-7 induces mesenchymal to epithelial transition in adult renal fibroblasts and facilitates regeneration of injured kidney. J Biol Chem. Mar 4;280(9):8094-100

Zhao B, Katagiri T, Toyoda H, Takada T, Yanai T, Fukuda T, Chung UI, Koike T, Takaoka K, Kamijo R (2006) Heparin potentiates the in vivo ectopic bone formation induced by bone morphogenetic protein-2. J Biol Chem. Aug 11;281(32):23246-53